1-1-2008

Robust Nonlinear Control Of Underactuated Satellite Formation

Geoffrey R. McVittie
Ryerson University

ROBUST NONLINEAR CONTROL OF UNDERACTUATED SATELLITE FORMATION

by

Geoffrey Robert McVittie
B.Eng., Electrical Engineering
Ryerson University, 2006

A thesis presented to Ryerson University

in partial fulfillment of the requirements for the degree of
Master of Applied Science
in the Program of
Electrical Engineering

Toronto, Ontario, Canada, 2008

AUTHOR'S DECLARATION

I hereby declare that I am the sole author of this thesis.

I authorize Ryerson University to lend this thesis to other institutions or individuals for the purpose of scholarly research.

____ _____

I further authorize Ryerson University to reproduce this thesis by photocopying or by other means, in total or in part, at the request of other institutions or individuals for the purpose of scholarly research.

_____ _____

ABSTRACT

ROBUST NONLINEAR CONTROL OF UNDERACTUATED SATELLITE FORMATION

Geoffrey Robert McVittie, Master of Applied Science, Electrical Engineering
Ryerson University, Toronto, 2008

In this thesis, the control of the underactuated satellite formation system is examined. The underactuated satellite formation consists of a leader-follower configuration where there is no control force available in the radial direction relative to the orbit of the leader satellite. Two new relay sliding mode controllers are proposed as a method of controlling the formation system. The first controller is developed using the Hill's equation of motion of the satellite formation and the sliding manifold is designed based on linear quadratic regulation and the algebraic Riccati equation. The second controller uses a 2^{nd} order state dependent time varying approximation of the satellite formation and the sliding manifold is chosen in real-time through the evaluation of the causal approximation of the differential Riccati equation. The incorporation of the nonlinearity and time varying properties of the system into the control law expands the operational range of application. The theoretical stability bounds of the two control laws are determined guaranteeing the robust nature of the closed loop system against both matched and unmatched disturbances. A series of numerical simulations are used to validate the stability and robustness of the proposed control laws. Finally, some simulations are provided to determine the effect of controller and system parameters on the control laws' performance.

ACKNOWLEDGMENTS

First, I would like to thank my thesis supervisors, Dr. Krishna Dev Kumar and Dr. Guangjun Liu, for their support, guidance, and encouragement during the course the research work. I would like to express my gratitude to Dr. Krishna Dev Kumar for providing advice and direction on the subject of satellite formation systems and general space system dynamics. I would like to express my gratitude to Dr. Guangjun Liu for his insight into the design and principles of control systems and helpful suggestions during the progress of the research.

I would like to thank Godard for helping me to prepare final thesis presentation as well as his valuable suggestions and discussions during this thesis work, which were valuable and positive. I am also very thankful to Kamran Shahid for setting up our SSDC lab and providing complete computer facilities with all tools I needed for research.

DEDICATION

This thesis is dedicated to my parents, Marianne and James R. McVittie, and my little brother, James H. McVittie, who gave me all the support I needed to complete my Masters of Applied Science degree.

TABLE OF CONTENTS

LIST OF TABLES

LIST OF FIGURES

NOMENCLATURE

θ	true anomaly
$\dot{\theta}$	orbital angular velocity
μ_e	gravitational parameter of Earth
x, y, z	relative radial, tangential, and normal positions
$\dot{x}, \dot{y}, \dot{z}$	relative velocities
y_s, z_s	integrals of relative tangential and normal positions
$\tilde{x}, \tilde{y}, \tilde{z}$	relative position tracking errors
r_c	orbital radius of leader satellite
r	orbital radius of follower satellite
V, T	potential and kinetic energy
L	lagrange function
m	mass of follower satellite
d_x, d_y, d_z	disturbances in the radial, tangential, and normal directions
$\overline{d}_x, \overline{d}_y, \overline{d}_z$	normalized disturbances
u_y, u_z	control force in the tangential and normal directions
$\overline{u}_y, \overline{u}_z$	normalized control force
$\mathbf{A}$	state matrix
$\mathbf{B}$	control matrix
$\mathbf{x}$	state vector
$\dot{\theta}_m$	mean orbital angular velocity
t	Time
τ	orbital frequency normalized time
$\Phi(t)$	state transition matrix
$\mathcal{L}$	laplace transform operator
r_d	desired formation radius
ΔV	fuel consumption measure

$\mathbf{Q}$	state weighting matrix
q	state weighting matrix coefficient
$\mathbf{R}$	control weighting matrix
$\mathbf{P}$	solution of riccati equation
$\alpha_{11}, \alpha_{12}, \beta_1, \alpha_{21}, \alpha_{22}, \gamma, \beta_2$	disturbance weighting coefficients
σ	Switching function
δ	dead zone boundary width
e	orbital eccentricity
$\text{sgn}(\bullet)$	sign function
η	Switching coefficient
$\|\bullet\|$	Euclidean norm
λ	eigenvalue
V_1, V_2	Lyapunov functions
Σ, Δ, Γ	robust stability regions
$\hat{a}, \overline{\mathbf{A}}, \mu$	compact notations
$\mathbf{x}_1$	unmatched states

"No, you can't always get what you want,
You can't always get what you want,
You can't always get what you want,
But if you try sometime you find,
You get what you need!"

- Mick Jagger and Keith Richards

Chapter 1
Introduction

In recent years, the satellite and space community has seen an increase in technological development brought about by the development of large scale launch systems, such as the European Space Agency's (ESA) Ariane-5 or NASA's cargo launch vehicle Ares-V, combined with the availability of inexpensive high-powered computing systems and sensor technology. This has resulted in the renewed interest of many missions and satellite applications that were once deemed either too expensive or high risk for serious investment. One such application is satellite formation flying.

A satellite formation consists of a group of satellites that operate together to accomplish a task that would either be too costly or impossible for a single satellite. In spite of the relatively low cost of formation deployment, it is always a primary goal in any satellite mission design to extend the operational lifespan of the mission. The control of the formation obviously becomes a key aspect in achieving the successful completion of the mission. Ideally, a satellite formation system can be controlled with high-precision using full and precise thrust available in all directions. However, in reality the satellite formation is subjected to disturbances and perturbations that need to be counteracted by the controllers. Furthermore, satellite hardware can be vulnerable to failure. When these failures occur, the control laws developed for the ideal system are no longer valid.

This thesis undertakes the challenge of developing a robust controller that will stabilize a satellite formation using a reduced number of thrusters and provide guaranteed operation in the presence of perturbing forces.

1.1 Motivation

The funding required for space mission is extremely high; with many companies and institutions only able to meet the financial requirements necessary for a single mission. As a result, the cost of failure can be devastating, both scientifically and financially. From 1990 to 2001, a total of 29% of all satellite failures, either partial or total, were attributed to the Guidance, Navigation and Control system (GN&C). Furthermore, 37% of the problems with the GN&C have resulted in a total loss of the mission [1]. In the case of satellite formations, if the formation consists of two satellites, the loss of either satellite would mean the loss of the entire mission. If the formation consists of more than two satellites, the mission may be able to tolerate the initial loss of one satellite in the formation and then it would be operating in reduced capacity and loss of vital scientific and experimental data.

The critical question to be answered here is, '*In the event of a failure, can the formation and the mission be salvaged?*' Since the satellite formation is already in orbit, any method that could be employed to extend the lifespan, especially following a failure, is beneficial. The failure that a satellite formation would be particularly prone to is the loss of thruster control, which is necessary to maintain the formation geometry. Therefore, the primary goal is the development of control methodologies capable of recovering the formation in a post-failure, reduced control state, specifically when the formation system is underactuated. Even the new control methods developed would still be subject to the realities of the original formation system, including constraints on available thrust and fuel; and, disturbances and perturbations acting on the satellites. Thus, determining the limits to which the new control technology would work is also a necessary aspect of the design.

1.2 Literature Review

The literature review is given in two parts. First, the research on the general area of satellite formation control with particular emphasis on the control methodologies is presented. Second, the specific area of underactuated satellite formation and the current control methodologies that have been explored in this area is outlined.

1.2.1 Satellite Formations

The development of satellite formation flying missions has become an active area of study in both theory and practice [2 – 14]. A variety of interesting scientific applications exist that require the use satellite formations. The two most notable applications are outlined here, including some of the missions in which they were employed. The first application for satellite formations is the distribution of sensor hardware over several satellites, reducing the power and mass costs on each individual satellite as well as the probability of a total mission failure. An example of this application is shown in Figure 1.1 where the formation consists of the Earth Observing 1 (EO-1) satellite in conjunction with LandSat 7. The satellites are able to simultaneously scan the same location of the Earth's surface with a variety of sensory equipment and gather high-fidelity climate information that would be too costly to acquire using a single satellite [2 – 4]. A second application of satellite formations is to achieve large separation distances between sensor modules, otherwise known as sparse aperture. In the case of imaging missions, the multiple low resolution sensors with large separation distances equivalent to a single, high-resolution sensor with large aperture. An illustration of this application is seen with TechSat 21 [5 – 6]. Each satellite in the formation is equipped with RADAR technology. Although the sensitivity of each satellite may be very small, the formation, as a whole, acts like a single large radio antenna. The TechSat 21 formation is shown in Figure 1.2. Another example of a formation employing large separation distances for measurement purposes is the Laser Interferometer Space Antenna (LISA) satellite mission where the formation of satellites is used to measure variations in the gravitational field [7].

In order to fulfill mission requirements, high-precision control of the satellite formation becomes crucial. As a result, several research initiatives have been directed toward controller design [15 – 28]. Linear control methodologies, including linear quadratic regulation (LQR), have been proven to be effective at stabilizing satellite formations [15 – 17]. Nonlinear control methodologies have also been proposed to stabilize the satellite formation systems, including feedback linearization [18], several forms of adaptive learning control [19 – 20], model predictive control [21], and sliding mode control [22 – 26]. Of these control methodologies, sliding mode control is particularly useful for the control of satellites due to the impulsive, or bang-bang, style of the controller output which is necessary due to the

physical operation of a typical thruster. An interesting design of the sliding mode control is proposed by Yeh et al. [26], where the basic sliding mode controller is enhanced though the addition of a dead zone, or boundary layer, around the sliding mode. This controller, also known as relay sliding mode control, is then able to stabilize the satellite formation while reducing the fuel consumption.

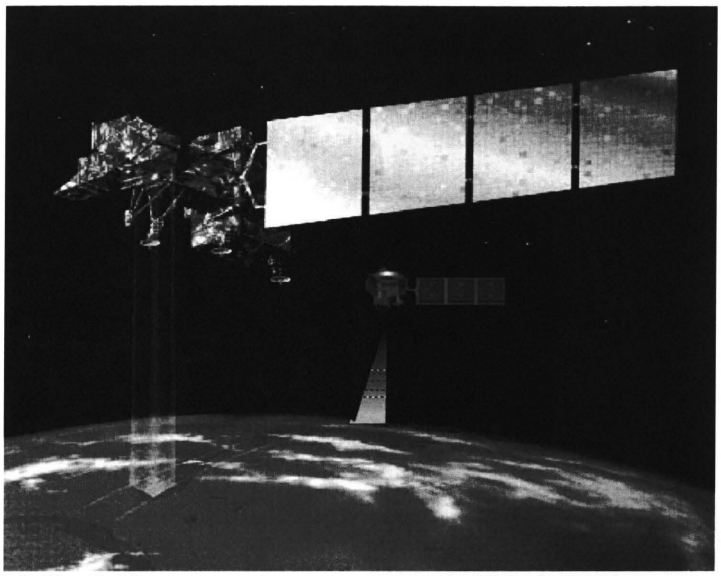

Figure 1.1: Earth Observing-1 (EO-1) and LandSat-7 in formation operation [2].

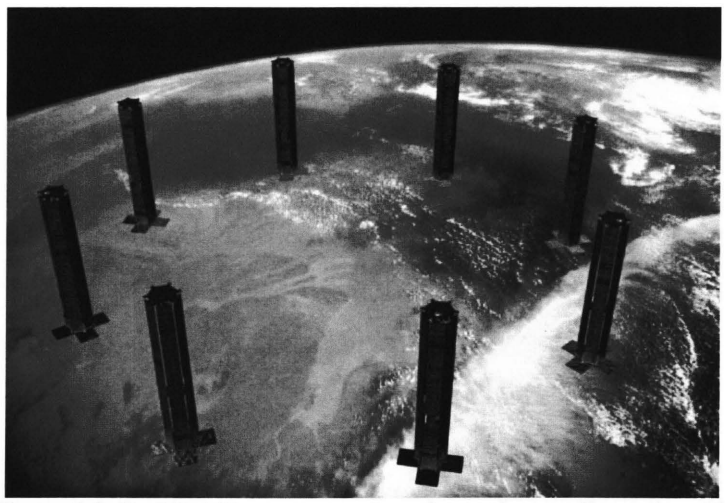

Figure 1.2: TechSat 21 sparse aperture formation configuration. [5]

1.2.2 Underactuated Satellite Formations

The special case of the underactuated satellite formation occurs when control force is not available along one axis, specifically the radial axis due as a result of controllability issues. There are several possible reasons for control thrust not being available in the radial direction. First, researchers have proposed that the satellites are designed with only one thruster in order to minimize complexity and mass [29 – 32]. A second reason is control achieved through the use of differential aerodynamic drag forces. Differential drag has the obvious advantage of not requiring any fuel but the control is only available in the tangential direction [33 – 34]. Finally, the thrusters can be physically disabled, due either to mechanical or electrical failure. Kumar et al. [29] have shown that proportional control can be applied to stabilize the underactuated LEO formation system. The proportional control was based on an ideal linear model and only marginally stable, which resulted in large tracking errors dependent on the initial conditions. The more advanced LQR was applied to the underactuated formation system and compared to the performance of the fully actuated system [30 – 32]. Although the LQR was able to stabilize the system, the requirement for variable thrust and the unconstrained control output makes it difficult to implement into a real satellite formation system. Furthermore, the LQR controller was developed from the linearized equations of motion and no considerations were given to disturbing forces acting on the system. Leonard et al. [33] applied a nonlinear, bang-bang controller to the system using linear phase-plane analysis. The phase-plane control is effective in its ability to restrict the control thrust and still drive the system to equilibrium. The only significant drawback of the phase-plane control law is the necessity to engage in maneuvers with large overshoot to bring the system to equilibrium. As with the proportional controller and LQR, the phase plane controller is developed from the linearized system model and there were no explicit consideration of disturbance forces acting on the formation.

1.3 Scope of Thesis

Based on the research that has already been conducted in the area of underactuated satellite control, the scope of the current research was established. In the current study, it is assumed that the attitude of the spacecraft in the formation is independently maintained. The disturbance forces acting on the spacecraft are restricted to the differential perturbations.

1.4 Research Objectives

The primary research objectives of this thesis are given as follows:

(1) Control of an underactuated satellite formation system, specifically without control actuation in the radial direction.

(2) A robust nonlinear control algorithm for underactuated satellite formation flying, developed from the linearized system model.

(3) A robust nonlinear control algorithm for underactuated satellite formation flying, developed from a time-varying 2^{nd} order approximation of the system model. The 2^{nd} order approximation is employed to expand the operational range of the linear controller.

(4) Precise formation keeping in the presence of model imperfections, external disturbances, and initial formation errors. This consideration is critical as these factors are responsible for the degradation and dispersal of the formation geometry.

1.5 Contributions of Thesis

The thesis makes several contributions and advancements in the area of underactuated satellite formation flying control. The key contributions are as follows:

(1) The application of closed-loop, nonlinear control for underactuated satellite formation flying, where all previous techniques have either been linear or open-loop.

(2) Proof of the stability and robustness of the linear time invariant sliding mode controller. The robustness is proven against matched and unmatched disturbance forces acting on the system. The robustness improves the reliability and feasibility in applying the control method to an actual system.

(3) Proof of the stability and robustness of the time-variant, state-dependent sliding mode controller against both matched and unmatched disturbing forces acting on the formation.

1.6 Thesis Organization

This thesis is organized as follows:

In Chapter 2 the nonlinear equations of motion for the underactuated satellite are derived through the Euler-Lagrange method. The nonlinear equations are simplified by first transforming them into a 2^{nd} order approximation and then into the classical Hill's equations, representing the linear, time-invariant (LTI) approximation. Next, the projected circular formation is presented as a stable configuration derived from the analytical solution of Hill's equations. Following the development of the system model and desired trajectory, the disturbing forces acting on the system are described. The dominant forces are due to the oblateness of the Earth, aerodynamic drag, and thruster imperfections. Finally, the chapter concludes with a description of the performance criteria used to evaluate the performance of the control laws to be developed in the proceeding chapter.

Chapter 3 begins with a brief review of variable structure control (VSC) and sliding mode control (SMC). This is followed by a description of the linear quadratic regulator (LQR) method and the state-dependent, time-variant quadratic regulator. The next section presents the design of the robust linear time invariant sliding mode controller. The controller is then redeveloped as the robust, state-dependent, time-varying sliding mode controller. In the design of both controllers, stability is ensured against both matched and unmatched disturbances acting on the system. The SMC laws are then modified into the relay control, with new boundaries established for the robustness of the system. Concluding remarks are then made concerning the issue of robustness and performance between the LTI and state-dependent, time-variant controllers.

Chapter 4 presents the numerical simulations used to validate the control laws designed Chapter 3 on the underactuated satellite formation system presented in Chapter 2. First, a detailed description of the simulation methodology and modeling is provided. Then a set of tests is made to verify the expected behavior of the control. This is followed by a series of simulations used to test the performance of the control laws under a variety of conditions that

would be typical of a satellite formation mission. These conditions include variations in disturbance forces and eccentricity of the leader satellite's orbit. A detailed analysis of the results of the simulations is performed with particular emphasis placed upon the fuel consumption and tracking performance. Chapter 4 ends with a discussion on the advantages and limitations of the proposed controllers.

Chapter 5 concludes the thesis with some remarks concerning the control laws developed for the underactuated formation system and possible directions on future work.

Chapter 2
Underactuated Satellite Formation

In this Chapter, the concept and model of a satellite formation flying system is developed. Section 2.1 develops the equations of motion of the satellite formation system through the Euler-Lagrange method. The nonlinear dynamics model is linearized about the equilibrium manifold and a framework for controllability is presented in Section 2.2. In Section 2.3, the analytical solution of the linear equations of motion and the resulting formation configurations are presented. Section 2.4 presents a general overview of the perturbing and disturbing forces acting on the satellite formation. Finally, Section 2.5 outlines the performance criteria to be used to evaluate the controllers in numerical simulation.

2.1 Model Formulation

A schematic of the satellite formation is shown in Figure 2.1, where $\vec{r}_c$ and $\vec{r}$ are respectively the position vectors of the leader and follower satellites relative to the Earth; $\vec{\rho} = [x \quad y \quad z]^T$ is the relative position vector between the leader and follower satellite; θ is the angular position of the leader satellite in the orbital plane; and finally, x, y, and z define the radial, tangential, and normal (RTN) coordinate frame of the follower satellite relative to the leader satellite, respectively [35]. Relative motion of a single follower satellite with respect to a leader satellite is considered in this study. A few assumptions concerning the formulation of the model will be established. The leader and follower satellites are treated as point masses in a geocentric inertial reference frame. A spherical Earth is assumed. Finally, it is assumed that no perturbations or control are acting on the leader satellite's orbit. As a result the behavior is defined by initial conditions.

Under these assumptions, the leader satellite's equations of motion are given as:

$$\ddot{r}_c = r_c\dot{\theta}^2 + \frac{\mu_e}{r_c^2} \tag{2-1}$$

$$\ddot{\theta} = -\frac{2\dot{\theta}\dot{r}_c}{r_c} \tag{2-2}$$

where r_c is the radius of the leader satellite's orbit, θ is and true anomaly of the leader satellite's orbit, and μ_e is the gravitational parameter of the Earth. From these assumptions, it is now possible to develop the relative equations of motion of the follower satellite.

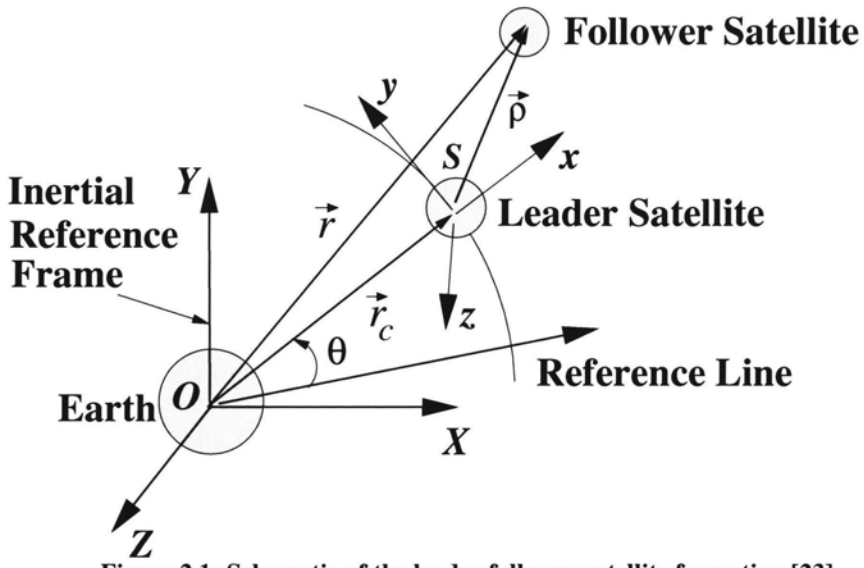

Figure 2.1: Schematic of the leader follower satellite formation [23]

2.1.1 Energy of the System

In order to apply the Euler-Langrage equation it is first necessary to derive the potential and kinetic energy of the system. The potential energy of the follower satellite is given as:

$$V = -\frac{\mu_e m}{r} = -\frac{\mu_e m}{\sqrt{(r_c + x)^2 + y^2 + z^2}} \tag{2-3}$$

where r_c is the distance of the leader, or chief, satellite from the Earth, and m is the mass of the follower satellite. The kinetic energy of the satellite in the inertial coordinate frame is given as:

$$T = \frac{1}{2} m \left(\dot{\vec{r}} \bullet \dot{\vec{r}} \right) \tag{2-4}$$

Since the goal is to find the relative equations of motion, Eq. (2-4) is transformed into the orbital coordinate frame as follows:

$$\begin{aligned} T &= \frac{m}{2} \left| \dot{\vec{r}}_c + \dot{\vec{\rho}} \right|^2 \\ &= \frac{m}{2} \left\{ \left| \dot{\vec{r}}_c \right|^2 + \left| \dot{\vec{\rho}} \right|^2 + 2 \dot{\vec{r}}_c \bullet \dot{\vec{\rho}} \right\} \\ &= \frac{m}{2} \left\{ \left[\dot{r}_c \hat{i} + r_c \dot{\theta} \hat{j} \right]^2 + \left[x\hat{i} + y\hat{j} + z\hat{k} + \vec{\omega} \times \vec{\rho} \right]^2 + 2 \left[\dot{r}_c \hat{i} + r_c \dot{\theta} \hat{j} \right] \bullet \left[x\hat{i} + y\hat{j} + z\hat{k} + \vec{\omega} \times \vec{\rho} \right] \right\} \\ &= \frac{m}{2} \left\{ \dot{r}_c^2 + r_c^2 \dot{\theta}^2 + \left(\dot{x} - \dot{\theta} y \right)^2 + \left(\dot{y} + \dot{\theta} x \right)^2 + \left(\dot{z} \right)^2 + 2 \left[\dot{r}_c \left(\dot{x} - \dot{\theta} y \right) + r_c \dot{\theta} \left(\dot{y} + \dot{\theta} x \right) \right] \right\} \end{aligned} \tag{2-5}$$

where $\dot{\theta}$ is the orbital angular velocity of the leader satellite.

2.1.2 Euler-Lagrange Equations of Motion

The Euler-Lagrange function of a system is defined as follows:

$$L = T - V \tag{2-6}$$

where T and V are the kinetic and potential energies defined earlier. The equations of motion are then derived using the following equations:

$$\frac{d}{dt} \left(\frac{\partial L}{\partial \dot{q}} \right) - \frac{\partial L}{\partial q} = U + D \tag{2-7}$$

Where $q = \begin{bmatrix} x & y & z \end{bmatrix}^T$ is a generalized coordinate vector, D is a generalized disturbance vector, and U is the generalized force vector. The partial derivatives of the potential energy of the system are given as follows:

$$\frac{\partial V}{\partial x} = \frac{\mu_e m}{r^3}(r_c + x) \tag{2-8}$$

$$\frac{\partial V}{\partial y} = \frac{\mu_e m}{r^3}(y) \tag{2-9}$$

$$\frac{\partial V}{\partial z} = \frac{\mu_e m}{r^3}(z) \tag{2-10}$$

The partial derivatives of the kinetic energy of the system are given as follows:

$$\frac{\partial T}{\partial x} = m\dot{\theta}\dot{y} + m\dot{\theta}^2 x + m r_c \dot{\theta}^2 \tag{2-11}$$

$$\frac{\partial T}{\partial y} = -m\dot{\theta}\dot{x} + m\dot{\theta}^2 y + m\dot{r}_c\dot{\theta} \tag{2-12}$$

$$\frac{\partial T}{\partial z} = 0 \tag{2-13}$$

Taking the time derivative of the partial derivatives of the system as follows:

$$\frac{d}{dt}\left(\frac{\partial T}{\partial \dot{x}}\right) = m\ddot{x} - m\ddot{\theta}y - m\dot{\theta}\dot{y} + m\ddot{r}_c \tag{2-14}$$

$$\frac{d}{dt}\left(\frac{\partial T}{\partial \dot{y}}\right) = m\ddot{y} + m\ddot{\theta}x + m\dot{\theta}\dot{x} + m\dot{r}_c\dot{\theta} + m r_c\ddot{\theta} \tag{2-15}$$

$$\frac{d}{dt}\left(\frac{\partial T}{\partial \dot{z}}\right) = m\ddot{z} \tag{2-16}$$

Combining (2-8), (2-11), and (2-14), and substituting the equation of motion of the leader satellite (2-1), the equation of motion for the x-axis is given as follows:

$$\begin{aligned} &\frac{d}{dt}\left(\frac{\partial L}{\partial \dot{x}}\right) - \frac{\partial L}{\partial x} = U_x + D_x \\ &m\ddot{x} - m\dot{\theta}^2 x - 2m\dot{\theta}\dot{y} - m\ddot{\theta}y - \frac{m\mu_e}{r_c^2} + \frac{\mu_e m}{r^3}(r_c + x) = U_x + D_x \end{aligned} \tag{2-17}$$

Similarly, combining (2-9), (2-12), and (2-15), the equation of the y-axis is given as:

$$\begin{aligned} &\frac{d}{dt}\left(\frac{\partial L}{\partial \dot{y}}\right) - \frac{\partial L}{\partial y} = U_y + D_y \\ &m\ddot{y} - m\dot{\theta}^2 y + 2m\dot{\theta}\dot{x} + m\ddot{\theta}x + \frac{\mu_e m}{r^3} y = U_y + D_y \end{aligned} \tag{2-18}$$

Finally, combining (2-10), (2-13), and (2-16) results in the equation for the z-axis:

$$\frac{d}{dt}\left(\frac{\partial L}{\partial \dot{z}}\right)-\frac{\partial L}{\partial z}=U_z+D_z$$
$$m\ddot{z}+\frac{\mu_e m}{r^3}z=U_z+D_z \tag{2-19}$$

Therefore, the fundamental equations of motion of the system are given as follows:

$$m\ddot{x}-m\dot{\theta}^2x-2m\dot{\theta}\dot{y}-m\ddot{\theta}y-\frac{\mu_e m}{r_c^2}+\frac{\mu_e m}{r^3}(r_c+x)+U_x+D_x=0 \tag{2-20}$$

$$m\ddot{y}-m\dot{\theta}^2y+2m\dot{\theta}\dot{x}+m\ddot{\theta}x+\frac{\mu_e m}{r^3}y+U_y+D_y=0 \tag{2-21}$$

$$m\ddot{z}+\frac{\mu_e m}{r^3}z+U_z+D_z=0 \tag{2-22}$$

where $D_{x,y,z}$ represents the perturbing forces acting along each axis and $U_{x,y,z}$ is the control forces applied along the tangential and normal axes, respectively. The underactuated nature of the formation system is achieved by removing control actuation in the radial direction, i.e. $U_x=0$. Equations (2-20), (2-21), and (2-22) can be simplified by normalizing the equations with respect to the mass of the follower satellite, m. The resulting equations are given as follows:

$$\ddot{x}=\dot{\theta}^2x+2\dot{\theta}\dot{y}+\ddot{\theta}y+\frac{\mu_e}{r_c^2}-\frac{\mu_e}{r^3}(r_c+x)+d_x \tag{2-23}$$

$$\ddot{y}=\dot{\theta}^2y-2\dot{\theta}\dot{x}-\ddot{\theta}x-\frac{\mu_e}{r^3}y+u_y+d_y \tag{2-24}$$

$$\ddot{z}=-\frac{\mu_e}{r^3}z+u_z+d_z \tag{2-25}$$

where $r=\sqrt{(r_c+x)^2+y^2+z^2}$, $u_{x,y,z}=U_{x,y,z}/m$ and $d_{x,y,z}=D_{x,y,z}/m$ represent the control and disturbance accelerations.

2.2 Model Approximations

In order to develop control laws, the nonlinear equations of motion, given by Eqs. (2-23), (2-24) and (2-25), are simplified. Two approximations of Eqs. (2-23), (2-24) and (2-25) are derived. The first approximation is a 2nd order state dependent time varying model. The second approximation is a linear time invariant model.

2.2.1 Second Order, Time-Varying Approximation

The most significant nonlinearity in the equations of motion (2-23), (2-24), and (2-25) is the radial norm of the follower satellite, r. Therefore, the function for r is substituted into (2-23), (2-24), and (2-25) and are rewritten in the following form:

$$\ddot{x} = \dot{\theta}^2 x + 2\dot{\theta}\dot{y} + \ddot{\theta} y + \frac{\mu_e}{r_c^2} - \frac{\mu_e (r_c + x)}{r_c^3}\left[1 + 2\frac{x}{r_c} + \frac{x^2}{r_c^2} + \frac{y^2}{r_c^2} + \frac{z^2}{r_c^2}\right]^{-3/2} + d_x \tag{2-26}$$

$$\ddot{y} = \dot{\theta}^2 y - 2\dot{\theta}\dot{x} - \ddot{\theta} x - \frac{\mu_e y}{r_c^3}\left[1 + 2\frac{x}{r_c} + \frac{x^2}{r_c^2} + \frac{y^2}{r_c^2} + \frac{z^2}{r_c^2}\right]^{-3/2} + u_y + d_y \tag{2-27}$$

$$\ddot{z} = -\frac{\mu_e z}{r_c^3}\left[1 + 2\frac{x}{r_c} + \frac{x^2}{r_c^2} + \frac{y^2}{r_c^2} + \frac{z^2}{r_c^2}\right]^{-3/2} + u_z + d_z \tag{2-28}$$

Although a variety of methods to linearize a system, the binomial series expansion is chosen due to the simplicity of its application. The binomial series is given as follows:

$$(1+X)^{\alpha} = 1 + \alpha X + \frac{\alpha(\alpha-1)}{2!}X^2 + \frac{\alpha(\alpha-1)(\alpha-2)}{3!}X^3 + \ldots \tag{2-29}$$

Using the assumption that the relative distance between the two satellites is much smaller than the orbital radius, i.e. $x, y, z \ll r_c$, the terms inside the square brackets can then be replaced with the two first terms of the binomial expansion as follows:

$$\ddot{x} = \dot{\theta}^2 x + 2\dot{\theta}\dot{y} + \ddot{\theta} y + \frac{\mu_e}{r_c^2} - \frac{\mu_e (r_c + x)}{r_c^3}\left[1 - 3\frac{x}{r_c} - \frac{3x^2}{2r_c^2} - \frac{3y^2}{2r_c^2} - \frac{3z^2}{2r_c^2} + \frac{15}{8}\left(\frac{2x}{r_c} + \frac{x^2}{r_c^2} + \frac{y^2}{r_c^2} + \frac{z^2}{r_c^2}\right)^2\right] + d_x \tag{2-30}$$

$$\ddot{y} = \dot{\theta}^2 y - 2\dot{\theta}\dot{x} - \ddot{\theta} x - \frac{\mu_e y}{r_c^3}\left[1 - 3\frac{x}{r_c} - \frac{3x^2}{2r_c^2} - \frac{3y^2}{2r_c^2} - \frac{3z^2}{2r_c^2} + \frac{15}{8}\left(\frac{2x}{r_c} + \frac{x^2}{r_c^2} + \frac{y^2}{r_c^2} + \frac{z^2}{r_c^2}\right)^2\right] + u_y + d_y \tag{2-31}$$

$$\ddot{z} = -\frac{\mu_e z}{r_c^3}\left[1 - 3\frac{x}{r_c} - \frac{3x^2}{2r_c^2} - \frac{3y^2}{2r_c^2} - \frac{3z^2}{2r_c^2} + \frac{15}{8}\left(\frac{2x}{r_c} + \frac{x^2}{r_c^2} + \frac{y^2}{r_c^2} + \frac{z^2}{r_c^2}\right)^2\right] + u_z + d_z \tag{2-32}$$

Expanding (2-30), (2-31), and (2-32), and neglecting the third and higher order terms, the 2nd order approximation of the equations of motion is expressed as:

$$\ddot{x} = \left(\dot{\theta}^2 + \frac{2\mu_e}{r_c^3} - \frac{3\mu_e x}{2r_c^4}\right)x + \left(\ddot{\theta} + \frac{3\mu_e y}{2r_c^4}\right)y + \left(\frac{3\mu_e z}{2r_c^4}\right)z + (0)\dot{x} + (2\dot{\theta})\dot{y} + (0)\dot{z} + d_x \tag{2-33}$$

$$\ddot{y} = \left(3\frac{\mu_e y}{r_c^4} - \ddot{\theta}\right)x + \left(\dot{\theta}^2 - \frac{\mu_e}{r_c^3}\right)y + (0)z + (-2\dot{\theta})\dot{x} + (0)\dot{y} + (0)\dot{z} + d_y + u_y \tag{2-34}$$

$$\ddot{z} = (0)x + (0)y + \left(3\frac{\mu_e x}{r_c^4} - \frac{\mu_e}{r_c^3}\right)z + (0)\dot{x} + (0)\dot{y} + (0)\dot{z} + d_z + u_z \tag{2-35}$$

The 2nd order approximation of the satellite can also be represented in state space form as:

$$\frac{d}{dt}\begin{bmatrix} x \\ y \\ z \\ \dot{x} \\ \dot{y} \\ \dot{z} \end{bmatrix} = \begin{bmatrix} 0 & 0 & 0 & 1 & 0 & 0 \\ 0 & 0 & 0 & 0 & 1 & 0 \\ 0 & 0 & 0 & 0 & 0 & 1 \\ \dot{\theta}^2 + \frac{2\mu_e}{r_c^3} - \frac{3\mu_e x}{2r_c^4} & \ddot{\theta} + \frac{3\mu_e y}{2r_c^4} & \frac{3\mu_e z}{2r_c^4} & 0 & 2\dot{\theta} & 0 \\ 3\frac{\mu_e y}{r_c^4} - \ddot{\theta} & \dot{\theta}^2 - \frac{\mu_e}{r_c^3} & 0 & -2\dot{\theta} & 0 & 0 \\ 0 & 0 & 3\frac{\mu_e x}{r_c^4} - \frac{\mu_e}{r_c^3} & 0 & 0 & 0 \end{bmatrix}\begin{bmatrix} x \\ y \\ z \\ \dot{x} \\ \dot{y} \\ \dot{z} \end{bmatrix} + \begin{bmatrix} 0 & 0 \\ 0 & 0 \\ 0 & 0 \\ 0 & 0 \\ 1 & 0 \\ 0 & 1 \end{bmatrix}\begin{bmatrix} u_y \\ u_z \end{bmatrix} + \begin{bmatrix} 0 \\ 0 \\ 0 \\ d_x \\ d_y \\ d_z \end{bmatrix} \tag{2-36}$$

2.2.2 Hill's Equations

The 2nd order system approximation can be simplified into a linear, time-invariant model. If it is assumed that the leader satellite is in a circular orbit, then the angular acceleration is reduced to zero, $\ddot{\theta} = 0$, and the angular velocity becomes a constant, $\dot{\theta} = n = \sqrt{\mu / r_c^3}$. Substituting these new relations and neglecting the 2nd order terms, Eqs. (2-33), (2-34), and (2-35) are reduced to the following:

$$\ddot{x} = 3n^2 x + 2n\dot{y} + d_x \tag{2-37}$$

$$\ddot{y} = -2n\dot{x} + u_y + d_y \tag{2-38}$$

$$\ddot{z} = -n^2 z + u_z + d_z \tag{2-39}$$

Equations (2-37), (2-38), and (2-39) are commonly referred to as either the Hill's or Clohessey-Wiltshire equations [36 – 37]. The Hill's equations can also be represented in the state space form as:

$$\frac{d}{dt}\begin{bmatrix} x \\ y \\ z \\ \dot{x} \\ \dot{y} \\ \dot{z} \end{bmatrix} = \begin{bmatrix} 0 & 0 & 0 & 1 & 0 & 0 \\ 0 & 0 & 0 & 0 & 1 & 0 \\ 0 & 0 & 0 & 0 & 0 & 1 \\ 3n^2 & 0 & 0 & 0 & 2n & 0 \\ 0 & 0 & 0 & -2n & 0 & 0 \\ 0 & 0 & -n^2 & 0 & 0 & 0 \end{bmatrix}\begin{bmatrix} x \\ y \\ z \\ \dot{x} \\ \dot{y} \\ \dot{z} \end{bmatrix} + \begin{bmatrix} 0 & 0 \\ 0 & 0 \\ 0 & 0 \\ 0 & 0 \\ 1 & 0 \\ 0 & 1 \end{bmatrix}\begin{bmatrix} u_y \\ u_z \end{bmatrix} + \begin{bmatrix} 0 \\ 0 \\ 0 \\ d_x \\ d_y \\ d_z \end{bmatrix} \tag{2-40}$$

A comparison of the uncontrolled, unperturbed tracking errors between the nonlinear model, and the 2nd order and LTI approximations are presented in Figure 2.2. The desired formation and tracking reference are defined in Section 2.3. The nonlinear model and the 2nd order approximation experience time varying tracking error in the radial and normal directions combined with a constant drift in the tangential direction. Furthermore, this illustrates the limits of linear time invariant approximation.

2.2.3 Controllability

After developing the model approximations in the previous section, it is necessary now to ensure that the approximations of the underactuated satellite formation system are controllable. A linear, time-invariant (LTI) system is defined to be controllable if the rank of the controllability matrix:

$$\mathbf{C} = \begin{bmatrix} \mathbf{B} & \mathbf{AB} & \mathbf{A}^2\mathbf{B} & \ldots & \mathbf{A}^{n-1}\mathbf{B} \end{bmatrix} \tag{2-41}$$

is equal to the number of system states [38]. For the Hill's equations, it is easily verified that the rank of the controllability matrix is equivalent to the number of states, specifically six. The concept of controllability can easily be extended to time-varying, state-dependent systems [39]. The generalized controllability test is defined as:

$$rank\left[\mathbf{B}(\mathbf{x},t) \quad \mathbf{A}(\mathbf{x},t)\mathbf{B}(\mathbf{x},t) \quad \mathbf{A}^2(\mathbf{x},t)\mathbf{B}(\mathbf{x},t) \quad \ldots \quad \mathbf{A}^{n-1}(\mathbf{x},t)\mathbf{B}(\mathbf{x},t)\right] = n \;\forall \mathbf{x},t \tag{2-42}$$

where n is the number of system states. In this formulation, the controllability of the system is defined for all points of $\mathbf{x}$ and over the entire time range. It is important to note that, unlike the LTI definition, controllability may only occur locally over a defined region of states. The 2nd order approximation of the underactuated satellite formation system can be verified as controllable in a realistic operational region surrounding the leader satellite, or reference point.

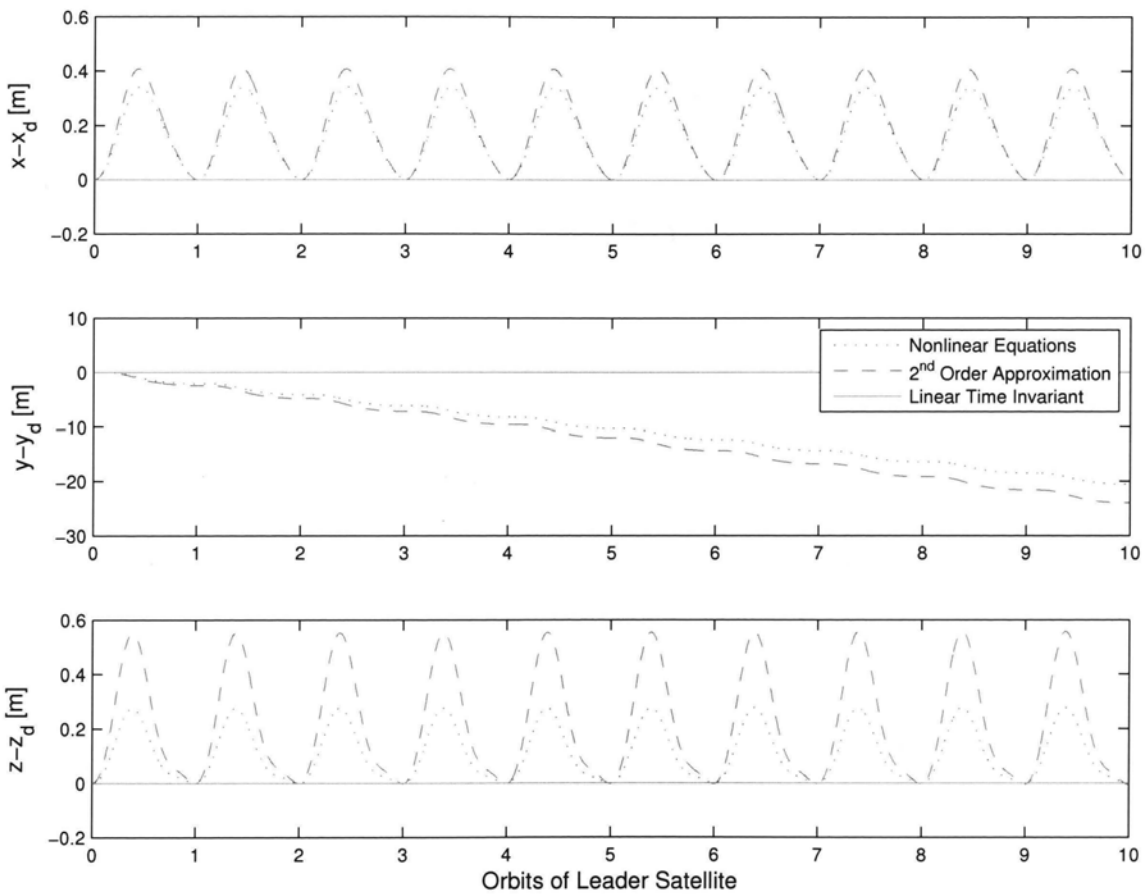

Figure 2.2: Comparison of approximation models

2.2.4 Normalization

In order to simplify the design and tuning of control laws for the satellite formation system, the equations of motion are normalized by the orbital frequency [25]. A new time base is defined as follows:

$$\tau = nt \tag{2-43}$$

where $n = \sqrt{\mu_e / a^3}$ is the mean orbital frequency. Using the new time base, the system states can be expressed as follows:

$$\begin{aligned} \dot{x} &= nx' & \ddot{x} &= n^2 x'' \\ \dot{y} &= ny' & \ddot{y} &= n^2 y'' \\ \dot{z} &= nz' & \ddot{z} &= n^2 z'' \end{aligned} \tag{2-44}$$

Substituting (2-44) into (2-34) and dividing through by $\dot{\theta}_m^2$, the normalized 2nd order approximation is then given as follows:

$$\frac{d}{d\tau}\begin{bmatrix} x \\ y \\ z \\ x' \\ y' \\ z' \end{bmatrix} = \begin{bmatrix} 0 & 0 & 0 & 1 & 0 & 0 \\ 0 & 0 & 0 & 0 & 1 & 0 \\ 0 & 0 & 0 & 0 & 0 & 1 \\ \dfrac{\dot{\theta}^2 + \dfrac{2\mu_e}{r_c^3} - \dfrac{3\mu_e x}{2r_c^4}}{n^2} & \dfrac{\ddot{\theta} + \dfrac{3\mu_e y}{2r_c^4}}{n^2} & \dfrac{\dfrac{3\mu_e z}{2r_c^4}}{n^2} & 0 & \dfrac{2\dot{\theta}}{n} & 0 \\ \dfrac{3\dfrac{\mu_e y}{r_c^4} - \ddot{\theta}}{n^2} & \dfrac{\dot{\theta}^2 - \dfrac{\mu_e}{r_c^3}}{n^2} & 0 & -\dfrac{2\dot{\theta}}{n} & 0 & 0 \\ 0 & 0 & \dfrac{3\dfrac{\mu_e x}{r_c^4} - \dfrac{\mu_e}{r_c^3}}{n^2} & 0 & 0 & 0 \end{bmatrix} \begin{bmatrix} x \\ y \\ z \\ x' \\ y' \\ z' \end{bmatrix} + \begin{bmatrix} 0 & 0 \\ 0 & 0 \\ 0 & 0 \\ 0 & 0 \\ 1 & 0 \\ 0 & 1 \end{bmatrix} \begin{bmatrix} \overline{u}_y \\ \overline{u}_z \end{bmatrix} + \begin{bmatrix} 0 \\ 0 \\ 0 \\ \overline{d}_x \\ \overline{d}_y \\ \overline{d}_z \end{bmatrix} \tag{2-45}$$

In the case of the Hill's equations, where it has been assumed that the leader satellite is in a circular orbit, the mean orbital frequency n is equal to $\dot{\theta}$. Substituting (2-44) into (2-40) and dividing through by n^2 results in the normalized Hill's equations, expressed in state space form as:

$$\frac{d}{dt}\begin{bmatrix} x \\ y \\ z \\ x' \\ y' \\ z' \end{bmatrix} = \begin{bmatrix} 0 & 0 & 0 & 1 & 0 & 0 \\ 0 & 0 & 0 & 0 & 1 & 0 \\ 0 & 0 & 0 & 0 & 0 & 1 \\ 3 & 0 & 0 & 0 & 2 & 0 \\ 0 & 0 & 0 & -2 & 0 & 0 \\ 0 & 0 & -1 & 0 & 0 & 0 \end{bmatrix}\begin{bmatrix} x \\ y \\ z \\ x' \\ y' \\ z' \end{bmatrix} + \begin{bmatrix} 0 & 0 \\ 0 & 0 \\ 0 & 0 \\ 0 & 0 \\ 1 & 0 \\ 0 & 1 \end{bmatrix}\begin{bmatrix} \bar{u}_y \\ \bar{u}_z \end{bmatrix} + \begin{bmatrix} 0 \\ 0 \\ 0 \\ \bar{d}_x \\ \bar{d}_y \\ \bar{d}_z \end{bmatrix} \tag{2-46}$$

where $\bar{d}_{x,y,z}$ and $\bar{u}_{y,z}$ are the frequency normalized disturbance and control accelerations.

2.2.5 Integral Augmentation

One of the major concerns in the development of any control system is achieving steady-state tracking around the equilibrium point; in particular, the elimination of any constant steady-state error. In order to address this concern, the system state vector and matrix can be augmented with additional integral states. In the case of the underactuated satellite formation system, two new integral states can be introduced. The new states are expressed as follows:

$$y_s = \int_0^t y(\tau)\,d\tau \tag{2-47}$$

$$z_s = \int_0^t z(\tau)\,d\tau \tag{2-48}$$

When (2-47) and (2-48) are combined with the normalized Hill's equations (2-46), the augmented system is expressed as follows:

$$\frac{d}{d\tau}\begin{bmatrix} y_s \\ z_s \\ x \\ y \\ z \\ x' \\ y' \\ z' \end{bmatrix} = \begin{bmatrix} 0 & 0 & 0 & 1 & 0 & 0 & 0 & 0 \\ 0 & 0 & 0 & 0 & 1 & 0 & 0 & 0 \\ 0 & 0 & 0 & 0 & 0 & 1 & 0 & 0 \\ 0 & 0 & 0 & 0 & 0 & 0 & 1 & 0 \\ 0 & 0 & 0 & 0 & 0 & 0 & 0 & 1 \\ 0 & 0 & 3 & 0 & 0 & 0 & 2 & 0 \\ 0 & 0 & 0 & 0 & 0 & -2 & 0 & 0 \\ 0 & 0 & 0 & 0 & -1 & 0 & 0 & 0 \end{bmatrix}\begin{bmatrix} y_s \\ z_s \\ x \\ y \\ z \\ x' \\ y' \\ z' \end{bmatrix} + \begin{bmatrix} 0 & 0 \\ 0 & 0 \\ 0 & 0 \\ 0 & 0 \\ 0 & 0 \\ 0 & 0 \\ 1 & 0 \\ 0 & 1 \end{bmatrix}\begin{bmatrix} \bar{u}_y \\ \bar{u}_z \end{bmatrix} + \begin{bmatrix} 0 \\ 0 \\ 0 \\ 0 \\ 0 \\ \bar{d}_x \\ \bar{d}_y \\ \bar{d}_z \end{bmatrix} \tag{2-49}$$

The 2nd order approximation of the system equations can similarly be augmented with integrator states. It should be noted that due to the underactuated configuration of the system,

specifically the absence of control actuation along the radial axis, the integration of the radial position error cannot be achieved as this would render the system uncontrollable, according to the definition given in Section 2.2.3. However, as the critical separation distance of the formation is on the y and z axes, a constant steady-state error on the x-axis can be tolerated.

2.3 Minimum Energy Configurations

One of the primary concerns with any satellite mission is the reduction of fuel consumption. Although there are an infinite number of possible satellite formation configurations, the configurations are typically chosen to minimize the fuel requirements of the controller. These formations are known as minimum energy configurations. The minimum energy configurations are derived from the analytical solution of Hill's equations [40]. As a result, the controller to be implemented is only required to counteract the unmodelled system nonlinearity and the external disturbance forces.

2.3.1 Analytical Solution of Hill's Equations

The analytical solutions of the Hill's equations are derived using the frequency domain method [41]. Assuming no disturbances or control forces are acting on the system, the state space representation of the system (2-40) can be expressed in the simplified notation given as:

$$\dot{\mathbf{x}} = \mathbf{A}\mathbf{x} \tag{2-50}$$

where $\mathbf{x}$ is the state vector and $\dot{\mathbf{x}}$ is the time derivative of the state vector. Taking the Laplace transform on both sides of (2-50) as follows:

$$s\mathbf{X}(s) - \mathbf{x}(0) = \mathbf{A}\mathbf{X}(s) \tag{2-51}$$

where $\mathbf{x}(0)$ is the state vector at time $t = 0$. Rearranging expression (2-51) as:

$$\mathbf{X}(s) = [s\mathbf{I} - \mathbf{A}]^{-1}\mathbf{x}(0) \tag{2-52}$$

Applying the inverse Laplace transform to both sides of (2-52) yields:

$$\begin{aligned}\mathbf{x}(t) &= \mathcal{L}^{-1}\left\{[s\mathbf{I}-\mathbf{A}]^{-1}\right\}\mathbf{x}(0) \\ &= \Phi(t)\mathbf{x}(0)\end{aligned} \tag{2-53}$$

where $\Phi(t)$ is the state transition matrix. For the satellite formation system, the state transition matrix is given as:

$$\Phi(t)=\begin{bmatrix} -3\cos(nt)+4 & 0 & 0 & \frac{\sin(nt)}{n} & -\frac{2\cos(nt)}{n}+\frac{2}{n} & 0 \\ -6nt+6\sin(nt) & 1 & 0 & \frac{2\cos(nt)}{n}-\frac{2}{n} & -3t+\frac{4\sin(nt)}{n} & 0 \\ 0 & 0 & \cos(nt) & 0 & 0 & \frac{\sin(nt)}{n} \\ 3n\sin(nt) & 0 & 0 & \cos(nt) & 2\sin(nt) & 0 \\ 6n\cos(nt)-6n & 0 & 0 & -2\sin(nt) & 4\cos(nt)-3 & 0 \\ 0 & 0 & -n\sin(nt) & 0 & 0 & \cos(nt) \end{bmatrix} \tag{2-54}$$

A number of interesting formation configurations can now be developed from (2-52). The most significant configurations include the in-plane, in-track, circular, and projected circular formations [40]. For brevity, only the projected circular formation will be considered in this thesis; however, the work can easily extended to the other formation configurations.

2.3.2 Projected Circular Formation

In the projected circular formation, the leader and follower satellites maintain a fixed separation distance in the yz-plane. In the 3-dimensional environment, the formation actually consists of the follower satellite traveling in an elliptical path around the leader satellite. Therefore, the desired formation is dictated by the following constraint:

$$y_{\mathrm{d}}^2 + z_{\mathrm{d}}^2 = r_{\mathrm{d}}^2 \tag{2-55}$$

where the subscript d represents the desired trajectory and r_d is the desired radius of the projected circle. As seen in (2-54), some terms are linearly proportional to time, t. In order to counteract the secular growth caused by these terms, the following constraints are applied to the initial conditions:

$$\dot{y}_0 = -2\dot{\theta}x_0 \tag{2-56}$$

Substituting (2-55) and (2-56) into (2-54) and after some algebraic manipulation, the equations for the desired motion of the projected formation are given as follows:

$$\begin{aligned}
x_d(t) &= \frac{r_d}{2}\sin(nt+\phi) \\
y_d(t) &= r_d\cos(nt+\phi) \\
z_d(t) &= r_d\sin(nt+\phi) \\
\dot{x}_d(t) &= \frac{r_d n}{2}\cos(nt+\phi) \\
\dot{y}_d(t) &= -r_d n\sin(nt+\phi) \\
\dot{z}_d(t) &= r_d n\cos(nt+\phi)
\end{aligned} \tag{2-57}$$

where ϕ is the phase of formation relative to the orbit of the leader satellite. A schematic of the projected circular formation is shown in Figure 2.3. The projected circular formation mission has a particular advantage for sparse aperture missions, where the projected distance between the satellites is required to be fixed.

With the desired trajectory of the projected satellite formation, it is now possible to derive the error states of the system. The error states are given as:

$$\begin{aligned}
\tilde{x} &= x - x_d & \dot{\tilde{x}} &= \dot{x} - \dot{x}_d \\
\tilde{y} &= y - y_d & \dot{\tilde{y}} &= \dot{y} - \dot{y}_d \\
\tilde{z} &= z - z_d & \dot{\tilde{z}} &= \dot{z} - \dot{z}_d
\end{aligned} \tag{2-58}$$

Since the desired trajectory is derived from the analytical solution of the Hill equations (2-40), they are also the equations for the error states.

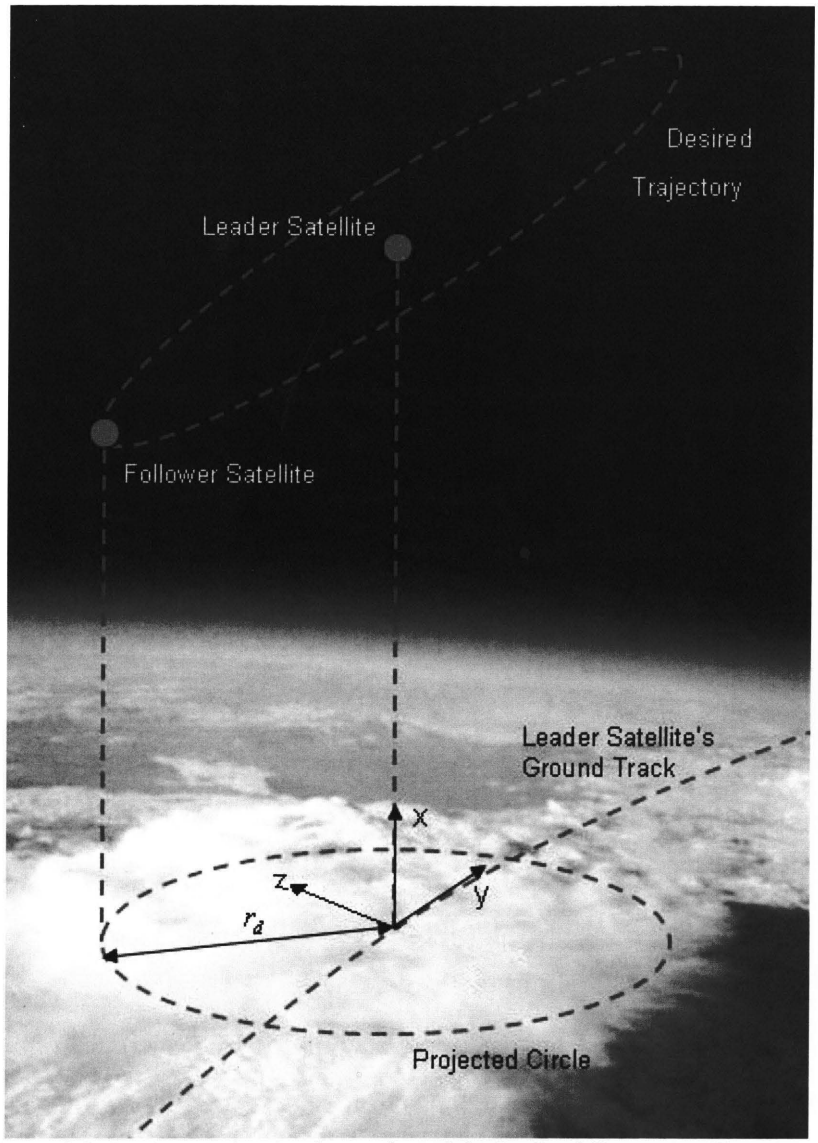

Figure 2.3: Projected circular formation of the leader follower satellite system

2.4 Perturbations and Disturbances

The Hill equations (2-40) describe the ideal behavior of the satellite formation. However, in reality there are many environmental factors affecting the orbital path of the satellites. The following subsections describe the dominant forces affecting the satellite formation.

2.4.1 J_2 Gravitational Effect

The most significant perturbing force acting on a satellite, while in low Earth orbit, is the variations in gravitational force of Earth. Of these variations, the second degree zonal

spherical harmonic, $J_2 = 1082\times10^{-6}$, produces the primary disturbing force due to the Earth oblateness [42]. The motion of the leader satellite a satellite in the inertial frame, see Figure 2.1, is described by the following equations:

$$\ddot{\vec{r}}_c = -\frac{\mu_e}{r_c^3}\vec{r}_c \tag{2-59}$$

where $\vec{r}_c = [X_c \quad Y_c \quad Z_c]$ is the geocentric position vector of the satellite and $\ddot{\vec{r}}$ is the corresponding acceleration. The equations of motion of a satellite with the J_2 disturbing are expressed in the inertial frame as:

$$\begin{aligned}
d_X &= -\frac{3\mu_e J_2 R_e^2}{2r^5}\left(1-5\frac{Z^2}{r^2}\right)X + \frac{3\mu_e J_2 R_e^2}{2r_c^5}\left(1-5\frac{Z_c^2}{r_c^2}\right)X_c \\
d_Y &= -\frac{3\mu_e J_2 R_e^2}{2r^5}\left(1-5\frac{Z^2}{r^2}\right)Y + \frac{3\mu_e J_2 R_e^2}{2r_c^5}\left(1-5\frac{Z_c^2}{r_c^2}\right)Y_c \\
d_Z &= -\frac{3\mu_e J_2 R_e^2}{2r^5}\left(3-5\frac{Z^2}{r^2}\right)Z + \frac{3\mu_e J_2 R_e^2}{2r_c^5}\left(3-5\frac{Z_c^2}{r_c^2}\right)Z_c
\end{aligned} \tag{2-60}$$

where r and r_c are the orbital radii of the leader and follower satellites and R_e is the radius of the Earth. The position of the follower satellite in the inertial frame, defined by $\vec{r} = [X \quad Y \quad Z]$, is determined from the position of the leader satellite and the relative position between the leader and follower satellites. The conversion is expressed as follows:

$$\begin{bmatrix} X \\ Y \\ Z \end{bmatrix} = R_3^T(\Omega) R_1^T(i) R_3^T(\omega+\theta) \begin{bmatrix} x+r_c \\ y \\ z \end{bmatrix} \tag{2-61}$$

where ω is the argument of periapsis, Ω is longitude of the ascending node, and i the inclination. By applying three rotations, the relative disturbance between the leader and follower satellites is expressed in the orbital frame of the leader satellite. The rotations sequence is given as follows:

$$\begin{bmatrix} d_x \\ d_y \\ d_z \end{bmatrix} = R_3(\omega+\theta)R_1(i)R_3(\Omega)\begin{bmatrix} d_X \\ d_Y \\ d_Z \end{bmatrix} \tag{2-62}$$

Since it is required to using numerical propagation to calculate the differential J_2 force, it will be strictly treated as a bounded disturbance $D_{x,y,z} = \begin{bmatrix} d_x & d_y & d_z \end{bmatrix}$ acting on the Eq. (2-26), (2-27), and (2-28) for the purposes of developing a control law.

2.4.2 Aerodynamic Drag

In LEO, the density of the Earth's atmosphere is sufficient to create a noticeable drag force on the spacecraft. The drag force, which is a function of the speed of the spacecraft, projected surface area, and density of the atmosphere, is typically modeled as a free molecular impact. As a result, the force on the spacecraft is continuous and in the direction opposite of travel. The drag force can also be radically varied by the effects of solar activity on the Earth's atmosphere. Although the drag force acting on each satellite in the formation can be very large, the relative drag force between them is much less. Kumar et al. [34] has determined the typical drift values caused by differential drag for a pair of 8 kg nano-satellites, with a 10% difference in projected surface area over a range of solar activity. The results of the study are given in Table 2.1.

Table 2.1: Drift due to differential aerodynamic drag [26]

	Low Solar Activity	Normal Solar Activity	High Solar Activity
Tangential Drift/day	15 m	110 m	460 m
Radial Drift/day	0.15 m	1.2 m	4.5 m

2.4.3 Thrusters

The third greatest contribution of perturbations to the satellite formation is the physical imperfections of the thrusters. There are two sources for deviations in thruster performance. The first is thruster alignment on the spacecraft or error in the spacecraft's attitude. The result is components of the control thrust along axes other than those desired, thus creating a

disturbing force. The second deviation is in the thruster output, which can be caused by variation in the fuel pressure or physical degradation of the thruster hardware.

2.5 Performance Criteria

In order to evaluate and tune the controller to be presented in the following chapter, it is necessary to establish a set of performance criteria. With any space mission, the two key requirements on the success of the mission are stabilizing the spacecraft to within a desired trajectory and on minimizing the magnitude and consumption of fuel, which is typically limited by the size and mass of the spacecraft. These criteria are presented in detail in the following subsections.

2.5.1 Projected Formation Error

The projected formation error is the distance between the satellite and desired path in the $yz-$plane. The projected formation error is given by the formula:

$$\tilde{r}_{y,z}(t)=\sqrt{\tilde{y}^2(t)+\tilde{z}^2(t)} \tag{2-63}$$

Since the projected error is critical for the success of any imaging or interferometer experiments, it serves as a quality performance measure for the control system. The proposed NASA mission for low Earth orbit (LEO) satellite formations suggested a projected separation distance error of no more than 5 meters [9]. Therefore, this will be the primary practical performance requirement, beyond stability, for the control system.

2.5.2 Fuel Consumption, ΔV

The fuel consumption of a spacecraft is typically measured in units of ΔV which is the summation of the changes of acceleration of the spacecraft over the period of an orbit. The formula for ΔV is given as follows:

$$\frac{\Delta V}{\text{orbit}}=\int_0^P\sqrt{u_y^2(\tau)+u_z^2(\tau)}d\tau \tag{2-64}$$

where P is the period of the leader satellite's orbit and $u_{y,z}$ are the mass normalized control forces. It is obvious that on any spacecraft, the length of a mission is determined by the

amount of fuel available. Therefore, after the critical requirement of maintain the projected formation error within bounds is met, the task is the reduction in the ΔV consumption.

2.5.3 In-Plane Formation Error

The third performance measure is the in-plane formation error. This is the error in distance from the desired trajectory in the orbital plane of the leader satellite, which is expressed as:

$$\tilde{r}_{x,y}(t) = \sqrt{\tilde{x}^2(t) + \tilde{y}^2(t)} \tag{2-65}$$

Although the in-plane error will not have a significant impact on the overall success of a formation mission, it does provide a useful check on the radial position and stability of the system.

Chapter 3
Robust Sliding Mode Control

In this chapter, the development of the robust sliding mode controller (SMC) is presented. First a brief introduction to variable structure control (VSC) and SMC is provided. This is followed by a review of the linear quadratic regulator (LQR) and state-dependent, time variant quadratic regulation. The robust linear, time-invariant SMC is then presented. This is followed by the robust state-dependent, time-varying SMC. Finally, the conventional switching control law is modified into the relay controller and the robustness bounds are redefined. The chapter concludes with some remarks on the tuning parameters of the controllers.

3.1 Review of Variable Structure Control

Variable structure control (VSC) is a powerful nonlinear control technique. The VSC, as its name suggests, achieves the desired response by switching control values in order to vary the dynamic structure of the system. Although individually each dynamic structure may be unstable, a stable response can be achieved by switching between the structures. Figure 3.1 shows the construction of a variable structure system. It is evident that although both subsystems are unstable, when combined the system will converge towards the equilibrium point at zero.

Referring to Figure 3.1, it is evident the VSC can be developed for 2^{nd} systems. However, for larger systems the design becomes more complicated; this resulted in the development of the sliding mode controller (SMC). The SMC is based on selecting a switching function, σ, that is composed of the system's state variables. When the switching function reaches zero, $\sigma = 0$, also known as the sliding manifold or surface, the system takes on the constrained behavior of the manifold. While the system state trajectory is on the sliding manifold, it is

known as the sliding mode. The sliding manifold is typically chosen to force the system states to converge to the desired reference states. Finally, when the system states have converged to zero on the sliding manifold, the system has achieved equilibrium. Figure 3.2 shows a representation of a typical SMC and the key components of the trajectory.

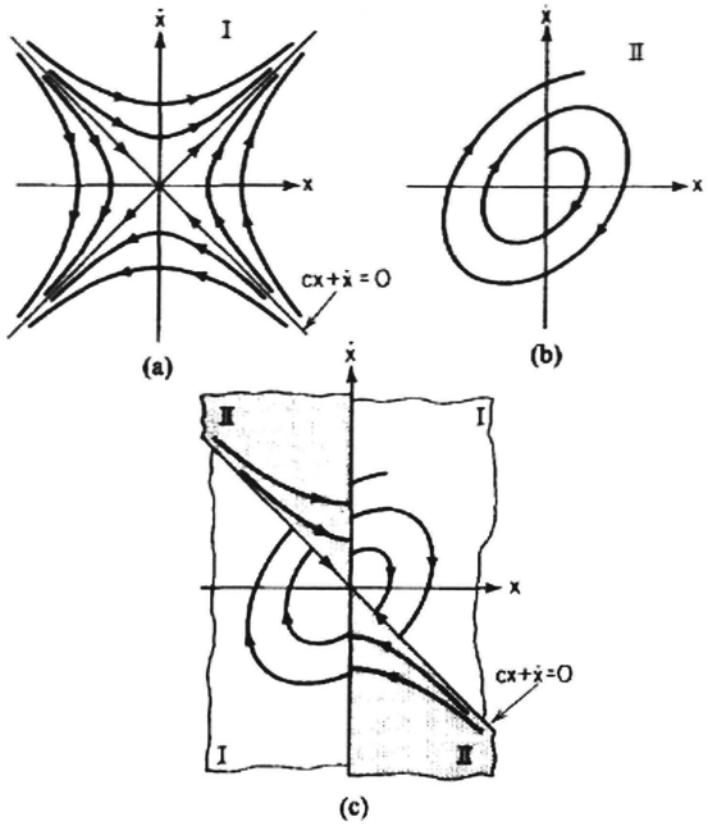

Figure 3.1: A stable variable structure system consisting of two unstable subsystems [43]

Although the SMC is a powerful controller, it does suffer from the problem known as chattering. Chattering is the high frequency switching of the controller when the system has reached the sliding manifold. A variety of techniques have been suggested to counteract the chattering effect, including the use of the sigmoid, or saturation functions [44]. For the case of spacecraft system, where control thrust is limited to fixed impulsive values, the relay controller, which incorporates a dead zone around the sliding manifold, is employed. Further detail of the relay controller is provided in Section 3.5. Before the development of the sliding mode controllers, a review of the linear quadratic regulator (LQR) is presented. The LQR

methodology will later be applied to the design of the sliding manifold due to its ability to guarantee the stability of both linear time-invariant (LTI) and state-dependent, time-varying (SDTV) control laws.

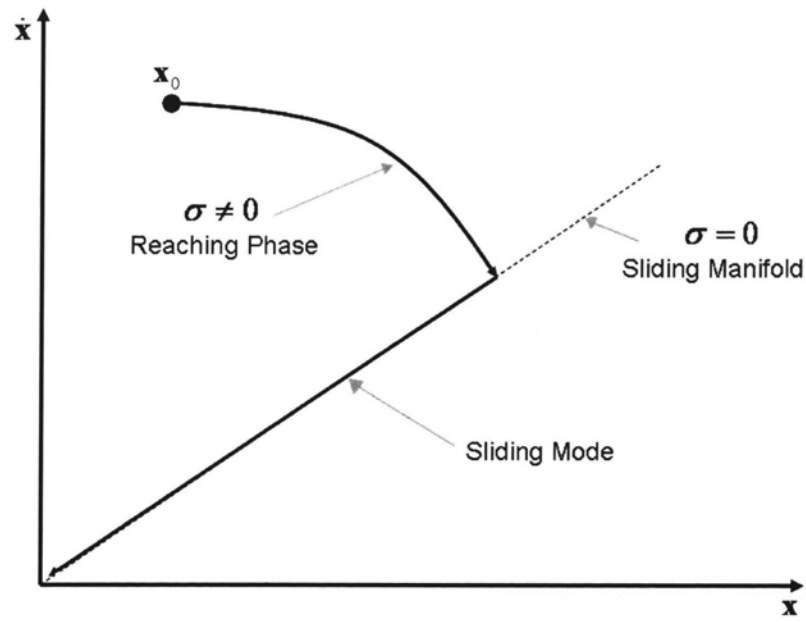

Figure 3.2: Sliding mode controller operation

3.2 Linear Quadratic Regulator

Consider the generic system represented in the following form:

$$\dot{\mathbf{x}} = \mathbf{A}\mathbf{x} + \mathbf{B}\mathbf{u} \tag{3-1}$$

where $\mathbf{x}(t) \in \mathbb{R}^n$ is the state vector; $\mathbf{A} \in \mathbb{R}^{n \times n}$ is the state matrix; $\mathbf{B} \in \mathbb{R}^{n \times m}$ is the control matrix; and, $\mathbf{u} \in \mathbb{R}^m$ is the control input vector. In order to evaluate the performance of a linear control law, a quadratic performance metric for the system is proposed as follows:

$$J = \int_t^{t_f} \left[\mathbf{x}^T(\tau)\mathbf{Q}\mathbf{x}(\tau) + \mathbf{u}^T(\tau)\mathbf{R}\mathbf{u}(\tau) \right] d\tau \tag{3-2}$$

where $\mathbf{Q} \in \mathbb{R}^{n \times n}$ and $\mathbf{R} \in \mathbb{R}^{m \times m}$ are the state and control weighting matrices, respectively; and $t \in \mathbb{R}^+$ and $t_f \in \mathbb{R}^+$ are the current and final times of the evaluation, respectively. A linear control law for the system (3-1) is proposed as follows:

$$\mathbf{u} = -\mathbf{B}^T\mathbf{P}\mathbf{x} \tag{3-3}$$

where $\mathbf{P} \in \mathbb{R}^{n\times n}$ is a positive semi-definite, symmetric matrix. The choice of $\mathbf{P}$ that minimizes the cost function (3-2) is determined by the solution of the differential Riccati equation (DRE). The DRE is expressed as follows:

$$\dot{\mathbf{P}} + \mathbf{P}\mathbf{A} + \mathbf{A}^T\mathbf{P} - \mathbf{P}\mathbf{B}\mathbf{R}^{-1}\mathbf{B}^T\mathbf{P} + \mathbf{Q} = 0 \tag{3-4}$$

where $\mathbf{P} \in \mathbb{R}^{n\times n}$ is a positive definite, symmetric matrix [38, 46 – 47]. Two particular cases exist for the solution of the DRE. These are presented in the following two subsections.

3.2.1 Linear, Time-Invariant

If the system (3-1) is linear time invariant (LTI), then the pair $(\mathbf{A},\mathbf{B})$ are constant. The cost metric (3-2) is then evaluated from $t_0 = 0$ to $t_f = \infty$ and the solution, $\mathbf{P}$, will be constant. As a result, the DRE (3-4) satisfying the modified cost metric can be reduced to the well known algebraic Riccati equation (ARE) given as:

$$\mathbf{P}\mathbf{A} + \mathbf{A}^T\mathbf{P} - \mathbf{P}\mathbf{B}\mathbf{R}^{-1}\mathbf{B}^T\mathbf{P} + \mathbf{Q} = 0 \tag{3-5}$$

The standard numerical solution to the ARE is found using the method presented by Zäk [38].

3.2.2 State Dependent, Time-Variant

In the case of the state dependent, time-variant (SDTV) system (3-1), the matrix pair $(\mathbf{A},\mathbf{B})$ is no longer constant. Therefore, the optimal control solution of the cost metric (3-2) is found by solving the differential Riccati equation (DRE). However, the solution of the DRE requires the system's states over the time span $t \le \tau \le t_f$. Since the solution uses future state values, it can be considered non-causal and not realizable in practice.

In order to resolve this problem, it has been suggested that the forward integration be changed to a backward integration [46, 47]. The time span of integration is then defined as $t_0 \le \tau \le t$. The modified differential Riccati equation is then expressed as:

$$-\dot{\mathbf{P}}' + \mathbf{P}'\mathbf{A} + \mathbf{A}^T\mathbf{P}' - \mathbf{P}'\mathbf{B}\mathbf{R}^{-1}\mathbf{B}^T\mathbf{P}' + \mathbf{Q} = 0 \tag{3-6}$$

where $\mathbf{P}'$ is a positive-definite, symmetric matrix. Although $\mathbf{P}'$ is a causal solution of the DRE, and realizable in practice, it is important to note that it only represents a realizable solution, not the optimal solution.

3.3 Robust Linear Time Invariant Sliding Mode Control

The design and proof of robustness for the linear time invariant sliding mode controller given is expansion on the method given by Hui et al. [48]. Specifically, the pole placement technique has been superseded with the application of linear quadratic regulation. Consider the linear time invariant (LTI) system expressed in the following form:

$$\dot{\mathbf{x}} = \mathbf{A}\mathbf{x} + \mathbf{B}\mathbf{u} + \mathbf{d} \tag{3-7}$$

where $\mathbf{x} \in \mathbb{R}^n$ is the state vector; $\mathbf{A} \in \mathbb{R}^{n \times n}$ is the state matrix; $\mathbf{B} \in \mathbb{R}^{n \times m}$ is the control matrix; $\mathbf{u} \in \mathbb{R}^m$ is the control input vector; and, $\mathbf{d} \in \mathbb{R}^n$ is the disturbance vector. The state vector can be decomposed into two state vectors, $\mathbf{x} = \begin{bmatrix} \mathbf{x}_1 & \mathbf{x}_2 \end{bmatrix}^T$, where $\mathbf{x}_1 \in \mathbb{R}^{n-m}$, $\mathbf{x}_2 \in \mathbb{R}^m$. The system (3-7) can now be expressed in the more specific form:

$$\begin{bmatrix} \dot{\mathbf{x}}_1 \\ \dot{\mathbf{x}}_2 \end{bmatrix} = \begin{bmatrix} \mathbf{A}_{11} & \mathbf{A}_{12} \\ \mathbf{A}_{21} & \mathbf{A}_{22} \end{bmatrix} \begin{bmatrix} \mathbf{x}_1 \\ \mathbf{x}_2 \end{bmatrix} + \begin{bmatrix} 0 \\ \mathbf{I} \end{bmatrix} \mathbf{u} + \begin{bmatrix} \mathbf{d}_1 \\ \mathbf{d}_2 \end{bmatrix} \tag{3-8}$$

where $\mathbf{A}_{11} \in \mathbb{R}^{(n-m)\times(n-m)}$, $\mathbf{A}_{12} \in \mathbb{R}^{(n-m)\times m}$, $\mathbf{A}_{21} \in \mathbb{R}^{m\times(n-m)}$, $\mathbf{A}_{22} \in \mathbb{R}^{m\times m}$ are the subsystem state matrices; $\mathbf{I} \in \mathbb{R}^{m\times m}$ is the identity matrix; and, $\mathbf{d}_1 \in \mathbb{R}^{(n-m)}$, $\mathbf{d}_2 \in \mathbb{R}^m$ are the matched and unmatched disturbances, respectively. Before the design of the controllers, two assumptions concerning the system (3-8) are required:

Assumption 1: The pair $(\mathbf{A}, \mathbf{B})$ is controllable for all $\mathbf{x} \in \mathbb{R}^n$.

Assumption 2: The matched and unmatched disturbances, $\mathbf{d}_1$ and $\mathbf{d}_2$ are bounded as:

$$\|\mathbf{d}_1\| \le \alpha_{11}\|\mathbf{x}_1\| + \alpha_{12}\|\mathbf{x}_2\| + \beta_1$$
$$\|\mathbf{d}_2\| \le \alpha_{21}\|\mathbf{x}_1\| + \alpha_{22}\|\mathbf{x}_2\| + \gamma\|\mathbf{u}\| + \beta_2 \quad \textbf{(3-9)}$$

where $\alpha_{11}, \alpha_{12}, \beta_1, \alpha_{21}, \alpha_{22}, \gamma, \beta_2$ are nonnegative constants and $\|\bullet\|$ represents the Euclidean norm of a vector or matrix.

Corollary 1: Since the pair $(\mathbf{A}, \mathbf{B})$ is controllable for all $\mathbf{x} \in \mathbb{R}^n$, then the sub-system defined by the pair $(\mathbf{A}_{11}, \mathbf{A}_{12})$ is also controllable for all $\mathbf{x} \in \mathbb{R}^n$.

From this framework, the robust LTI sliding mode controller is next developed.

3.3.1 Switching Function

The switching function is defined as follows:

$$\sigma = \mathbf{A}_{12}^T \mathbf{P}\mathbf{x}_1 + \mathbf{x}_2, \ \sigma \in \mathbb{R}^m \quad \textbf{(3-10)}$$

where $\mathbf{P} \in \mathbb{R}^{(n-m)\times(n-m)}$ is a positive definite, symmetric matrix that is to be determined. The objective here is to select a set of Lyapunov functions for the switching function, σ, and unmatched states, $\mathbf{x}_1$, to prove the stability of the controlled system. Therefore, the system disturbances are redefined in terms of σ and $\mathbf{x}_1$. Rearranging the switching function, Eq. (3-10) is given as:

$$\mathbf{x}_2 = \sigma - \mathbf{A}_{12}^T \mathbf{P}\mathbf{x}_1 \quad \textbf{(3-11)}$$

The norm of (3-11) can be expressed:

$$\|\mathbf{x}_2\| = \|\sigma - \mathbf{A}_{12}^T \mathbf{P}\mathbf{x}_1\| \le \|\sigma\| + \|\mathbf{A}_{12}^T \mathbf{P}\| \cdot \|\mathbf{x}_1\| \quad \textbf{(3-12)}$$

Substituting (3-12) into (3-9), the disturbance norms are written as:

$$\|\mathbf{d}_1\| \le \left(\alpha_{11} + \alpha_{12}\|\mathbf{A}_{12}^T \mathbf{P}\|\right)\|\mathbf{x}_1\| + \alpha_{12}\|\sigma\| + \beta_1$$
$$\|\mathbf{d}_2\| \le \left(\alpha_{21} + \alpha_{22}\|\mathbf{A}_{12}^T \mathbf{P}\|\right)\|\mathbf{x}_1\| + \alpha_{22}\|\sigma\| + \gamma\|\mathbf{u}\| + \beta_2 \quad \textbf{(3-13)}$$

Equation (3-13) is expressed in the simplified form:

$$\begin{aligned}\|\mathbf{d}_1\| &\le \bar{\alpha}_{11}\|\mathbf{x}_1\| + \alpha_{12}\|\sigma\| + \beta_1 \\ \|\mathbf{d}_2\| &\le \bar{\alpha}_{21}\|\mathbf{x}_1\| + \alpha_{22}\|\sigma\| + \gamma\|\mathbf{u}\| + \beta_2\end{aligned} \tag{3-14}$$

where $\bar{\alpha}_{11} = \alpha_{11} + \alpha_{12}\left\|\mathbf{A}_{12}^T\mathbf{P}\right\| \ge 0$ and $\bar{\alpha}_{21} = \alpha_{21} + \alpha_{22}\left\|\mathbf{A}_{12}^T\mathbf{P}\right\| \ge 0$.

A candidate Lyapunov function for the unmatched states, $\mathbf{x}_1$, is considered as:

$$V_1 = \mathbf{x}_1^T\mathbf{P}\mathbf{x}_1 \tag{3-15}$$

where $\mathbf{P} \in \mathbb{R}^{(n-m)\times(n-m)}$ is the positive definite, symmetric matrix mentioned earlier. Taking the derivative of the V_1 results in the following:

$$\begin{aligned}\dot{V}_1 &= \dot{\mathbf{x}}_1^T\mathbf{P}\mathbf{x}_1 + \mathbf{x}_1^T\mathbf{P}\dot{\mathbf{x}}_1 \\ &= \left(\mathbf{A}_{11}\mathbf{x}_1 + \mathbf{A}_{12}\mathbf{x}_2 + \mathbf{d}_1\right)^T\mathbf{P}\mathbf{x}_1 + \mathbf{x}_1^T\mathbf{P}\left(\mathbf{A}_{11}\mathbf{x}_1 + \mathbf{A}_{12}\mathbf{x}_2 + \mathbf{d}_1\right) \\ &= \mathbf{x}_1^T\left(\mathbf{A}_{11}^T\mathbf{P} + \mathbf{P}\mathbf{A}_{11}\right)\mathbf{x}_1 + \mathbf{x}_2^T\mathbf{A}_{12}^T\mathbf{P}\mathbf{x}_1 + \mathbf{x}_1^T\mathbf{P}\mathbf{A}_{12}\mathbf{x}_2 + \mathbf{d}_1^T\mathbf{P}\mathbf{x}_1 + \mathbf{x}_1^T\mathbf{P}\mathbf{d}_1\end{aligned} \tag{3-16}$$

Substituting (3-11) into (3-16) yields:

$$\begin{aligned}\dot{V}_1 &= \mathbf{x}_1^T\left(\mathbf{A}_{11}^T\mathbf{P} + \mathbf{P}\mathbf{A}_{11}\right)\mathbf{x}_1 + \left(\sigma - \mathbf{A}_{12}^T\mathbf{P}\mathbf{x}_1\right)^T\mathbf{A}_{12}^T\mathbf{P}\mathbf{x}_1 + \mathbf{x}_1^T\mathbf{P}\mathbf{A}_{12}\left(\sigma - \mathbf{A}_{12}^T\mathbf{P}\mathbf{x}_1\right) + \mathbf{d}_1^T\mathbf{P}\mathbf{x}_1 + \mathbf{x}_1^T\mathbf{P}\mathbf{d}_1 \\ &= \mathbf{x}_1^T\left(\mathbf{A}_{11}^T\mathbf{P} + \mathbf{P}\mathbf{A}_{11} - 2\mathbf{P}\mathbf{A}_{12}\mathbf{A}_{12}^T\mathbf{P}\right)\mathbf{x}_1 + \sigma^T\mathbf{A}_{12}^T\mathbf{P}\mathbf{x}_1 + \mathbf{x}_1^T\mathbf{P}\mathbf{A}_{12}\sigma + \mathbf{d}_1^T\mathbf{P}\mathbf{x}_1 + \mathbf{x}_1^T\mathbf{P}\mathbf{d}_1\end{aligned} \tag{3-17}$$

The Algebraic Riccati Equation (ARE) described earlier is restated here as:

$$\mathbf{A}_{11}^T\mathbf{P} + \mathbf{P}\mathbf{A}_{11} - \mathbf{P}\mathbf{A}_{12}\mathbf{R}^{-1}\mathbf{A}_{12}^T\mathbf{P} + \mathbf{Q} = 0 \tag{3-18}$$

where $\mathbf{Q} \in \mathbb{R}^{(n-m)\times(n-m)}$ is a positive definite symmetric matrix. In order to reduce the complexity of the design, the $\mathbf{R}$ matrix defined in Eq. (3-2) has been assumed to be the identity matrix. Substituting the ARE into the Lyapunov derivative and rearranging the terms results in the following expression:

$$\dot{V}_1 = -\mathbf{x}_1^T\left(\mathbf{Q} + 2\mathbf{P}\mathbf{A}_{12}\mathbf{A}_{12}^T\mathbf{P} - \mathbf{P}\mathbf{A}_{12}\mathbf{R}^{-1}\mathbf{A}_{12}^T\mathbf{P}\right)\mathbf{x}_1 + 2\mathbf{x}_1^T\mathbf{P}\mathbf{A}_{12}\sigma + 2\mathbf{x}_1^T\mathbf{P}\mathbf{d}_1 \tag{3-19}$$

where $\mathbf{Q} + 2\mathbf{P}\mathbf{A}_{12}\mathbf{A}_{12}^T\mathbf{P} - \mathbf{P}\mathbf{A}_{12}\mathbf{R}^{-1}\mathbf{A}_{12}^T\mathbf{P}$ is a positive definite symmetric matrix. Applying a property of the eigenvalues:

Property 1: If $\mathbf{M}$ is a positive definite, square matrix, and $\mathbf{q}$ is a state vector, then the following property exists:

$$\min\left(|\lambda_{\mathbf{M}}|\right)\|\mathbf{q}\|^2 \le \mathbf{q}^T\mathbf{M}\mathbf{q} \le \max\left(|\lambda_{\mathbf{M}}|\right)\|\mathbf{q}\|^2 \tag{3-20}$$

where $\lambda_{\mathbf{M}} = \left\{\lambda_1,...,\lambda_{(n-m)}\right\}$ are the eigenvalues of $\mathbf{M}$.

and taking the norm of (3-19), $\dot{V}_1$ can be expressed as:

$$\begin{aligned}\dot{V}_1 &\le -\min\left(\left|\lambda_{\mathbf{Q}+2\mathbf{P}\mathbf{A}_{12}\mathbf{A}_{12}^T\mathbf{P}-\mathbf{P}\mathbf{A}_{12}\mathbf{R}^{-1}\mathbf{A}_{12}^T\mathbf{P}}\right|\right)\|\mathbf{x}_1\|^2 + 2\|\mathbf{x}_1\|\cdot\|\mathbf{P}\mathbf{A}_{12}\|\cdot\|\sigma\| + 2\|\mathbf{x}_1\|\cdot\|\mathbf{P}\|\cdot\|\mathbf{d}_1\| \\ &\le \left\{-\min\left(\left|\lambda_{\mathbf{Q}+2\mathbf{P}\mathbf{A}_{12}\mathbf{A}_{12}^T\mathbf{P}-\mathbf{P}\mathbf{A}_{12}\mathbf{R}^{-1}\mathbf{A}_{12}^T\mathbf{P}}\right|\right)\|\mathbf{x}_1\| + 2\|\mathbf{P}\mathbf{A}_{12}\|\cdot\|\sigma\| + 2\|\mathbf{P}\|\cdot\|\mathbf{d}_1\|\right\}\|\mathbf{x}_1\|\end{aligned} \tag{3-21}$$

Denoting $\lambda = \min\left(\left|\lambda_{\mathbf{Q}+2\mathbf{P}\mathbf{A}_{12}\mathbf{A}_{12}^T\mathbf{P}-\mathbf{P}\mathbf{A}_{12}\mathbf{R}^{-1}\mathbf{A}_{12}^T\mathbf{P}}\right|\right)$ and $a_{12} = 2\|\mathbf{P}\mathbf{A}_{12}\|$, (3-21) is reduced to the following expression:

$$\dot{V}_1 \le \left\{-\lambda\|\mathbf{x}_1\| + a_{12}\|\sigma\| + 2\|\mathbf{P}\|\cdot\|\mathbf{d}_1\|\right\}\|\mathbf{x}_1\| \tag{3-22}$$

Substituting the unmatched disturbance norm relation (3-14) into (3-22) gives:

$$\dot{V}_1 \le \left\{-\lambda\|\mathbf{x}_1\| + a_{12}\|\sigma\| + 2\|\mathbf{P}\|\left(\bar{\alpha}_{11}\|\mathbf{x}_1\| + \alpha_{12}\|\sigma\| + \beta_1\right)\right\}\|\mathbf{x}_1\| \tag{3-23}$$

Collecting the terms together results in:

$$\dot{V}_1 \le \left\{-\hat{a}_{11}\|\mathbf{x}_1\| + \hat{a}_{12}\|\sigma\| + \hat{\beta}_1\right\}\|\mathbf{x}_1\| \tag{3-24}$$

where $\hat{a}_{11} = \lambda - 2\|\mathbf{P}\|\left(\alpha_{11} + \alpha_{12}\left\|\mathbf{A}_{12}^T\mathbf{P}\right\|\right)$, $\hat{a}_{12} = a_{12} + 2\|\mathbf{P}\|\alpha_{12}$, and $\hat{\beta}_1 = 2\|\mathbf{P}\|\beta_1$. This completes the derivation Lyapunov function of the unmatched states and its derivative. The significance of this Lyapunov function to the stability and robustness of the closed loop system will be discussed in Section 3.3.3.

3.3.2 Reaching Law Design

A candidate Lyapunov function for the switching surface is chosen as follows:

$$V_2 = \|\sigma\| \tag{3-25}$$

Taking the time derivative of (3-25) yields:

$$\dot{V}_2 = \frac{\sigma^T \dot{\sigma}}{\|\sigma\|} = \frac{\sigma^T}{\|\sigma\|}\left(\mathbf{A}_{12}^T \mathbf{P}\dot{\mathbf{x}}_1 + \dot{\mathbf{x}}_2\right) \tag{3-26}$$

Substituting the equations of motion (3-8) and the rearranged switching function (3-11) into (3-26) results in:

$$\begin{aligned}
\dot{V}_2 &= \frac{\sigma^T}{\|\sigma\|}\left(\mathbf{A}_{12}^T \mathbf{P}\left(\mathbf{A}_{11}\mathbf{x}_1 + \mathbf{A}_{12}\mathbf{x}_2 + \mathbf{d}_1\right) + \left(\mathbf{A}_{21}\mathbf{x}_1 + \mathbf{A}_{22}\mathbf{x}_2 + \mathbf{u} + \mathbf{d}_2\right)\right) \\
&= \frac{\sigma^T}{\|\sigma\|}\left(\left(\mathbf{A}_{12}^T \mathbf{P}\mathbf{A}_{11} + \mathbf{A}_{21}\right)\mathbf{x}_1 + \left(\mathbf{A}_{12}^T \mathbf{P}\mathbf{A}_{12} + \mathbf{A}_{22}\right)\mathbf{x}_2 + \mathbf{u} + \mathbf{A}_{12}^T \mathbf{P}\mathbf{d}_1 + \mathbf{d}_2\right) \\
&= \frac{\sigma^T}{\|\sigma\|}\left(\left(\mathbf{A}_{12}^T \mathbf{P}\mathbf{A}_{11} + \mathbf{A}_{21}\right)\mathbf{x}_1 + \left(\mathbf{A}_{12}^T \mathbf{P}\mathbf{A}_{12} + \mathbf{A}_{22}\right)\left(\sigma - \mathbf{A}_{12}^T \mathbf{P}\mathbf{x}_1\right) + \mathbf{u} + \mathbf{A}_{12}^T \mathbf{P}\mathbf{d}_1 + \mathbf{d}_2\right) \\
&= \frac{\sigma^T}{\|\sigma\|}\begin{pmatrix}\left(\mathbf{A}_{21} + \mathbf{A}_{12}^T \mathbf{P}\mathbf{A}_{11} - \mathbf{A}_{12}^T \mathbf{P}\mathbf{A}_{12}\mathbf{A}_{12}^T \mathbf{P} - \mathbf{A}_{22}\mathbf{A}_{12}^T \mathbf{P}\right)\mathbf{x}_1 \\ +\left(\mathbf{A}_{22} + \mathbf{A}_{12}^T \mathbf{P}\mathbf{A}_{12}\right)\sigma + \mathbf{u} + \mathbf{A}_{12}^T \mathbf{P}\mathbf{d}_1 + \mathbf{d}_2\end{pmatrix}
\end{aligned} \tag{3-27}$$

Using the simplified notation given by $\bar{\mathbf{A}}_{21} = \mathbf{A}_{21} + \mathbf{A}_{12}^T \mathbf{P}\mathbf{A}_{11} - \mathbf{A}_{12}^T \mathbf{P}\mathbf{A}_{12}\mathbf{A}_{12}^T \mathbf{P} - \mathbf{A}_{22}\mathbf{A}_{12}^T \mathbf{P}$ and $\bar{\mathbf{A}}_{22} = \mathbf{A}_{22} + \mathbf{A}_{12}^T \mathbf{P}\mathbf{A}_{12}$, the Lyapunov derivative (3-27) can expressed in the following form:

$$\dot{V}_2 = \frac{\sigma^T}{\|\sigma\|}\left(\bar{\mathbf{A}}_{21}\mathbf{x}_1 + \bar{\mathbf{A}}_{22}\sigma + \mathbf{u} + \mathbf{A}_{12}^T \mathbf{P}\mathbf{d}_1 + \mathbf{d}_2\right) \tag{3-28}$$

A control law for the system is proposed as:

$$\mathbf{u} = -\eta\begin{bmatrix}\operatorname{sgn}(\sigma_1) \\ \operatorname{sgn}(\sigma_2) \\ \vdots \\ \operatorname{sgn}(\sigma_m)\end{bmatrix} = -\eta \operatorname{sgn}(\sigma) \tag{3-29}$$

where η is a positive constant. The signum function is defined by:

$$\operatorname{sgn}(q)=\begin{cases}+1 & for \quad q>0\\ 0 & for \quad q=0\\ -1 & for \quad q<0\end{cases} \tag{3-30}$$

where $q\in\mathbb{R}$ is a variable. Substituting (3-29) into (3-28) yields:

$$\dot{V}_2=\frac{\sigma^T}{\|\sigma\|}\left(\bar{\mathbf{A}}_{21}\mathbf{x}_1+\bar{\mathbf{A}}_{22}\sigma-\eta\operatorname{sgn}(\sigma)+\mathbf{A}_{12}^T\mathbf{P}\mathbf{d}_1+\mathbf{d}_2\right) \tag{3-31}$$

Taking the norm of the Lyapunov derivative (3-31) yields:

$$\dot{V}_2\le\left\|\bar{\mathbf{A}}_{21}\right\|\cdot\|\mathbf{x}_1\|+\left\|\bar{\mathbf{A}}_{22}\right\|\cdot\|\sigma\|+\left\|\mathbf{A}_{12}^T\mathbf{P}\right\|\cdot\|\mathbf{d}_1\|+\|\mathbf{d}_2\|-\eta\sum_{i=1}^{m}\frac{|\sigma_i|}{\|\sigma\|} \tag{3-32}$$

Using the relation given by $\sum_{i=1}^{m}|\sigma_i|\ge\|\sigma\|$ and substituting the disturbance norms (3-14), the Lyapunov derivative can be expressed as:

$$\begin{aligned}\dot{V}_2&\le\left\|\bar{\mathbf{A}}_{21}\right\|\cdot\|\mathbf{x}_1\|+\left\|\bar{\mathbf{A}}_{22}\right\|\cdot\|\sigma\|+\left\|\mathbf{A}_{12}^T\mathbf{P}\right\|\cdot\|\mathbf{d}_1\|+\|\mathbf{d}_2\|-\eta\\ &\le\left\|\bar{\mathbf{A}}_{21}\right\|\cdot\|\mathbf{x}_1\|+\left\|\bar{\mathbf{A}}_{22}\right\|\cdot\|\sigma\|+\left\|\mathbf{A}_{12}^T\mathbf{P}\right\|\left[\bar{\alpha}_{11}\|\mathbf{x}_1\|+\alpha_{12}\|\sigma\|+\beta_1\right]\\ &+\bar{\alpha}_{21}\|\mathbf{x}_1\|+\alpha_{22}\|\sigma\|+\gamma\|\mathbf{u}\|+\beta_2-\eta\end{aligned} \tag{3-33}$$

Using the relation for the control input $\|\mathbf{u}\|=\eta\sqrt{m}$ and applying the following notational simplifications:

$$\begin{aligned}\hat{a}_{21}&=\left\|\bar{\mathbf{A}}_{21}\right\|+\bar{\alpha}_{11}\left\|\mathbf{A}_{12}^T\mathbf{P}\right\|+\bar{\alpha}_{21}\\ \hat{a}_{22}&=\left\|\bar{\mathbf{A}}_{22}\right\|+\alpha_{12}\left\|\mathbf{A}_{12}^T\mathbf{P}\right\|+\alpha_{22}\\ \mu&=\eta\left(1-\gamma\sqrt{m}\right)-\left\|\mathbf{A}_{12}^T\mathbf{P}\right\|\beta_1-\beta_2\end{aligned} \tag{3-34}$$

the derivative of the second Lyapunov function (3-33) is expressed as:

$$\dot{V}_2\le\hat{a}_{21}\|\mathbf{x}_1\|+\hat{a}_{22}\|\sigma\|-\mu \tag{3-35}$$

This completes the derivation of the Lyapunov function of the switching function and it derivative.

3.3.3 Stability Bounds

The region of stability for the controlled system is determined by the region satisfying the Lyapunov theorem for local stability. This theorem is stated as follows:

> *Theorem 1*: If, in a ball $\mathbf{B}$, there exists a scalar function $V(\mathbf{x})$ with continuous first partial derivatives such that
>
> - $V(\mathbf{x})$ is positive definite (locally in $\mathbf{B}$)
> - $\dot{V}(\mathbf{x})$ is negative semi-definite (locally in $\mathbf{B}$)
>
> then the equilibrium point 0 is stable. If, actually, the derivative $\dot{V}(\mathbf{x})$ is locally negative definite in $\mathbf{B}$, then the stability is asymptotic [43].

The two Lyapunov functions (3-15) and (3-25) satisfy the first requirement of *Theorem 1*. The derivative of the first Lyapunov function is given as follows:

$$\dot{V}_1 \leq \left\{-\hat{a}_{11}\|\mathbf{x}_1\| + \hat{a}_{12}\|\sigma\| + \hat{\beta}_1\right\}\|\mathbf{x}_1\| \tag{3-36}$$

Since the norm of the unmatched states, $\|\mathbf{x}_1\|$, is always positive, the derivative of the Lyapunov function (3-36) will be negative, semi-definite, given the following condition:

$$-\hat{a}_{11}\|\mathbf{x}_1\| + \hat{a}_{12}\|\sigma\| + \hat{\beta}_1 < 0 \tag{3-37}$$

The derivative of the second Lyapunov function is given by the following

$$\dot{V}_2 \leq \hat{a}_{21}\|\mathbf{x}_1\| + \hat{a}_{22}\|\sigma\| - \mu \tag{3-38}$$

In order to satisfy the second requirement of Theorem 1, the following condition can be applied to (3-38):

$$\hat{a}_{21}\|\mathbf{x}_1\| + \hat{a}_{22}\|\sigma\| - \mu < 0 \tag{3-39}$$

The first boundary on the stability is determined by substituting (3-37) into (3-39) as follows:

$$\|\sigma\| < \frac{\mu\hat{a}_{11} - \hat{a}_{21}\hat{\beta}_1}{\hat{a}_{22}\hat{a}_{11} + \hat{a}_{12}\hat{a}_{21}} \tag{3-40}$$

Therefore, the outer boundary on the region of stability is defined as:

$$\Sigma = \left\{ (x_1, \sigma) \left| \|\sigma\| < \frac{\mu\hat{a}_{11} - \hat{a}_{21}\hat{\beta}_1}{\hat{a}_{22}\hat{a}_{11} + \hat{a}_{12}\hat{a}_{21}}, \hat{a}_{21}\|\mathbf{x}_1\| + \hat{a}_{22}\|\sigma\| < \mu \right. \right\} \tag{3-41}$$

With the outer boundary of the region of stability defined, the inner boundary can now be developed. Upon reaching the sliding manifold, $\sigma = 0$, the derivative of the first Lyapunov function (3-36), can be simplified to the following relationship:

$$\dot{V}_1 \leq \left\{ -\hat{a}_{11}\|\mathbf{x}_1\| + \hat{\beta}_1 \right\} \|\mathbf{x}_1\| \tag{3-42}$$

The lower boundary on the region of stability is defined as the boundary of the interior region of instability. Specifically, the boundary layer occurs when $V_1 > 0$; this implies:

$$\|\mathbf{x}_1\| < \frac{\hat{\beta}_1}{\hat{a}_{11}} \tag{3-43}$$

The inner boundary of the stability region is defined as:

$$\Gamma = \left\{ (x_1, 0) \left| \|x_1\| < \frac{\hat{\beta}_1}{\hat{a}_{11}} \right. \right\} \tag{3-44}$$

Therefore, any trajectory starting inside the region defined by Σ in Eq. (3-41) will asymptotically converge to the region Γ and remain there for all future time. This behavior is guaranteed by *Theorem 1*, thus proving the stability and robustness of the system.

3.4 Robust State Dependent Time Varying Sliding Mode Control

In order to further improve the tracking performance of the controller, the more generalized robust, state dependent, time varying (SDTV) sliding mode controller is derived from the LTI SMC law developed in the previous section. The system model is defined as follows:

$$\dot{\mathbf{x}}(t) = \mathbf{A}(\mathbf{x},t)\mathbf{x}(t) + \mathbf{B}(\mathbf{x},t)\mathbf{u}(t) + \mathbf{d}(\mathbf{x},t) \tag{3-45}$$

where $\mathbf{x}(t) \in \mathbb{R}^n$ is the state vector; $\mathbf{A}(\mathbf{x},t) \in \mathbb{R}^{n \times n}$ is the state matrix; $\mathbf{B}(\mathbf{x},t) \in \mathbb{R}^{n \times m}$ is the control matrix; $\mathbf{u}(\mathbf{x},t) \in \mathbb{R}^m$ is the control input vector; and, $\mathbf{d}(\mathbf{x},t) \in \mathbb{R}^n$ is the disturbance vector. For the derivation presented here, the system is assumed to be in the more specific form:

$$\begin{bmatrix} \dot{\mathbf{x}}_1 \\ \dot{\mathbf{x}}_2 \end{bmatrix} = \begin{bmatrix} \mathbf{A}_{11}(\mathbf{x},t) & \mathbf{A}_{12}(\mathbf{x},t) \\ \mathbf{A}_{21}(\mathbf{x},t) & \mathbf{A}_{22}(\mathbf{x},t) \end{bmatrix} \begin{bmatrix} \mathbf{x}_1 \\ \mathbf{x}_2 \end{bmatrix} + \begin{bmatrix} 0 \\ \mathbf{I} \end{bmatrix} \mathbf{u} + \begin{bmatrix} \mathbf{d}_1(\mathbf{x},t) \\ \mathbf{d}_2(\mathbf{x},t) \end{bmatrix} \tag{3-46}$$

where $\mathbf{x}_1 \in \mathbb{R}^{n-m}$, $\mathbf{x}_2 \in \mathbb{R}^m$ are the matched and unmatched states, respectively; $\mathbf{A}_{11} \in \mathbb{R}^{(n-m)\times(n-m)}$, $\mathbf{A}_{12} \in \mathbb{R}^{(n-m)\times m}$, $\mathbf{A}_{21} \in \mathbb{R}^{m\times(n-m)}$, $\mathbf{A}_{22} \in \mathbb{R}^{m\times m}$ are the subsystem state matrices; $\mathbf{I} \in \mathbb{R}^{m\times m}$ is the identity matrix; and, $\mathbf{d}_1 \in \mathbb{R}^{(n-m)}$, $\mathbf{d}_2 \in \mathbb{R}^m$ are the matched and unmatched disturbances, respectively. For simplification, the $(\mathbf{x},t)$ notation representing the state and time dependence is removed.

The following assumptions concerning the system are made:

Assumption 1: The pair $(\mathbf{A},\mathbf{B})$ is controllable for all $\mathbf{x} \in \mathbb{R}^n$ and $t \in \mathbb{R}^+$.

Assumption 2: The matched and unmatched disturbances, $\mathbf{d}_1$ and $\mathbf{d}_2$ are bounded as:

$$\begin{aligned} \|\mathbf{d}_1\| &\le \alpha_{11}\|\mathbf{x}_1\| + \alpha_{12}\|\mathbf{x}_2\| + \beta_1 \\ \|\mathbf{d}_2\| &\le \alpha_{21}\|\mathbf{x}_1\| + \alpha_{22}\|\mathbf{x}_2\| + \gamma\|\mathbf{u}\| + \beta_2 \end{aligned} \tag{3-47}$$

where $\alpha_{11}, \alpha_{12}, \beta_1, \alpha_{21}, \alpha_{22}, \gamma, \beta_2$ are nonnegative constants and $\|\bullet\|$ represents the Euclidean norm of a vector or matrix.

Corollary 1: Since the pair $(\mathbf{A}, \mathbf{B})$ is controllable for all $\mathbf{x} \in \mathbb{R}^n$ and $t \in \mathbb{R}^+$, then the sub-system defined by the pair $(\mathbf{A}_{11}, \mathbf{A}_{12})$ is also controllable for all $\mathbf{x} \in \mathbb{R}^n$ and $t \in \mathbb{R}^+$.

3.4.1 Switching Function

The switching function is given as:

$$\sigma = \mathbf{A}_{12}^T \mathbf{P}' \mathbf{x}_1 + \mathbf{x}_2 \in \mathbb{R}^m \tag{3-48}$$

where $\mathbf{P}'(\mathbf{x}, t) \in \mathbb{R}^{(n-m)\times(n-m)}$ is a positive definite, symmetric matrix. Since the desired result is to have the switching function, σ, and the unmatched states, $\mathbf{x}_1$, converge to zero, it will be useful to rearrange the switching function (3-48) into the following form:

$$\mathbf{x}_2 = \sigma - \mathbf{A}_{12}^T \mathbf{P}' \mathbf{x}_1 \tag{3-49}$$

Using the same method used in Section 3.3.1, the disturbance forces (3-47) can be expressed as follows:

$$\begin{aligned} \|\mathbf{d}_1\| &\le \bar{\alpha}_{11} \|\mathbf{x}_1\| + \alpha_{12} \|\sigma\| + \beta_1 \\ \|\mathbf{d}_2\| &\le \bar{\alpha}_{21} \|\mathbf{x}_1\| + \alpha_{22} \|\sigma\| + \gamma \|\mathbf{u}\| + \beta_2 \end{aligned} \tag{3-50}$$

where $\bar{\alpha}_{11} = \alpha_{11} + \alpha_{12} \|\mathbf{A}_{12}^T \mathbf{P}'\| \ge 0$ and $\bar{\alpha}_{21} = \alpha_{21} + \alpha_{22} \|\mathbf{A}_{12}^T \mathbf{P}'\| \ge 0$.

A candidate Lyapunov function for the unmatched states is assumed as:

$$V_1 = \mathbf{x}_1^T \mathbf{P}' \mathbf{x}_1 \tag{3-51}$$

Taking the time derivative of the Lyapunov function yields:

$$\begin{aligned}\dot{V}_1 &= \mathbf{x}_1^T\dot{\mathbf{P}}'\mathbf{x}_1 + \dot{\mathbf{x}}_1^T\mathbf{P}'\mathbf{x}_1 + \mathbf{x}_1^T\mathbf{P}'\dot{\mathbf{x}}_1 \\ &= \mathbf{x}_1^T\dot{\mathbf{P}}'\mathbf{x}_1 + \left(\mathbf{A}_{11}\mathbf{x}_1 + \mathbf{A}_{12}\mathbf{x}_2 + \mathbf{d}_1\right)^T\mathbf{P}'\mathbf{x}_1 + \mathbf{x}_1^T\mathbf{P}'\left(\mathbf{A}_{11}\mathbf{x}_1 + \mathbf{A}_{12}\mathbf{x}_2 + \mathbf{d}_1\right) \\ &= \mathbf{x}_1^T\left(\dot{\mathbf{P}}' + \mathbf{A}_{11}^T\mathbf{P}' + \mathbf{P}'\mathbf{A}_{11}\right)\mathbf{x}_1 + \mathbf{x}_2^T\mathbf{A}_{12}^T\mathbf{P}'\mathbf{x}_1 + \mathbf{x}_1^T\mathbf{P}'\mathbf{A}_{12}\mathbf{x}_2 + \mathbf{d}_1^T\mathbf{P}'\mathbf{x}_1 + \mathbf{x}_1^T\mathbf{P}'\mathbf{d}_1\end{aligned} \tag{3-52}$$

Substituting the rearranged switching function (3-49) into (3-52) yields:

$$\begin{aligned}\dot{V}_1 &= \mathbf{x}_1^T\left(\dot{\mathbf{P}}' + \mathbf{A}_{11}^T\mathbf{P}' + \mathbf{P}'\mathbf{A}_{11}\right)\mathbf{x}_1 + \left(\sigma - \mathbf{A}_{12}^T\mathbf{P}'\mathbf{x}_1\right)^T\mathbf{A}_{12}^T\mathbf{P}'\mathbf{x}_1 \\ &\quad + \mathbf{x}_1^T\mathbf{P}'\mathbf{A}_{12}\left(\sigma - \mathbf{A}_{12}^T\mathbf{P}'\mathbf{x}_1\right) + \mathbf{d}_1^T\mathbf{P}'\mathbf{x}_1 + \mathbf{x}_1^T\mathbf{P}'\mathbf{d}_1 \\ &= \mathbf{x}_1^T\left(\dot{\mathbf{P}}' + \mathbf{A}_{11}^T\mathbf{P}' + \mathbf{P}'\mathbf{A}_{11} - 2\mathbf{P}'\mathbf{A}_{12}\mathbf{A}_{12}^T\mathbf{P}'\right)\mathbf{x}_1 \\ &\quad + \sigma^T\mathbf{A}_{12}^T\mathbf{P}'\mathbf{x}_1 + \mathbf{x}_1^T\mathbf{P}'\mathbf{A}_{12}\sigma + \mathbf{d}_1^T\mathbf{P}'\mathbf{x}_1 + \mathbf{x}_1^T\mathbf{P}'\mathbf{d}_1\end{aligned} \tag{3-53}$$

The state dependent differential ricatti equation (SDDRE), described in Section 3.2.2, is expressed in the current framework as:

$$-\dot{\mathbf{P}}' + \mathbf{P}'\mathbf{A}_{11} + \mathbf{A}_{11}^T\mathbf{P}' - \mathbf{P}'\mathbf{A}_{12}\mathbf{R}^{-1}\mathbf{A}_{12}^T\mathbf{P}' + \mathbf{Q} = 0 \tag{3-54}$$

where $\mathbf{Q} \in \mathbb{R}^{(n-m)\times(n-m)}$ is a positive definite symmetric matrix, again the $\mathbf{R}$ matrix defined in Eq. (3-2) has been assumed to be the identity matrix. Substituting the SDDRE into (3-54) yields:

$$\dot{V}_1 = -\mathbf{x}_1^T\left(\mathbf{Q} + 2\mathbf{P}'\mathbf{A}_{12}\mathbf{A}_{12}^T\mathbf{P}' - \mathbf{P}'\mathbf{A}_{12}\mathbf{R}^{-1}\mathbf{A}_{12}^T\mathbf{P}' - 2\dot{\mathbf{P}}'\right)\mathbf{x}_1 + 2\mathbf{x}_1^T\mathbf{P}'\mathbf{A}_{12}\sigma + 2\mathbf{x}_1^T\mathbf{P}'\mathbf{d}_1 \tag{3-55}$$

Taking the norm of (3-55) and applying Property 1 from Section 3.3.1, the following relation for $\dot{V}_1$ is achieved:

$$\dot{V}_1 \le \left\{-\lambda\|\mathbf{x}_1\| + a_{12}\|\sigma\| + 2\|\mathbf{P}'\|\cdot\|\mathbf{d}_1\|\right\}\|\mathbf{x}_1\| \tag{3-56}$$

where $\lambda = \min\left(\left|\lambda_{\mathbf{Q}+2\mathbf{P}'\mathbf{A}_{12}\mathbf{A}_{12}^T\mathbf{P}'-\mathbf{P}'\mathbf{A}_{12}\mathbf{R}^{-1}\mathbf{A}_{12}^T\mathbf{P}'-2\dot{\mathbf{P}}'}\right|\right)$ and $a_{12} = 2\|\mathbf{P}'\mathbf{A}_{12}\|$. In order to guarantee that the eigenvalue, λ, is positive and *Property 1* holds, the following constraint is applied:

$$\mathbf{Q} + 2\mathbf{P}'\mathbf{A}_{12}\mathbf{A}_{12}^T\mathbf{P}' - \mathbf{P}'\mathbf{A}_{12}\mathbf{R}^{-1}\mathbf{A}_{12}^T\mathbf{P}' - 2\dot{\mathbf{P}}' > 0 \qquad \forall t \in \mathbb{R}^+ \tag{3-57}$$

Substituting the disturbance terms (3-50) into (3-56) gives:

$$\dot{V}_1 \le \left\{-\lambda\|\mathbf{x}_1\| + a_{12}\|\sigma\| + 2\|\mathbf{P}'\|\left[\left(\alpha_{11} + \alpha_{12}\left\|\mathbf{A}_{12}^T\mathbf{P}'\right\|\right)\|\mathbf{x}_1\| + \alpha_{12}\|\sigma\| + \beta_1\right]\right\}\|\mathbf{x}_1\| \tag{3-58}$$

Collecting the terms together, (3-58) can be simplified into the following expression:

$$\dot{V}_1 \le \left\{-\hat{a}_{11}\|\mathbf{x}_1\| + \hat{a}_{12}\|\sigma\| + \hat{\beta}_1\right\}\|\mathbf{x}_1\| \tag{3-59}$$

where $\hat{a}_{11} = \lambda - 2\|\mathbf{P}'\|\left(\alpha_{11} + \alpha_{12}\left\|\mathbf{A}_{12}^T\mathbf{P}'\right\|\right)$, $\hat{a}_{12} = a_{12} + 2\|\mathbf{P}'\|\alpha_{12}$, and $\hat{\beta}_1 = 2\|\mathbf{P}'\|\beta_1$.

3.4.2 Reaching Law Design

A candidate Lyapunov function for the switching surface is then chosen as follows:

$$V_2 = \|\sigma\| \tag{3-60}$$

Taking the derivative of the second Lyapunov function (3-60) yields:

$$\dot{V}_2 = \frac{\sigma^T\dot{\sigma}}{\|\sigma\|} = \frac{\sigma^T}{\|\sigma\|}\left(\dot{\mathbf{A}}_{12}^T\mathbf{P}'\mathbf{x}_1 + \mathbf{A}_{12}^T\dot{\mathbf{P}}'\mathbf{x}_1 + \mathbf{A}_{12}^T\mathbf{P}'\dot{\mathbf{x}}_1 + \dot{\mathbf{x}}_2\right) \tag{3-61}$$

Substituting the equations of motion (3-46) and the rearranged switching function (3-49) into (3-61) results in:

$$\begin{aligned}
\dot{V}_2 &= \frac{\sigma^T}{\|\sigma\|}\begin{pmatrix}\dot{\mathbf{A}}_{12}^T\mathbf{P}'\mathbf{x}_1 + \mathbf{A}_{12}^T\dot{\mathbf{P}}'\mathbf{x}_1 + \mathbf{A}_{12}^T\mathbf{P}'\left(\mathbf{A}_{11}\mathbf{x}_1 + \mathbf{A}_{12}\mathbf{x}_2 + \mathbf{d}_1\right)\\ +\left(\mathbf{A}_{21}\mathbf{x}_1 + \mathbf{A}_{22}\mathbf{x}_2 + \mathbf{u} + \mathbf{d}_2\right)\end{pmatrix}\\
&= \frac{\sigma^T}{\|\sigma\|}\begin{pmatrix}\left(\dot{\mathbf{A}}_{12}^T\mathbf{P}' + \mathbf{A}_{12}^T\dot{\mathbf{P}}' + \mathbf{A}_{12}^T\mathbf{P}'\mathbf{A}_{11} + \mathbf{A}_{21}\right)\mathbf{x}_1\\ +\left(\mathbf{A}_{12}^T\mathbf{P}'\mathbf{A}_{12} + \mathbf{A}_{22}\right)\mathbf{x}_2 + \mathbf{u} + \mathbf{A}_{12}^T\mathbf{P}'\mathbf{d}_1 + \mathbf{d}_2\end{pmatrix}\\
&= \frac{\sigma^T}{\|\sigma\|}\begin{pmatrix}\left(\dot{\mathbf{A}}_{12}^T\mathbf{P}' + \mathbf{A}_{12}^T\dot{\mathbf{P}}' + \mathbf{A}_{12}^T\mathbf{P}'\mathbf{A}_{11} + \mathbf{A}_{21}\right)\mathbf{x}_1\\ +\left(\mathbf{A}_{12}^T\mathbf{P}'\mathbf{A}_{12} + \mathbf{A}_{22}\right)\left(\sigma - \mathbf{A}_{12}^T\mathbf{P}'\mathbf{x}_1\right) + \mathbf{u} + \mathbf{A}_{12}^T\mathbf{P}'\mathbf{d}_1 + \mathbf{d}_2\end{pmatrix}\\
&= \frac{\sigma^T}{\|\sigma\|}\begin{pmatrix}\left(\dot{\mathbf{A}}_{12}^T\mathbf{P}' + \mathbf{A}_{12}^T\dot{\mathbf{P}}' + \mathbf{A}_{21} + \mathbf{A}_{12}^T\mathbf{P}'\mathbf{A}_{11} - \mathbf{A}_{12}^T\mathbf{P}'\mathbf{A}_{12}\mathbf{A}_{12}^T\mathbf{P}' - \mathbf{A}_{22}\mathbf{A}_{12}^T\mathbf{P}'\right)\mathbf{x}_1\\ +\left(\mathbf{A}_{22} + \mathbf{A}_{12}^T\mathbf{P}'\mathbf{A}_{12}\right)\sigma + \mathbf{u} + \mathbf{A}_{12}^T\mathbf{P}'\mathbf{d}_1 + \mathbf{d}_2\end{pmatrix}
\end{aligned} \tag{3-62}$$

Using the following simplified notation:

$$\begin{aligned}\bar{\mathbf{A}}_{21} &= \mathbf{A}_{21} + \dot{\mathbf{A}}_{12}^T\mathbf{P}' + \mathbf{A}_{12}^T\dot{\mathbf{P}}' + \mathbf{A}_{12}^T\mathbf{P}'\mathbf{A}_{11} - \mathbf{A}_{12}^T\mathbf{P}'\mathbf{A}_{12}\mathbf{A}_{12}^T\mathbf{P}' - \mathbf{A}_{22}\mathbf{A}_{12}^T\mathbf{P}' \\ \bar{\mathbf{A}}_{22} &= \mathbf{A}_{22} + \mathbf{A}_{12}^T\mathbf{P}'\mathbf{A}_{12}\end{aligned} \tag{3-63}$$

the Lyapunov derivative function is expressed in the following form:

$$\dot{V}_2 = \frac{\sigma^T}{\|\sigma\|}\left(\bar{\mathbf{A}}_{21}\mathbf{x}_1 + \bar{\mathbf{A}}_{22}\sigma + \mathbf{u} + \mathbf{A}_{12}^T\mathbf{P}'\mathbf{d}_1 + \mathbf{d}_2\right) \tag{3-64}$$

The control law (3-29) proposed in Section 3.3.2, is also applied to the time-variant, state-dependent system. The control law is restated here as:

$$\mathbf{u} = -\eta\,\mathrm{sgn}(\sigma) \tag{3-65}$$

Substituting the controller into (3-65) yields:

$$\dot{V}_2 = \frac{\sigma^T}{\|\sigma\|}\left(\bar{\mathbf{A}}_{21}\mathbf{x}_1 + \bar{\mathbf{A}}_{22}\sigma - \eta\,\mathrm{sgn}(\sigma) + \mathbf{A}_{12}^T\mathbf{P}'\mathbf{d}_1 + \mathbf{d}_2\right) \tag{3-66}$$

Taking the norm of the Lyapunov function derivative (3-66) as follows:

$$\dot{V}_2 \le \left\|\bar{\mathbf{A}}_{21}\right\|\cdot\|\mathbf{x}_1\| + \left\|\bar{\mathbf{A}}_{22}\right\|\cdot\|\sigma\| + \left\|\mathbf{A}_{12}^T\mathbf{P}'\right\|\cdot\|\mathbf{d}_1\| + \|\mathbf{d}_2\| - \eta\sum_{i=1}^{m}\frac{|\sigma_i|}{\|\sigma\|} \tag{3-67}$$

Using the relation given by $\sum_{i=1}^{m}|\sigma_i| \ge \|\sigma\|$ and substituting the disturbance norms (3-50), the Lyapunov derivative (3-67) can be expressed as:

$$\begin{aligned}\dot{V}_2 &\le \left\|\bar{\mathbf{A}}_{21}\right\|\cdot\|\mathbf{x}_1\| + \left\|\bar{\mathbf{A}}_{22}\right\|\cdot\|\sigma\| + \left\|\mathbf{A}_{12}^T\mathbf{P}'\right\|\cdot\|\mathbf{d}_1\| + \|\mathbf{d}_2\| - \eta \\ &\le \left\|\bar{\mathbf{A}}_{21}\right\|\cdot\|\mathbf{x}_1\| + \left\|\bar{\mathbf{A}}_{22}\right\|\cdot\|\sigma\| + \left\|\mathbf{A}_{12}^T\mathbf{P}'\right\|\left[\bar{\alpha}_{11}\|\mathbf{x}_1\| + \alpha_{12}\|\sigma\| + \beta_1\right] \\ &\quad + \bar{\alpha}_{21}\|\mathbf{x}_1\| + \alpha_{22}\|\sigma\| + \gamma\|\mathbf{u}\| + \beta_2 - \eta\end{aligned} \tag{3-68}$$

Substituting the relation for the control input, $\|\mathbf{u}\| = \eta\sqrt{m}$, and applying the following notational simplifications:

$$\begin{aligned}\hat{a}_{21} &= \left\|\bar{\mathbf{A}}_{21}\right\| + \bar{\alpha}_{11}\left\|\mathbf{A}_{12}^{T}\mathbf{P}'\right\| + \bar{\alpha}_{21} \\ \hat{a}_{22} &= \left\|\bar{\mathbf{A}}_{22}\right\| + \alpha_{12}\left\|\mathbf{A}_{12}^{T}\mathbf{P}'\right\| + \alpha_{22} \\ \mu &= \eta\left(1-\gamma\sqrt{m}\right) - \left\|\mathbf{A}_{12}^{T}\mathbf{P}'\right\|\beta_1 - \beta_2\end{aligned} \tag{3-69}$$

The derivative of the second Lyapunov function is expressed as:

$$\dot{V}_2 \le \hat{a}_{21}\left\|\mathbf{x}_1\right\| + \hat{a}_{22}\left\|\sigma\right\| - \mu \tag{3-70}$$

With the second Lyapunov function, the stability bounds on the system can be determined.

3.4.3 Stability Bounds

The region of stability for the state-dependent, time-varying controller is obtained using the same method as discussed in Section 3.3.3 for the LTI controller. The outer and inner boundaries on the region of stability are given by:

$$\Sigma = \left\{ (x_1, \sigma) \left| \left\|\sigma\right\| < \frac{\mu\hat{a}_{11} - \hat{a}_{21}\hat{\beta}_1}{\hat{a}_{22}\hat{a}_{11} + \hat{a}_{12}\hat{a}_{21}}, \hat{a}_{21}\left\|\mathbf{x}_1\right\| + \hat{a}_{22}\left\|\sigma\right\| < \mu \right. \right\} \tag{3-71}$$

$$\Gamma = \left\{ (x_1, 0) \left| \left\|x_1\right\| < \frac{\hat{\beta}_1}{\hat{a}_{11}} \right. \right\} \tag{3-72}$$

respectively. Again, any trajectory starting within Σ will converge asymptotically towards Γ, and remain for all future time. It is important to note, however, that both Σ and Γ are now time dependent regions.

3.5 Relay Control

In the design of any control law, particularly for space applications, a major consideration is always on the reduction of fuel consumption. For the robust LTI and SDTV sliding mode controllers presented above, the switching control law:

$$\mathbf{u} = -\eta\,\mathrm{sgn}(\sigma) \tag{3-73}$$

is subject to the undesirable effect known as chattering. In order to counteract the chattering effect, the more effective relay controller is introduced. The controller is expressed as follows:

$$\mathbf{u} = \begin{cases} -\eta \operatorname{sgn}(\sigma_i) & for \quad |\sigma_i| > \delta \\ 0 & for \quad |\sigma_i| \le \delta \end{cases}, \quad i = 1...m \tag{3-74}$$

where δ is a positive constant. The relay controller derives its name from the similarity to a physical relay which experiences a momentary dead zone while being switched between states [26]. When the switching function is outside of the dead zone, $|\sigma| > \delta$, the relay control law (3-74) is identical to the switching controller (3-73) and it achieves improved performance by removing control action around the sliding manifold, which eliminates the chattering effect. Furthermore, since any control action while the system is within the interior Γ region has no guaranteed effect on the system behavior, eliminating the control input in the region will conserve fuel that would otherwise be wasted.

3.5.1 Modified Boundary Conditions

With the relay controller, it is necessary to redevelop the boundaries on the systems stability. Three regions are provided that determine the behavior of the system. The first region defining the stability of the system is defined by:

$$\Sigma = \left\{ (x_1, \sigma) \middle| \delta\sqrt{m} < \|\sigma\| < \frac{\mu\hat{a}_{11} - \hat{a}_{21}\hat{\beta}_1}{\hat{a}_{22}\hat{a}_{11} + \hat{a}_{12}\hat{a}_{21}}, \hat{a}_{21}\|\mathbf{x}_1\| + \hat{a}_{22}\|\sigma\| < \mu \right\} \tag{3-75}$$

which shows that the norm switching function will converge asymptotically towards δ. Upon reaching this point, the systems performance is governed by the derivation of the second Lyapunov function (3-36). The second region is given as:

$$\Delta = \left\{ (x_1, \sigma) \middle| \frac{\mu - \hat{a}_{22}\delta\sqrt{m}}{\hat{a}_{21}} > \|x_1\| > \frac{\hat{a}_{12}}{\hat{a}_{11}}\delta\sqrt{m} + \frac{\hat{\beta}_1}{\hat{a}_{11}}, \|\sigma\| < \delta\sqrt{m} \right\} \tag{3-76}$$

where the norm of the switching function is bounded and the unmatched states, $\|\mathbf{x}_1\|$, will converge asymptotically towards zero. The final, unstable interior region is given by the following expression:

$$\Gamma = \left\{ (x_1, \sigma) \middle| \left(\|x_1\| < \frac{\hat{a}_{12}}{\hat{a}_{11}} \delta\sqrt{m} + \frac{\hat{\beta}_1}{\hat{a}_{11}} \right) \bigcap \left(\|\sigma\| < \delta\sqrt{m} \right) \right\} \tag{3-77}$$

Therefore, any trajectory starting in Σ (3-75) converges asymptotically towards either Δ (3-76) or Γ (3-77). Any trajectory entering or starting in Δ (3-76) then converges asymptotically to Γ (3-77). Thus, the relay controller is proven to be stable by Lyapunov stability theory, i.e. *Theorem 1*. The regions of stability can be more easily visualized in Figure 3.3.

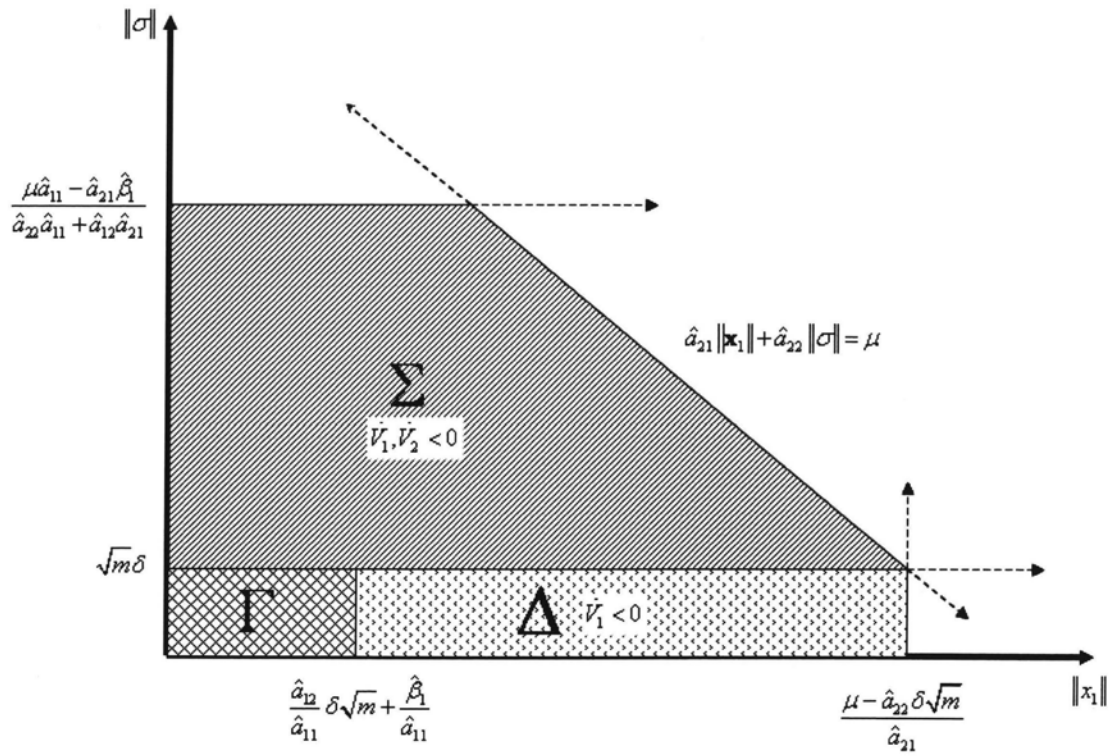

Figure 3.3: Robust stability map for the relay sliding mode controller

3.6 Conclusions

From the analysis presented in this Chapter, it has been successfully proven that both the conventional switching and relay laws can provide robust stability to LTI and state-dependent, time-varying systems in the presence of both matched and unmatched disturbance forces. The tuning and hence performance of the controllers are dependent on the parameters $\mathbf{Q}$, which define the behavior of the sliding manifold, and η, which affects the reaching operation of the controller. Furthermore, the relay control law is additionally dependent on the width of the dead zone, δ, surrounding the sliding manifold. It is also apparent that the control output has been developed in the form of bang-bang style actuation, allowing for its application to typical thruster hardware on satellite systems. With the derivation of the new sliding mode control laws and their associated stability proofs, presented in this chapter, it is now possible to apply them to the underactuated satellite formation flying system.

Chapter 4
Numerical Simulations

In this chapter, the proposed robust relay controllers developed in Chapter 3 are applied to the underactuated satellite formation system. The primary concern in the design of the controller is to maintain the projected formation. In order to ensure this requirement, the integral augmented Hill's equation and 2^{nd} order approximation state space models developed in Section 2.2 are employed. Using the augmented system models, the LTI and SDTV relay controllers, proposed in Chapter 3, are applied to the augmented Hill and 2^{nd} order models, respectively. In order to validate the control laws on the underactuated formation flying system, it is necessary to perform numerical simulations. The numerical simulations are developed through the SIMULINK® modeling environment in the MATLAB® programming system. The simulations are propagated through the use of a variable-step fourth order Runge-Kutta ordinary differential numerical integrator [49].

4.1 Controller Design

The performance of the proposed controllers is determined by three parameters, the sliding manifold weighting matrix $\mathbf{Q}$, the switching coefficient η, and the dead zone width δ. In order to simplify the analysis, the weighting matrix is redefined as:

$$\mathbf{Q} = q\mathbf{I}_{6\times 6} \tag{4-1}$$

where q is a positive scalar and $\mathbf{I}_{6\times 6}$ is a 6×6 identity matrix. Thus, the choice of the weighting matrix is reduced to the selection of the scalar q. In addition, the control weighting matrix has been chosen as $\mathbf{R} = \frac{1}{2}\mathbf{I}_{2\times 2}$. Upon substitution of the control weighting matrix, eigenvalues in the robustness proof reduce to the eigenvalues of $\mathbf{Q}$. Since the

augmented state space models are already in the specific state space form (3-8), the relay control laws for the underactuated satellite formation system is given as follows:

$$u_y = \begin{cases} -\eta \operatorname{sgn}(\sigma_y) & for \quad |\sigma_y| > \delta \\ 0 & for \quad |\sigma_y| \le \delta \end{cases} \tag{4-2}$$

$$u_z = \begin{cases} -\eta \operatorname{sgn}(\sigma_z) & for \quad |\sigma_z| > \delta \\ 0 & for \quad |\sigma_z| \le \delta \end{cases} \tag{4-3}$$

where the sliding manifolds are defined as follows:

$$\begin{aligned} \sigma &= \mathbf{A}_{12}^T \mathbf{P}(q) \mathbf{x}_1 + \mathbf{x}_2 \\ \begin{bmatrix} \sigma_y \\ \sigma_z \end{bmatrix} &= \mathbf{A}_{12}^T \mathbf{P}(q) [y_s \quad z_s \quad x \quad y \quad z \quad \dot{x}]^T + \begin{bmatrix} \dot{y} \\ \dot{z} \end{bmatrix} \end{aligned} \tag{4-4}$$

and $\mathbf{P}$ is the solution of the Riccati equation (3-4).

4.2 Simulation Model

The particular scenario considered here consists of formation operating in a near circular, sun-synchronous, low Earth orbit (LEO) with an altitude of 500 km. In the simulation, the system model is defined by Eq. (2-23), (2-24), and (2-25) for the relative motion between the leader and follower satellites, and by Eq. (2-1) and (2-2) for the motion of the leader satellite in orbit about the Earth. In order to maintain consistency throughout the analysis, all simulations use the parameters given in Table 4.1, unless explicitly stated otherwise. The dominant force acting on the formation is the differential J_2 force, see Section 2.4.1. Figure 4.1 shows the disturbance responses over the course of five orbits while the system follower satellite is in the projected formation.

In the case of the state dependent, time varying sliding mode controller, the solution of the realizable differential Riccati equation is evaluated numerically. The matrix $\mathbf{P}$ in the case of the SDTV controller is initialized to the solution of the simpler algebraic Riccati equation. With the formation configuration and parameters defined, it is now possible to establish the controllers' stability bounds.

Table 4.1: Simulation parameters for the formation tests

Parameter	Value
System	
Gravitational Parameter of Earth, μ	$398600\,\mathrm{km}^3/\mathrm{s}^2$
Radius of the Earth, R_E	6378 km
Semi-Major Axis of Leader Satellite, a	6878 km
Eccentricity of Leader Satellite, e	1×10^{-3}
Inclination of Leader Satellite, i	97.38°
Ascending Node of Leader Satellite, Ω	0.0°
Periapsis of Leader Satellite, ω	0.0°
Desired Projected Formation Radius, r_d	0.50 km
Formation Phase, φ	45°
Sliding Mode Controller	
Manifold Tuning Parameter, q	1×10^{-3}
Switching Coefficient, η	1
Dead Zone Boundary, δ	1

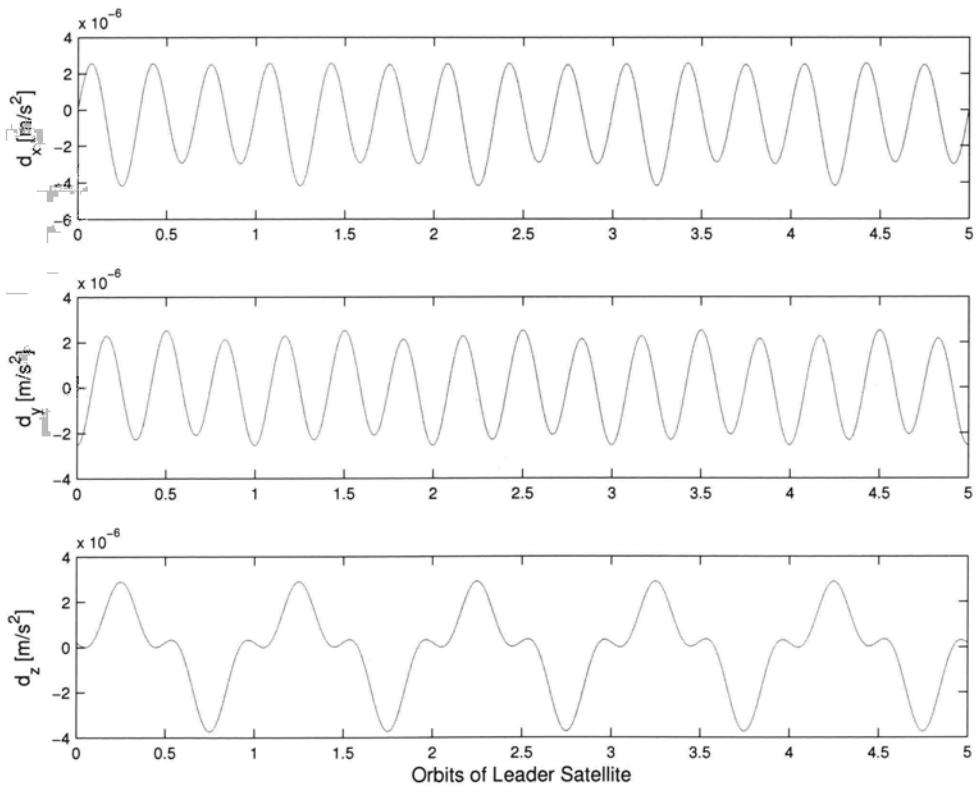

Figure 4.1: External disturbance acting on the follower satellite

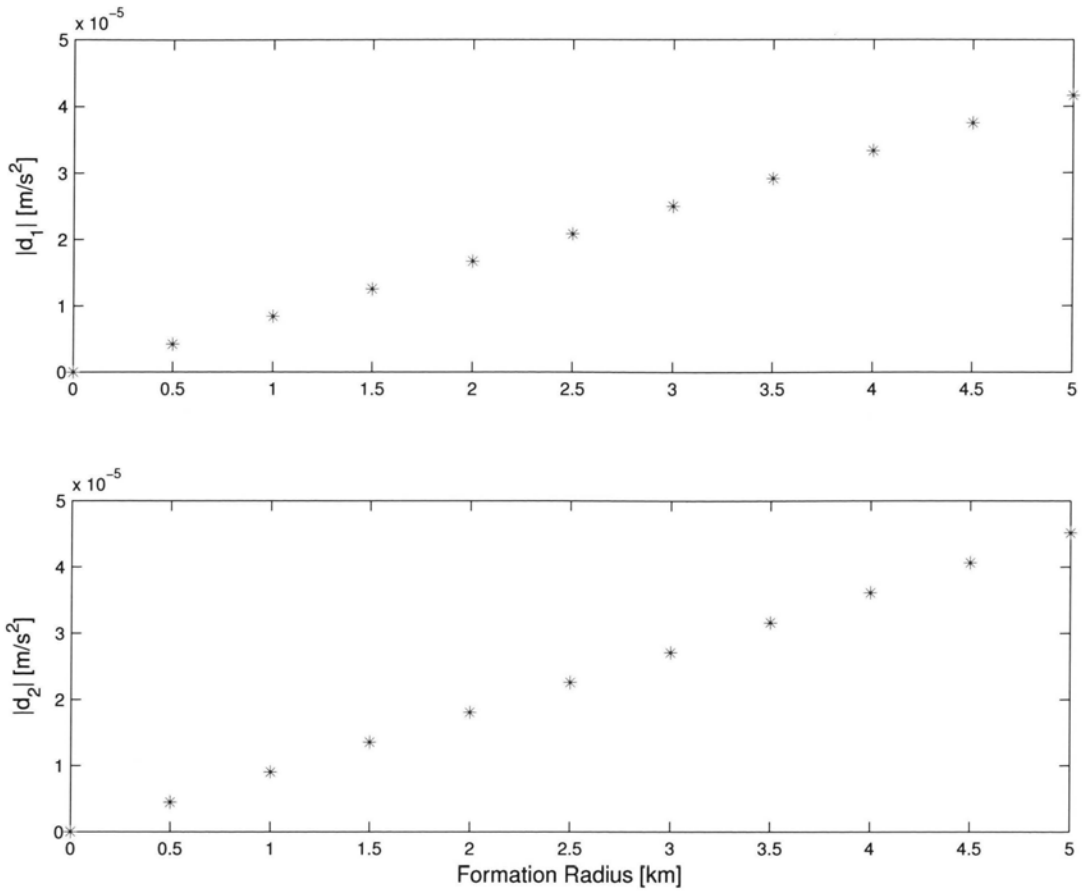

Figure 4.2: Matched and unmatched disturbance forces resulting from differential J_2 disturbance compared to formation radii

4.3 Robustness

The first step in defining the bounds on the stability is to develop the equations of the disturbance forces acting on the system. Referring to Eq. (3-9) the boundary approximations for a disturbance are restated as follows:

$$\begin{aligned} \|\mathbf{d}_1\| &\le \alpha_{11}\|\mathbf{x}_1\| + \alpha_{12}\|\mathbf{x}_2\| + \beta_1 \\ \|\mathbf{d}_2\| &\le \alpha_{21}\|\mathbf{x}_1\| + \alpha_{22}\|\mathbf{x}_2\| + \gamma\|\mathbf{u}\| + \beta_2 \end{aligned} \tag{4-5}$$

Using the relation between the disturbance forces and the formation radius as shown in Figure 4.2, the values of the coefficients in Eq. (4-5) can be derived. The values of the coefficients and constants of Eq. (4-5) are defined in Table 4.2.

Table 4.2: Disturbance parameterization

Disturbance Parameters	Value
α_{11}	6.8569×10^{-3}
α_{12}	0
α_{21}	6.8569×10^{-3}
α_{22}	0
β_1	4.0815
β_2	4.0815
γ	0

Following the procedure developed in Section 3.5 of Chapter 3, the regions of stability for the formation system are defined as follows:

$$\begin{aligned}\Sigma &= \left\{(x_1,\sigma)\left|\delta<\|\sigma\|<\frac{\mu\hat{a}_{11}-\hat{a}_{21}\hat{\beta}_1}{\hat{a}_{22}\hat{a}_{11}+\hat{a}_{12}\hat{a}_{21}},\hat{a}_{21}\|\mathbf{x}_1\|+\hat{a}_{22}\|\sigma\|<\mu\right.\right\}\\ &=\left\{(x_1,\sigma)\left|1.4142<\|\sigma\|<22.2246,\ 7.2696\|\mathbf{x}_1\|+2.851\|\sigma\|<8140.3053\right.\right\}\end{aligned} \tag{4-6}$$

$$\begin{aligned}\Delta &= \left\{(x_1,\sigma)\left|\frac{\mu-\hat{a}_{22}\delta}{\hat{a}_{21}}>\|x_1\|>\frac{\hat{a}_{12}}{\hat{a}_{11}}\delta+\frac{\hat{\beta}_1}{\hat{a}_{11}},\|\sigma\|<\delta\right.\right\}\\ &=\left\{(x_1,\sigma)\left|1119.2256>\|x_1\|>463.9729,\|\sigma\|<1.4142\right.\right\}\end{aligned} \tag{4-7}$$

$$\begin{aligned}\Gamma &= \left\{(x_1,\sigma)\left|\left(\|x_1\|<\frac{\hat{a}_{12}}{\hat{a}_{11}}\delta+\frac{\hat{\beta}_1}{\hat{a}_{11}}\right)\bigcap(\|\sigma\|<\delta)\right.\right\}\\ &=\left\{(x_1,\sigma)\left|(\|x_1\|<1.4142)\bigcap(\|\sigma\|<1)\right.\right\}\end{aligned} \tag{4-8}$$

where Σ is the region of convergence for the unmatched states and switching function, Δ is the convergence region for the unmatched states only, and Γ is the inner unstable region. The specific values of the coefficients for the satellite formation system are provided in Table 4.3. These regions define the guaranteed stability and response of the formation system based on the current knowledge of the system dynamics and disturbance forces.

Table 4.3: Robustness boundary parameters

Robustness Boundary Parameters	Value
$\hat{a}_{11}$	0.2932
$\hat{a}_{12}$	9.1155
$\hat{a}_{21}$	7.2696
$\hat{a}_{22}$	2.8510
$\hat{\beta}_1$	123.1235
μ	8140.3

4.4 Simulation Responses

In this section, the responses of two numerical simulations are presented. The first simulation assumes that the satellite formation starts in the formation with no initial error. The second simulation evaluates the controller when a 5% offset from the ideal initial positions is present.

4.4.1 Ideal Initial Conditions

The first simulation assumes that the follower satellite has no initial offset error from the desired formation trajectory. The specific starting conditions for the follower satellite are given in Table 4.4. The steady-state tracking errors as shown in Figure 4.3, demonstrate the stabilizing effect of the controller on the formation system. The y error, at steady-state, is bounded to within $\pm 2\,\mathrm{m}$ and is centered at zero. Similarly, the x error demonstrates a bounded steady-state operation in the range of $\pm 1.5\,\mathrm{m}$. However, it is evident that the oscillations do not converge around zero but have a minor offset instead. The steady-state operation of the y error around zero and offset in the x error can be directly attributed to the presence of the integral error terms in the design of the sliding manifold. The z error, exhibits similar response to the x y error, demonstrating a bounded response to within the $\pm 1.5\,\mathrm{m}$.

Table 4.4: Ideal initial state conditions of the satellite formation system

System States	Value
Radial position, x	176.8 m
Tangential position, y	353.6 m
Normal position, z	353.6 m
Radial velocity, $\dot{x}$	0.1956 m/s
Tangential velocity, $\dot{y}$	–0.3913 m/s
Normal velocity, $\dot{z}$	0.3913 m/s

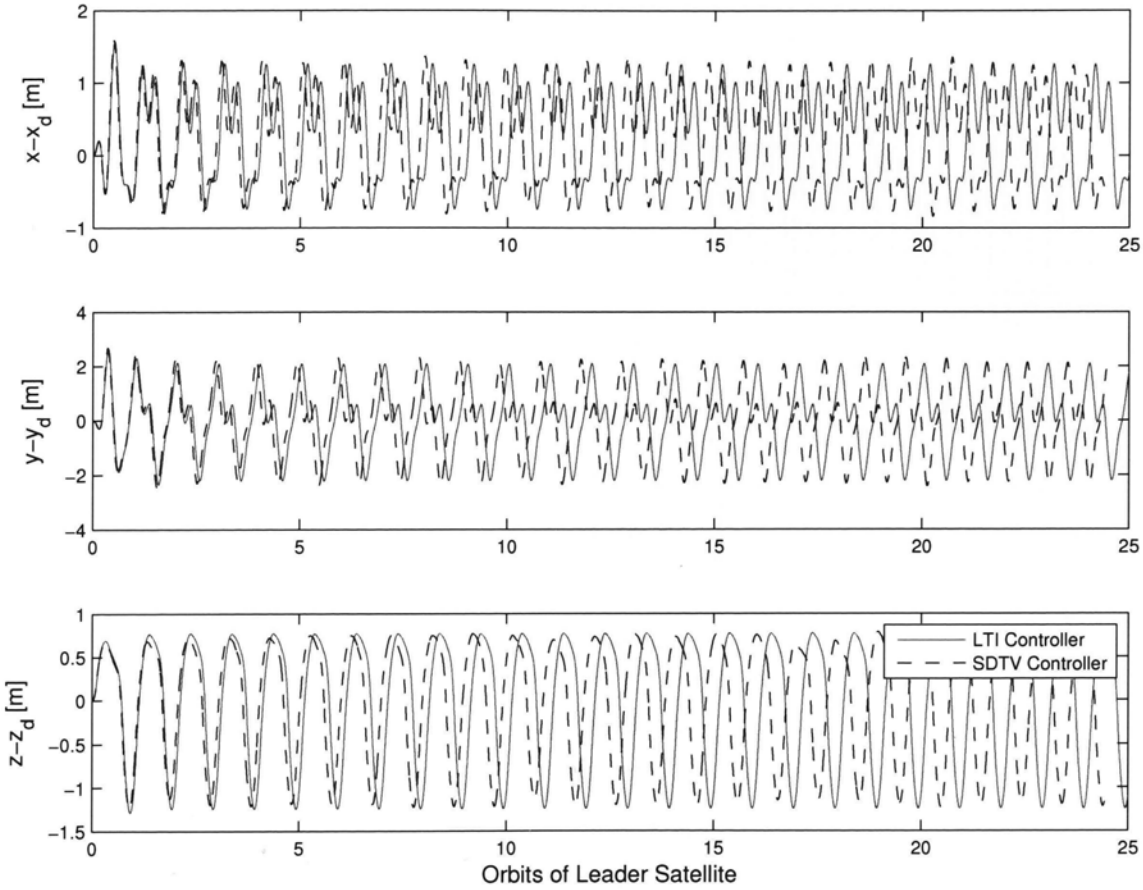

Figure 4.3: Satellite formation tracking errors with ideal initial conditions

The control forces in the tangential and normal directions have fixed magnitudes of either 0 or $\pm 10\,\text{mN/kg}$; this behavior is better known as bang-bang style of control. When the control force profile is compared to the response of the switching functions, as shown in Figure 4.5, it is found that the control force acts to keep the switching function within the

dead zone boundary, δ. Furthermore, while the switching functions are within the dead zone region, no control action is taken.

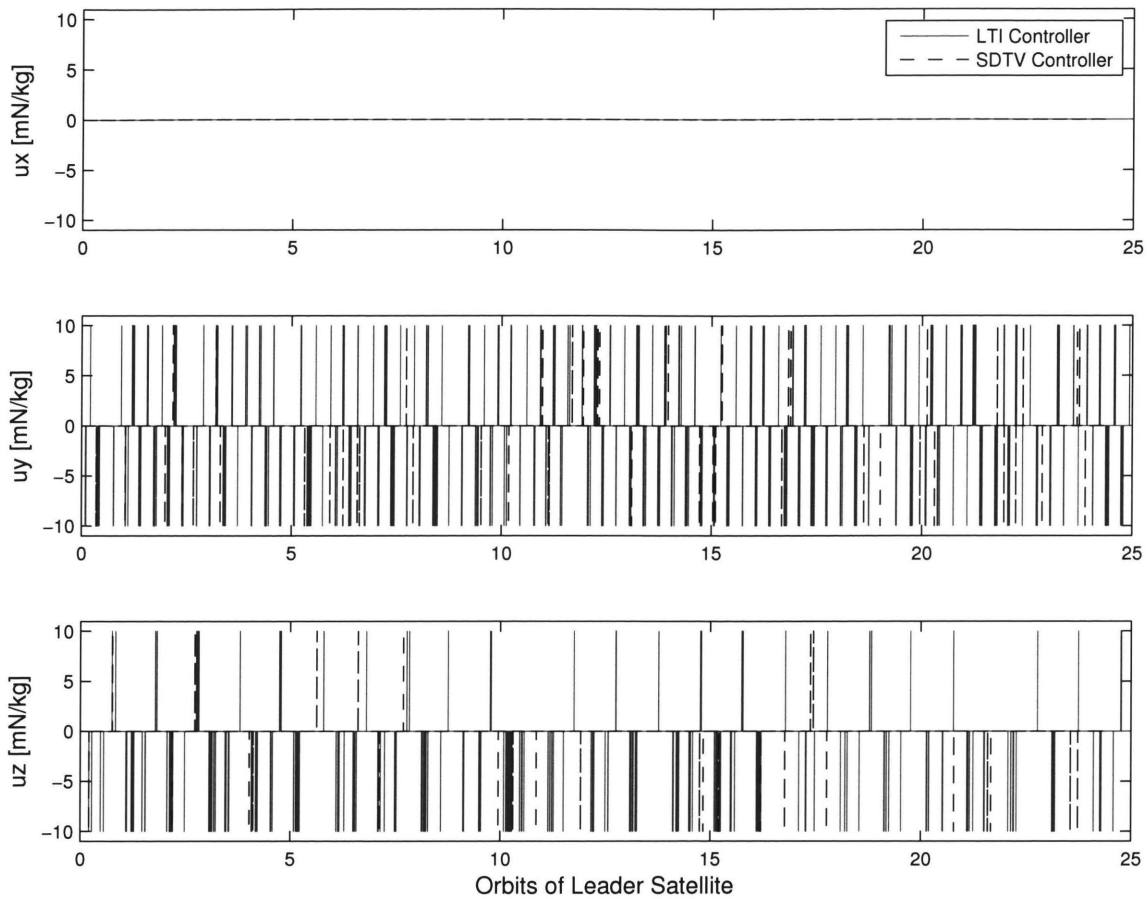

Figure 4.4: Controller output response with ideal initial conditions

Finally, the responses of the LTI and SDTV relay controllers are found to be similar with slight variation in phase following the 5th orbit. The probable cause for this difference might be due to the DRE, which changes as a result of the initial controller activity and then eventually reach a steady-state response.

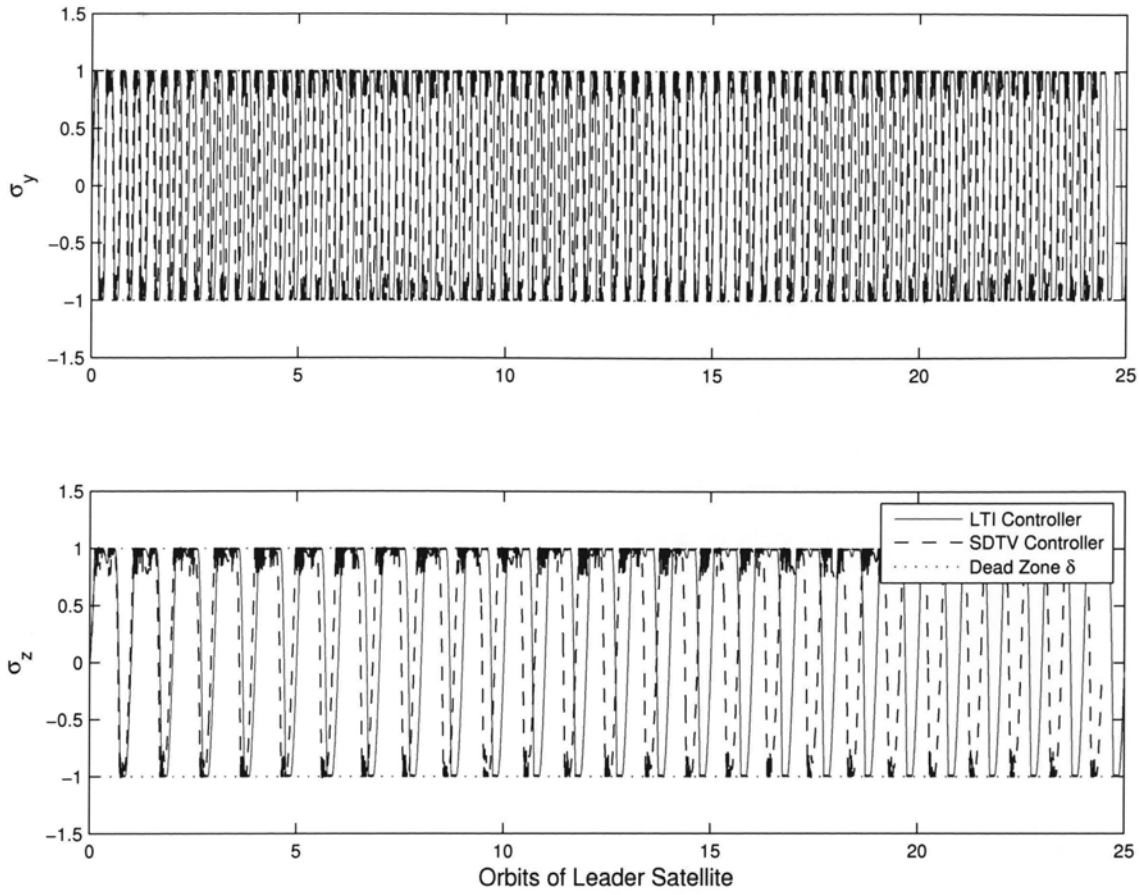

Figure 4.5: Switching function response with ideal initial conditions

4.4.2 Ten Percent Offset in Initial Conditions

In the second simulation, the system is initialized with a 5% offset in the position errors from the ideal formation. The initial values of the position errors and the norms of the switching functions and unmatched states are given in Table 4.5. From the robustness bounds defined in Section 4.2, the system starts within the region of convergence, Σ. As a result, the formation tracking error states, and the switching function and unmatched state norms, are guaranteed to converge toward the inner stability region, Γ.

The first response, as shown in Figure 4.6, clearly demonstrates the follower satellite's convergence towards the desired projected formation configuration. Similarly, the formation tracking error response shows convergence towards a region around the equilibrium, see Figure 4.7. In both the plots, it is quite evident that the overall system response is stable, which was guaranteed by the robustness of the control law.

Table 4.5: Initial error states with a 5% offset from ideal conditions

Error States	Value
Tangential integral, $\tilde{y}_s$	$0\,\mathrm{m}\cdot\mathrm{s}$
Normal integral, $\tilde{z}_s$	$0\,\mathrm{m}\cdot\mathrm{s}$
Radial position, $\tilde{x}$	$8.84\,\mathrm{m}$
Tangential position, $\tilde{y}$	$17.67\,\mathrm{m}$
Normal position, $\tilde{z}$	$17.68\,\mathrm{m}$
Radial velocity, $\dot{\tilde{x}}$	$0.0\,\mathrm{m/s}$
Tangential velocity, $\dot{\tilde{y}}$	$0.0\,\mathrm{m/s}$
Normal velocity, $\dot{\tilde{z}}$	$0.0\,\mathrm{m/s}$
Norm States	
Unmatched states, $\|\mathbf{x}_1\|$	26.5165
Switching functions, $\|\sigma\|$	16.567

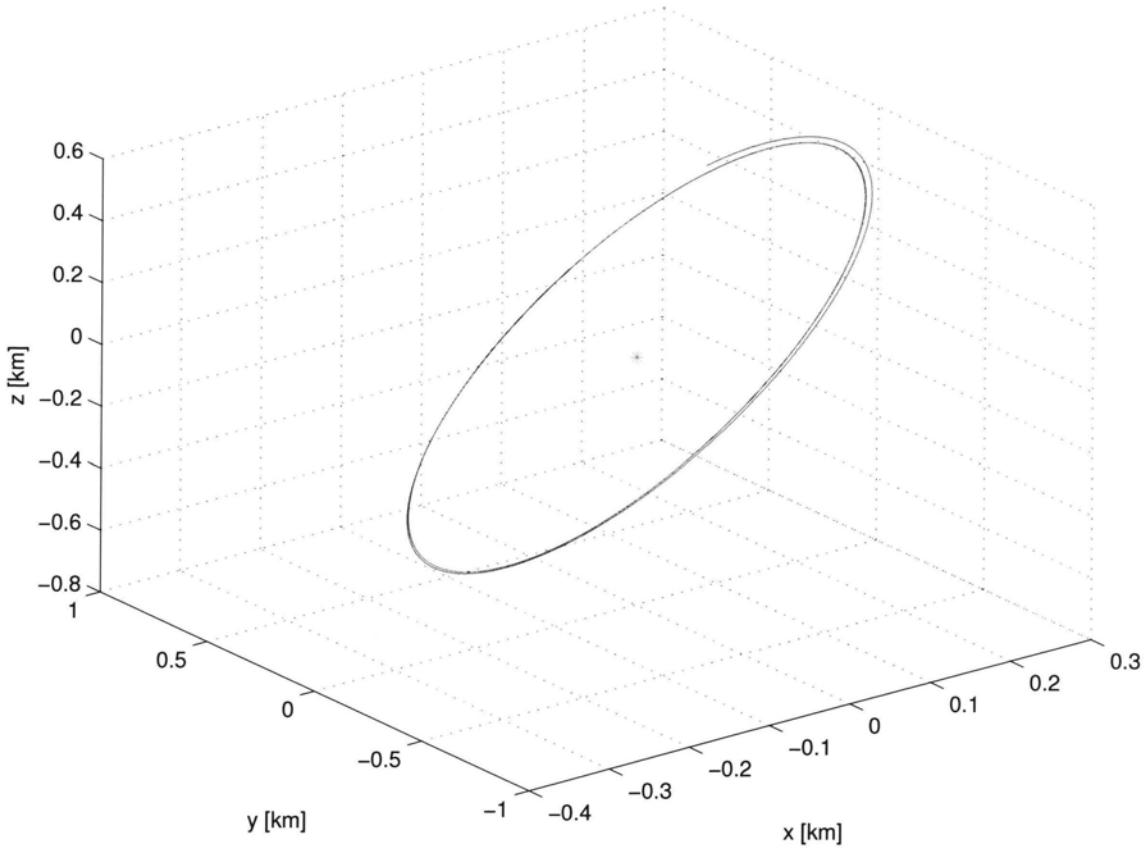

Figure 4.6: Satellite position state response with 5% initial offset from ideal starting conditions

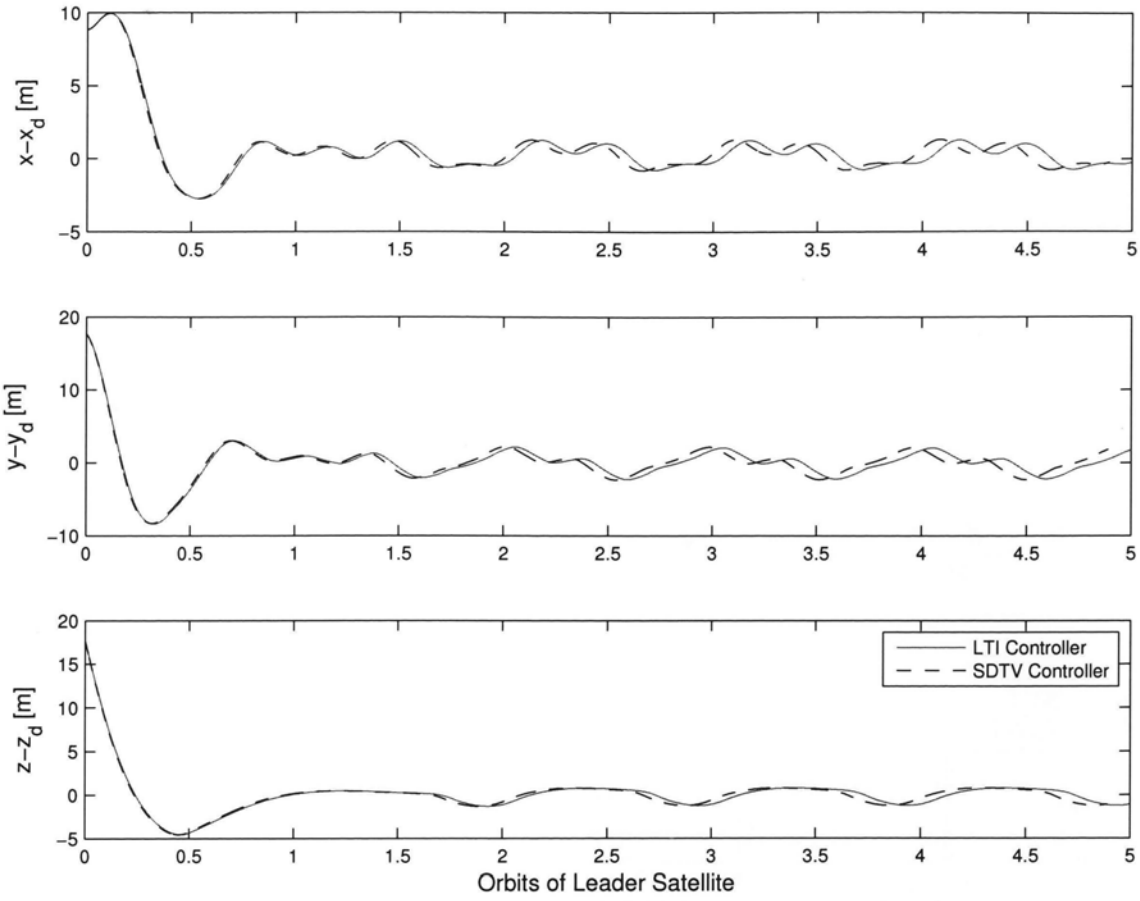

Figure 4.7: Tracking error response with 5% initial offset from ideal positions

Figure 4.8 shows the response of the control thrusters. During the first orbit, while the tracking errors converge towards the steady-state, the controller experiences a short continuous pulse followed by an intense period of high-frequency control actuation. The short pulse is a result of the controller driving the switching functions to the sliding manifold. The high-frequency oscillations are due to the follower not being in the desired trajectory, which only requires control action to counteract the disturbing forces and nonlinearities that were not included in the model approximations.

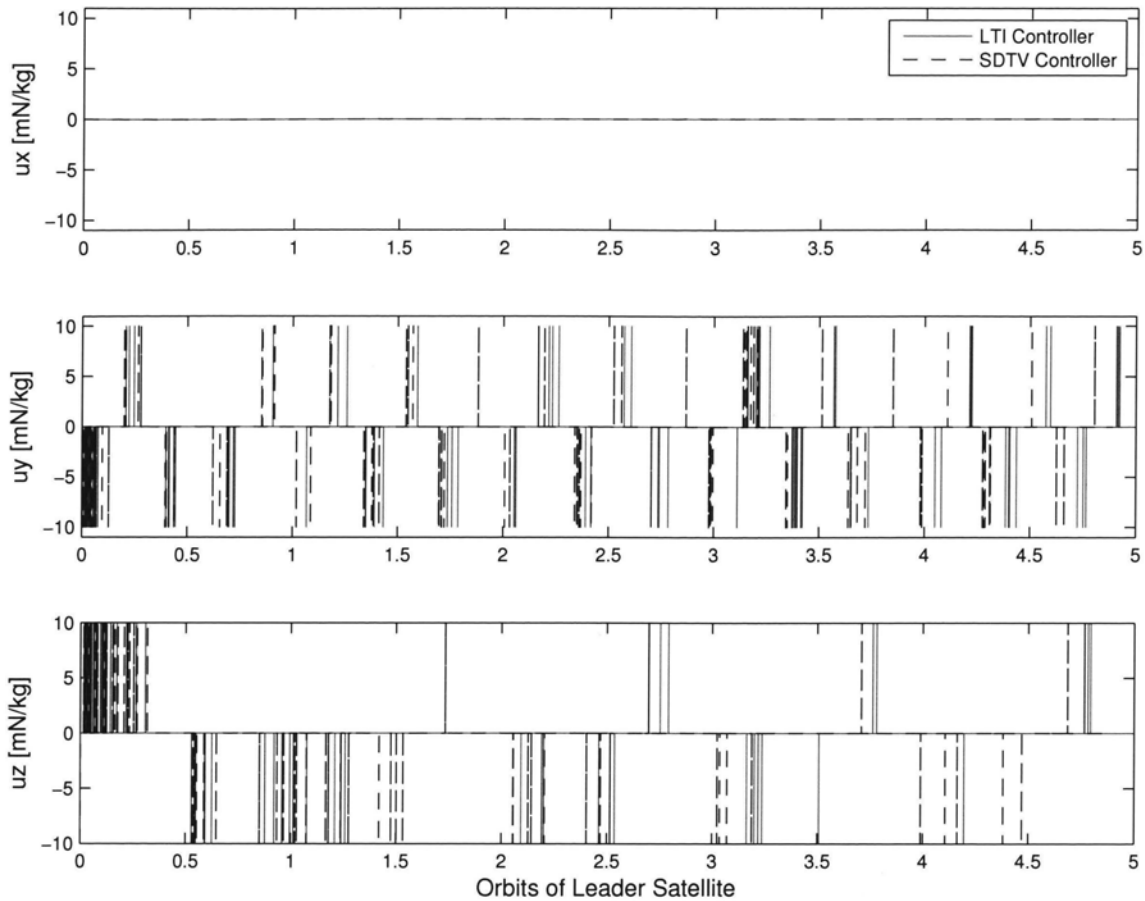

Figure 4.8: Controller response for 5% offset from ideal initial positions

The most interesting results are shown in the responses of the norms switching functions and unmatched states, given in Figure 4.9 and Figure 4.10, respectively. The trajectory of the norm of the switching function, which is initially within the Σ convergence region, moves directly to the $\Delta - \Gamma$ region, where it remains. This behavior was the expected result of the robustness analysis which guaranteed the convergence of the switching function to the $\Delta - \Gamma$ if the trajectory started inside the Σ region. Furthermore, since the norm of the switching functions is also the Lyapunov function, while in the Σ region, the slope of the trajectory is negative, satisfying the Lyapunov stability. It is evident that the norm of the switching function converges within an extremely short period of time. However, this action only represents the reaching phase of the control law. The actual system states do not achieve steady-state for a full orbit.

Although the norm of the unmatched states begins within the Σ region and enters the Γ region, it continues to demonstrate convergence to a much smaller value than was predicted by the robustness boundaries. It is important to note that the boundaries of Γ determine the maximum outer bounds, but the norm trajectories may settle to a much smaller value, as is demonstrated in the response of Figure 4.10.

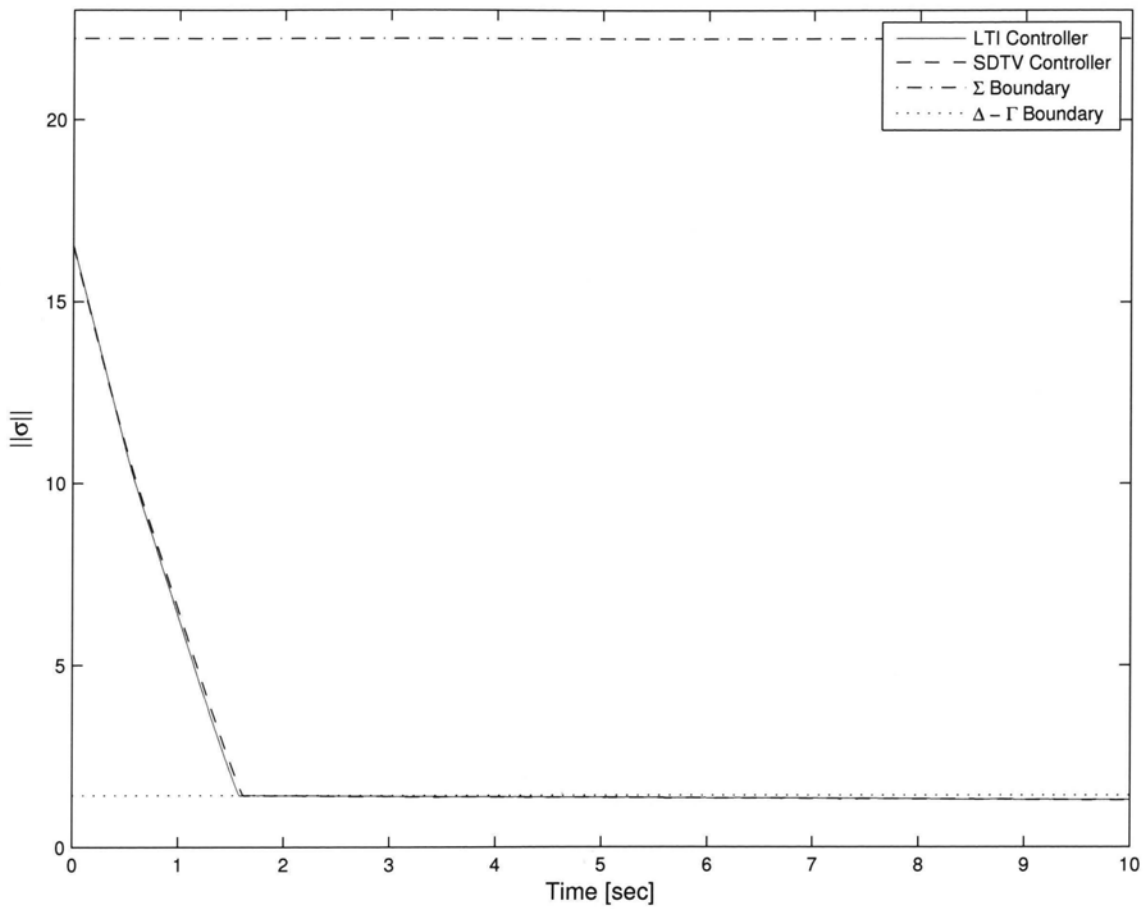

Figure 4.9: Norm of switching functions response with 5% initial offset from ideal positions

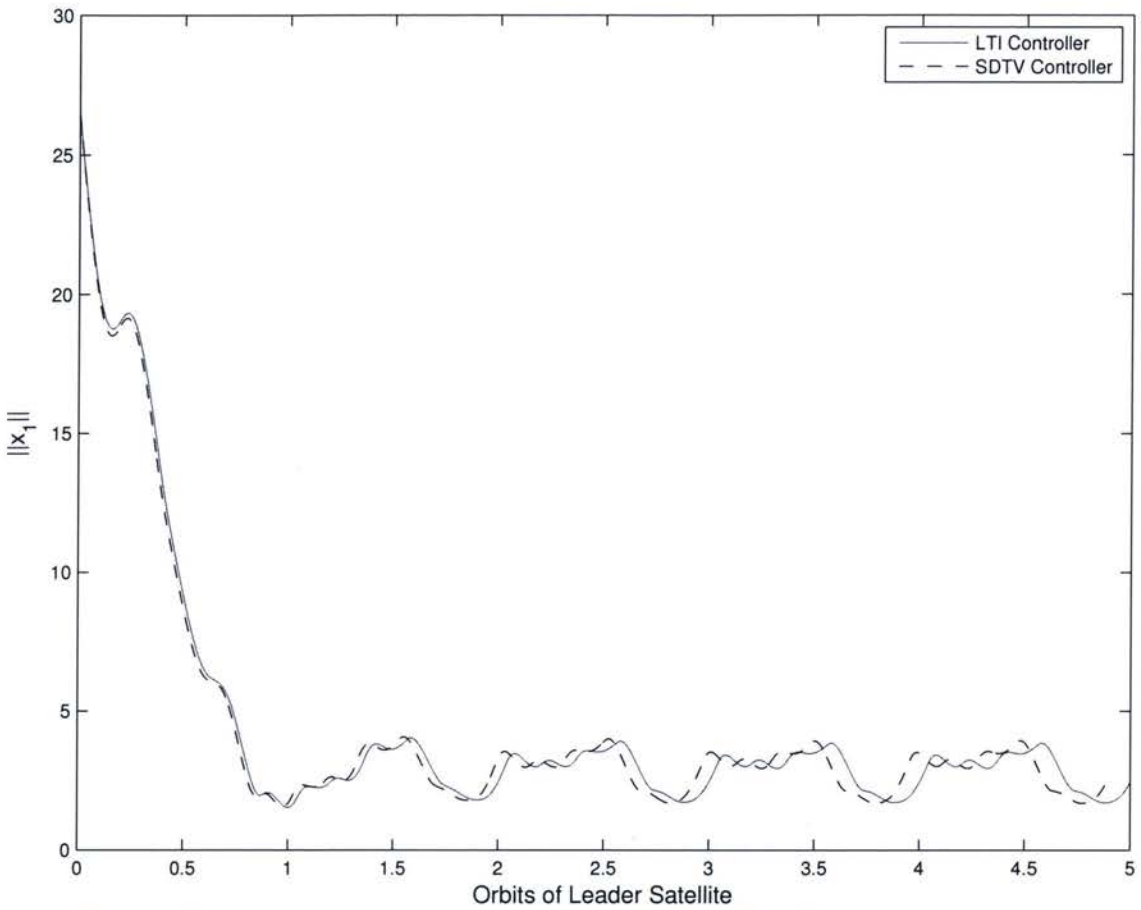

Figure 4.10: Norm of unmatched states response with 5% initial offset from ideal positions

4.5 Controller Tuning and Performance Trade-Offs

In controlling the satellite formation, the performance of the formation is affected by several parameters. To achieve the desired performance, three tuning variables can be adjusted. The tuning variables are the sliding manifold gain, q; the switching coefficient, η; and, the dead zone boundary width, δ. The following subsections analyze, through numerical simulations, the effect of the control variables on the formation performance criteria proposed in Section 4.1.

4.5.1 Sliding Manifold Gain, q

The largest contributing factor affecting the performance of the controller is the design of the sliding manifold. As described in Section 4.1, the design of the sliding manifold can be reduced to the selection of a single positive constant gain, q. Figure 4.11 and Figure 4.12

show the transient responses of the performance criteria of the formation system with a 5% initial offset for a range of q. It is apparent that, although each transient response shares a similar profile, the value of q is directly influencing the settling time of the transients. In the case of the tracking errors, increasing the values of q results in shorter response times of the transients. However, the ΔV performance demonstrates the opposite trend with decreasing fuel consumption when q is increased, particularly for values of $q > 1$. Therefore, in order to achieve a settling time of within 1-2 orbits and reduce the total ΔV, the sliding manifold gain $q = 0.5$.

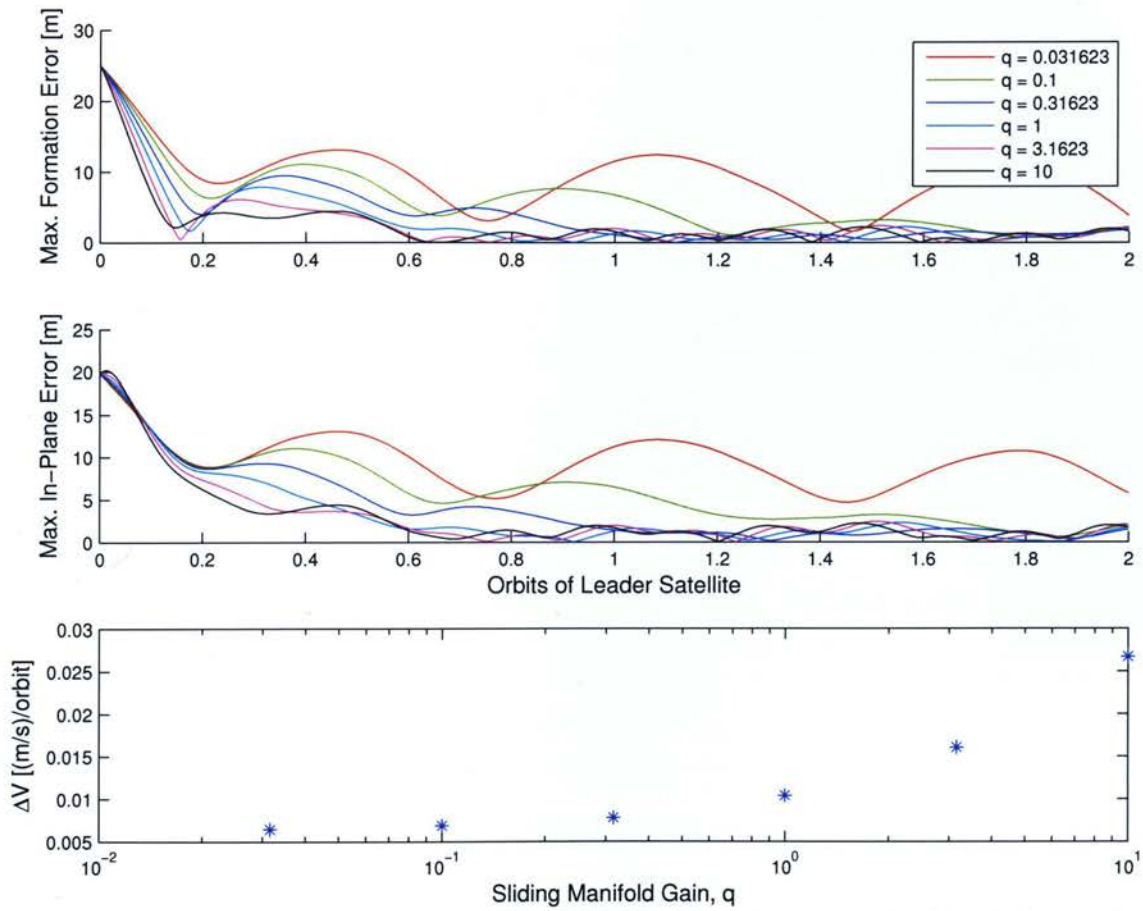

Figure 4.11: Comparison of the manifold tuning gain against the performance criteria for the linear time invariant sliding mode controller

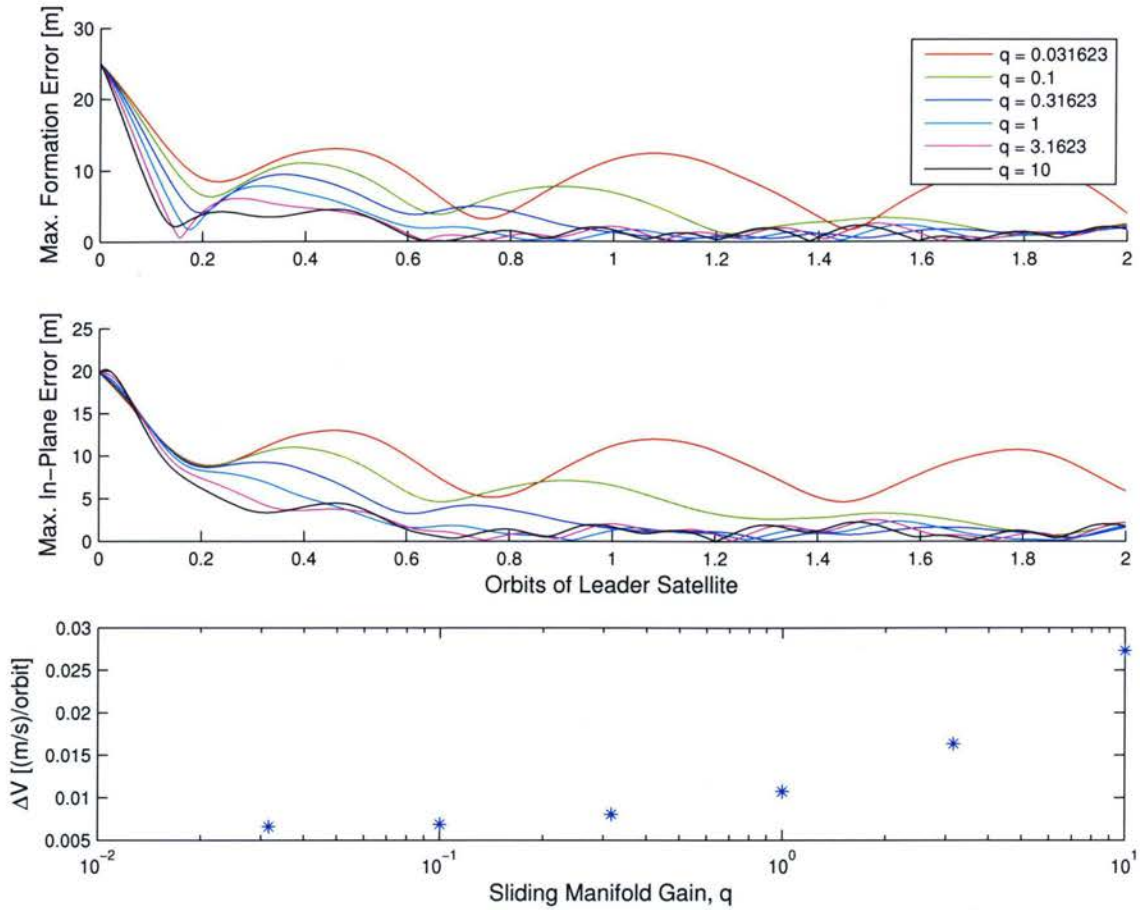

Figure 4.12: Comparison of the manifold tuning gain against the performance criteria for the state dependent, time varying sliding mode controller

4.5.2 Switching Coefficient, η

The second factor affecting the performance of the satellite formation is the switching coefficient, η. In Figure 4.13, a comparison between the performance criteria and the switching coefficient is provided. The formation tracking errors show no discernable relation to the switching coefficient. In contrast, for values of $\eta > 2$, the ΔV consumption decreases exponentially; after which, the ΔV becomes relatively constant. Therefore, choosing $\eta \approx 10$ will reduce the fuel consumption to a reasonable level but ensure the controller is still capable of reaching the sliding manifold upon initialization.

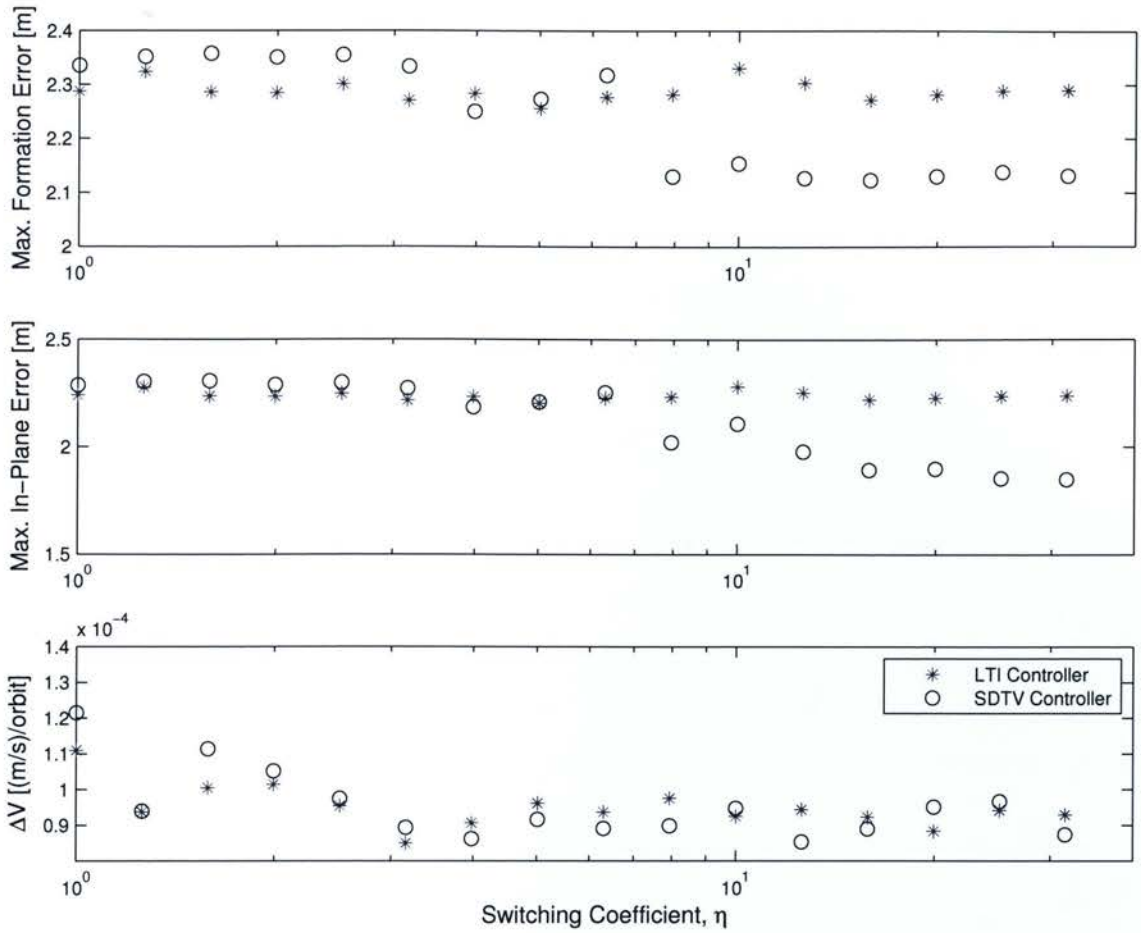

Figure 4.13: Comparison of the switching coefficient against the formation performance criteria

4.5.3 Dead Zone Width, δ

The final controller parameter is the dead zone width, δ. Figure 4.14 shows the formation performance criteria against the width of the dead zone boundary. It is evident that for increasing values of δ, the formation tracking errors also increase. This is expected since the interior stability region Γ, which is a function δ, defines maximum expected steady-state error. The ΔV performance shows the exact opposite trend. For values of $\delta \geq 1$, the ΔV remains constant with changes in the dead zone width; however, as $\delta \to 0$ the fuel consumption begins to increase dramatically, by nearly an order of magnitude. This result is expected since at $\delta = 0$, the relay controller simplifies to the basic switching controller, $\mathbf{u} = -\eta \operatorname{sgn}(\sigma)$. The switching controller attempts to bring the switching function to exactly zero, which requires significantly greater control action, causes chattering, and provides no

significant improvement in the formation tracking error performance. Therefore, in order to reduce the fuel consumption and the tracking errors, the dead zone width should be chosen as $\delta \approx 1$.

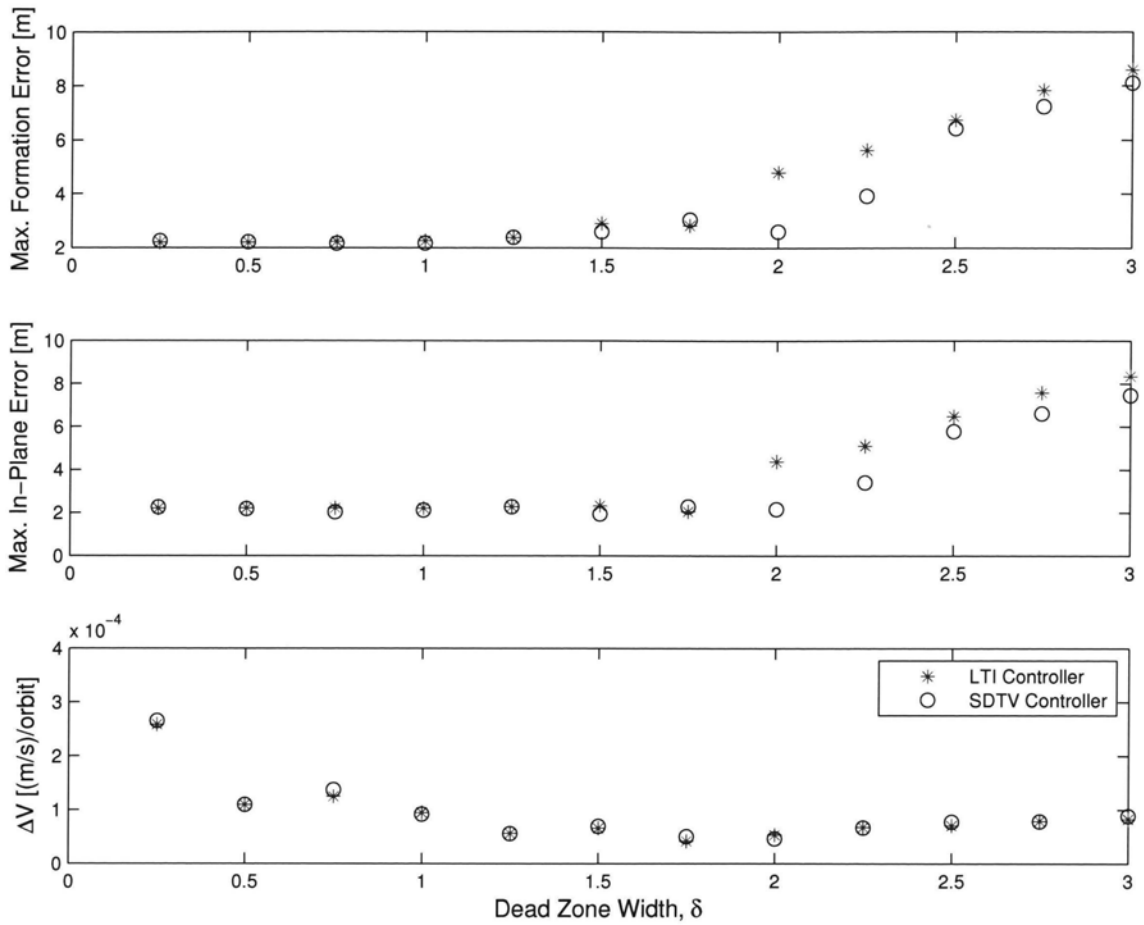

Figure 4.14: Dead zone bandwidth compared to the performance criteria

4.6 Physical and Formation Parameters

Although the performance of the system can be adjusted through the careful selection of the control parameters q, η, and δ, there are many other factors that effect the performance of the system. The most significant factors are the phase and radius of the satellite formation, and the eccentricity of the leader satellite's orbit. The following subsections evaluate the effects of each of these variables on the formation performance.

4.6.1 Formation Phase, φ

As the leader-follower formation can be expanded to include multiple follower satellites, it is desirable to determine the effect of the phase of the follower on the formation performance criteria. A comparison of the formation's phase and the performance criteria is shown in Figure 4.15. Although the phase of the formation has no significant influence on the fuel consumption, it does demonstrate an effect on the tracking errors. In particular, minimums in the formation tracking errors occur when $\varphi = 90^o, 270^o$ and maximums when $\varphi = 30^o, 210^o$.

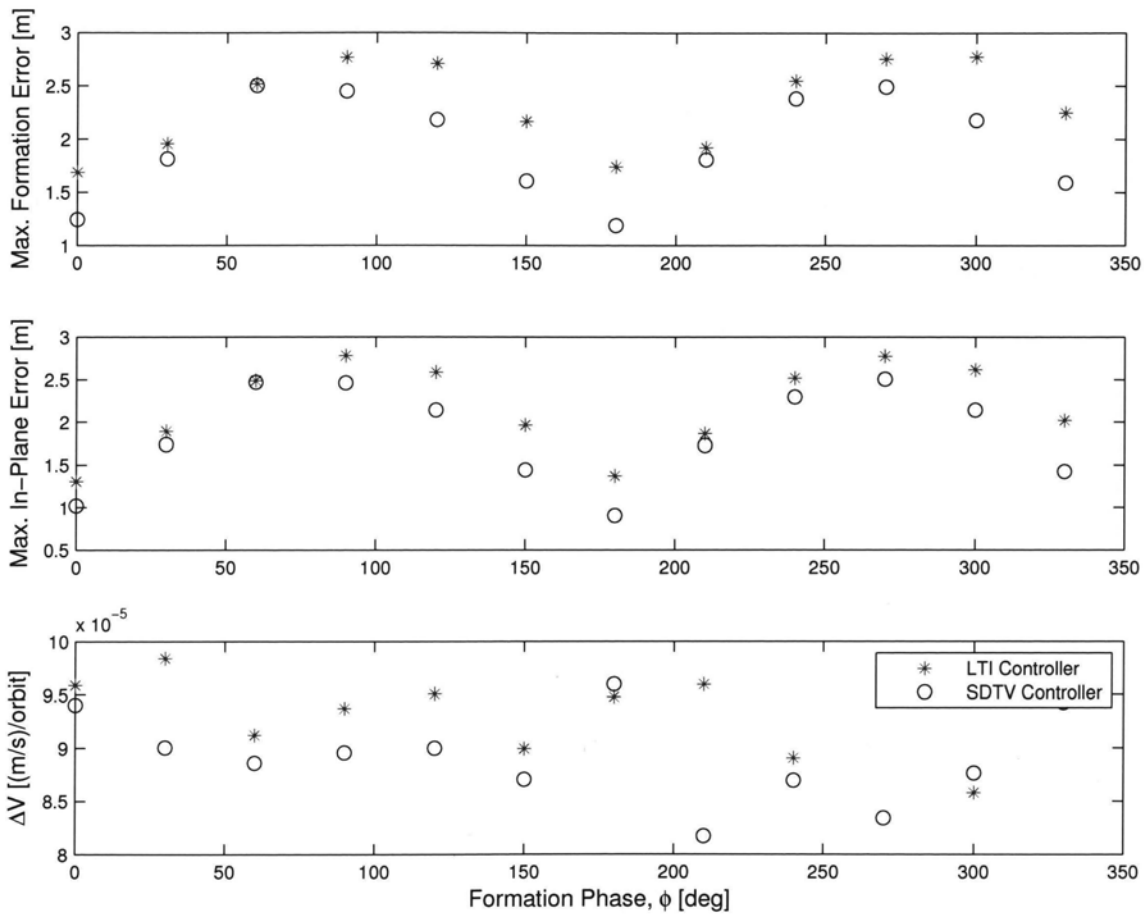

Figure 4.15: Performance measures compared to formation phase

4.6.2 Formation Radius, r_d

Figure 4.16 shows the effects of formation radii on the performance criteria. It is evident that both the formation tracking errors and the fuel consumption all exhibit a positive linear relationship with increasing values of the radius. It is interesting to note that although the

formation tracking error is increasing with the larger formations, the ratio of the tracking error to the formation radius stays constant at approximately 0.3%.

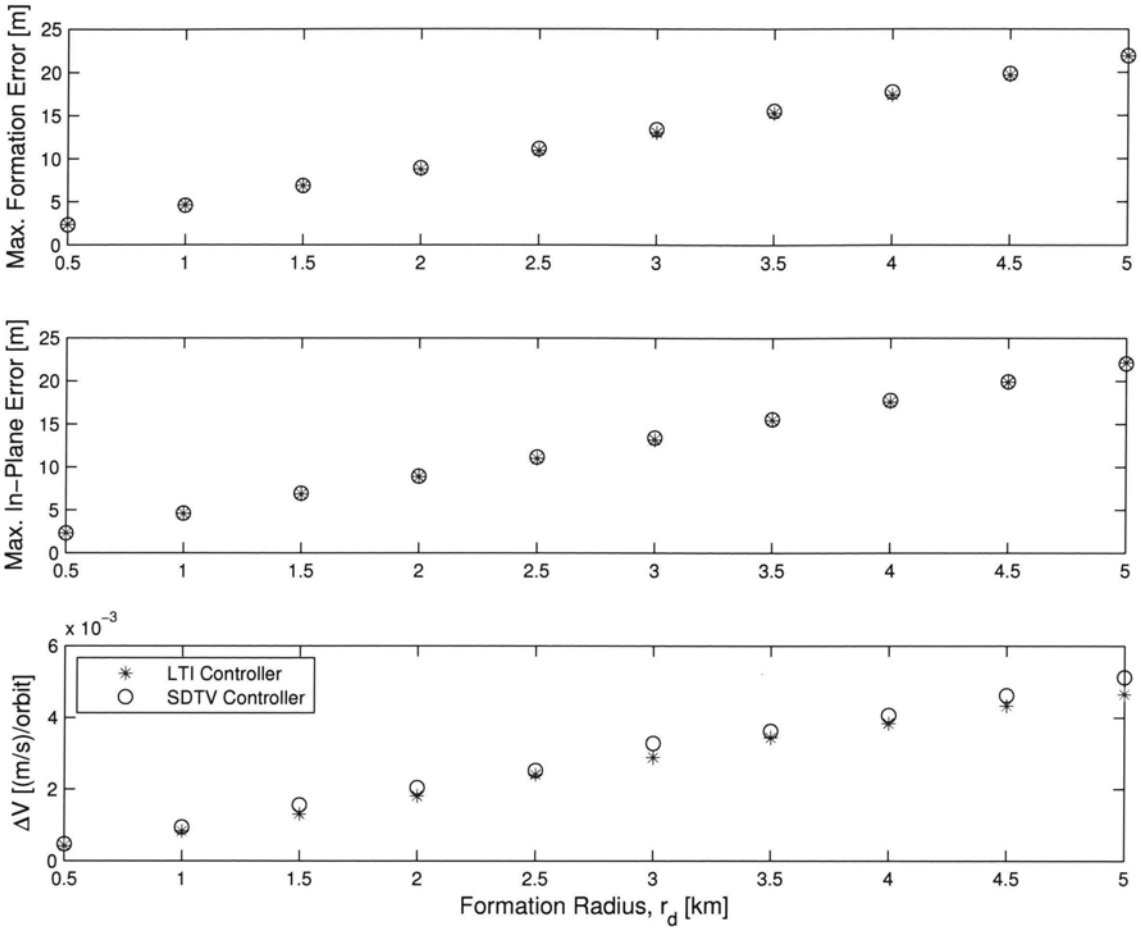

Figure 4.16: Comparison of the satellite formation radius against the performance criteria

4.6.3 Formation Eccentricity, e

A critical factor affecting the behavior of the satellite formation is the eccentricity of the leader satellite's orbit. As shown in Figure 4.17, the formation performance criteria are measured against the eccentricity of the leader satellite. Although no direct effect is evident between the eccentricity and the tracking performance, there is a clear degradation in the ΔV performance with increasing eccentricity. However, the more important result is the difference between the LTI and SDTV relay controllers. Although it would be expected that the SDTV relay controller should perform better since it is able to account for some of the system nonlinearities, which increase with eccentricity, the LTI relay controller uses the

optimal solution of the ARE as opposed to the SDTV relay controller which uses the realizable solution of the DRE. The result is the optimal solution of the ARE in fact performs better than the realizable DRE solution.

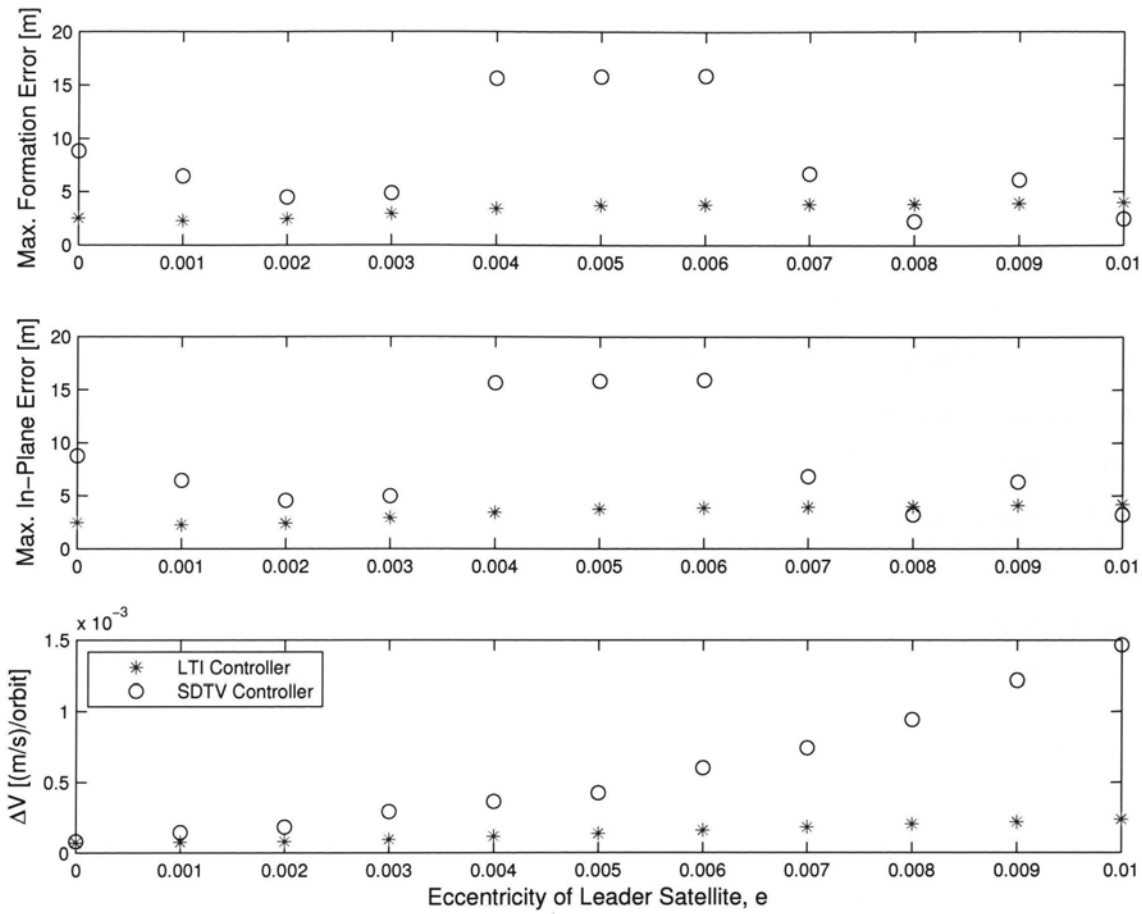

Figure 4.17: Comparison of the eccentricity of the leader satellite's orbit and the performance criteria

4.7 Conclusions

The results of the numerical simulations have revealed many important properties of the relay controllers' effects on the underactuated satellite formation. First and foremost, the theoretical stability and robustness bounds predicted by Chapter 3 were verified through the numerical simulations. Second, through careful selection of the control parameters, the system can be tuned to provide relatively good performance. Finally, the performances of both the controllers were found to be similar in most cases.

Chapter 5
Conclusions & Future Work

In this thesis, the control of an underactuated satellite formation using robust nonlinear techniques was examined. Two new sliding mode control laws were developed in Chapter 3, the first using the linear, time-invariant model of the formation system, also known as the Hill's equations, and the second using a 2^{nd} approximation of the equations of motion. Regions of stability, in the presence of matched and unmatched disturbing forces, were determined for both controllers. The control laws were further advanced by modifying them into the form of a relay sliding mode control, which incorporates a dead zone boundary around the sliding manifold, the desired effect being a reduction in fuel consumption and the chattering effect. Through the numerical simulations, presented in Chapter 4, the robustness of the proposed control laws were demonstrated to match the theoretical robustness boundaries determined from Chapter 3.

5.1 Conclusions

The most significant result of the study has been the development of the robust sliding mode control methods for the underactuated satellite formation system. This represents a significant step forward since the previous control methodologies applied to the system have not explicitly considered controller's stability in the presence of disturbing forces. A secondary result was the use of the 2^{nd} order approximation of the equations of motion in the design of the control law, where only the Hill's equation had been applied previously. It was found that the state dependent, time varying control law did not show any noticeable improvement in the performance.

Through numerical simulations, the control laws were tested against a range of tuning parameters and formation variations. The results of the simulation showed that controllers could be tuned to achieve steady-state formation tracking errors within $\pm 5\,\mathrm{m}$ and ΔV

consumption on the order of $1\times10^{-3}\,(\mathrm{m/s})/\mathrm{orbit}$. Although larger degradation in the controller performance occurred for more extreme formation radii, i.e. $r_d > 3\mathrm{km}$, and orbital eccentricities, i.e. $e > 0.005$, this would be expected since the nonlinear equations of motion would start to show significant deviations from the Hill's and 2nd order approximation equations.

5.2 Future Work

Despite the advances in the control of the underactuated satellite formation developed in this thesis, the control laws have only been tested within a small range test conditions. The first recommendation, therefore, is to expand the range of testing scenarios for the proposed control laws. This includes the use of alternative formation configurations, larger parameters variations and high-fidelity models of the disturbing forces, and extending the simulations over larger time-spans to evaluate the long-term fuel consumption. The second area of development is to evaluate the performance of robust control laws in the task of formation reconfiguration. The third improvement in the development of the underactuated satellite formation is to redevelop the robust control laws in the discrete time domain. As the final spacecraft hardware is only capable discrete operation, the advancement to discrete control laws is a necessity.

References

[1] Robertson, B. and Stoneking, E., "Satellite GN&C Anomaly Trends," *Advances in the Astronautical Sciences*, Vol. 113, 2003, pp. 531 – 542.

[2] Folta, D. and Quinn, D., "Enhanced formation Flying for the Earth Observing-1 (EO-1) New Millennium Mission," *Proceedings of the Flight Mechanics Symposium*, NASA Goddard Space Flight Center, Greenbelt, MD, 1997, pp. 405-406.

[3] Folta, D., Bristow, J., Hawkins, A., and Dell, G., "NASA's autonomous formation flying technology demonstration, Earth Observing-1," *First International Symposium on Formation Flying Missions and Technologies*, Centre National d'Etudes Spatiales, Toulouse, France, Oct 29-30 2002.

[4] Folta, D. and Hawkins, A., "Results of NASA's first autonomous formation flying experiment: Earth Observing-1 (EO-1)," *AIAA/AAS Astrodynamics Specialist Conference and Exhibit*, Monterey, California, 5-8 August, 2002.

[5] Burns, R., McLaughlin, C., Leitner, J., and Martin, M., "TechSat 21: Formation design, control, and simulation," *Proceedings of the IEEE Aerospace Conference*, Vol. 7, Big Sky, MT, 2000, pp. 19 - 25.

[6] Das, A. and Cobb, R., "TechSat 21: Space missions using collaborating constellations and satellites," *Proceedings of the 12th AIAA/USU Annual Conference on Small Satellites*, Reston, VA, 1998.

[7] Folkner, W., Bender, P., and Stebbins, R., "LISA misison concept study: Laser Interferometer Space Antenna for the detection and observation of gravitational waves," *Jet Propulsion Laboratory Report*, JPL 97-16, California Institute of Technology, Pasadena, CA, March 2 1998.

[8] How, J., Twiggs, R., Weidow, D., Hartman, K., and Bauer, F., "ORION: A low-cost demonstration of formation flying in space using GPS," *AIAA/AAS Astrodynamics Specialist Conference*, AIAA-98-4398, Boston, MA, August 1998, pp. 276-286.

[9] Cabeza, I. and Martinez, A., "SMART-2: An ESA mission to demonstrate the key technologies for formation flying and drag-free control," *First International Symposium on Formation Flying Missions and Technologies*, Center National d'Etudes Spatiales, Toulouse, France, Oct 29-30 2002.

[10] Bristow, J., Folta, D., and Hartman, K., "A formation flying technology vision," *AIAA Space 2000 Conference and Exposition*, Long Beach, CA, September 19-21 2000, AIAA-2000-5194.

[11] Neeck, S. P., Magner, T. J., and Paules, G. E., "NASA's small satellite missions for Earth observation," *Acta Astronautica*, Vol. 56, No. 1-2, 2005, pp. 187-192.

[12] Carpenter, J. R., Leitner, J. A., Folta, D. C., and Burns, R. D., "Benchmark problems for spacecraft formation flying missions," *AIAA Guidance, Navigation, and Control Conference and Exhibit*, AIAA-2003-5364, Austin, Texas, August 11-12, 2003.

[13] Persson, S., Jacobsson, B., and Gill, E., "Prisma - Demonstration mission for advanced rendezvous and formation flying technologies and sensors," *International Astronautical Federation - 56th International Astronautical Congress 2005*, Vol. 4, Fukuoka, Japan, Oct 17-21 2005, pp. 2403 - 2412.

[14] Bauer, F., Bristow, J., Carpenter, J., Garrison, J., Hartman, K., Lee, T., Long, A., Kelbel, D., Lu, V., How, J., Busse, F., Axelrad, P., and Moreau, M., "Enabling spacecraft formation flying in any Earth orbit through spaceborne GPS and enhanced autonomy technologies," *Space Technology*, Vol. 20, No. 4, 2001, pp. 175-185.

[15] Ulybyshev, Y., "Long-Term Formation Keeping of Satellite Constellation Using Linear-Quadratic Control," *AIAA Journal of Guidance, Control, and Dynamics*, Vol. 21, No. 1, 1998, pp. 109-115.

[16] Kapila, V., Sparks, A. G., Buffington, J. M., and Yan, Q., "Spacecraft Formation Flying: Dynamics and Control," AIAA *Journal of Guidance, Control, and Dynamics: Engineering Notes*, Vol. 23, No. 3, 2000, pp. 561-563.

[17] Sparks, A., "Linear Control of Satellite Formation Flying," *AIAA Guidance, Navigation, and Control Conference*, A00-37335, Vol. 1, AIAA, Denver, CO, 2000, pp. 1-5.

[18] Dixon, W. E., Behal, A., Dawson, D. M., and Nagarkatti, S. P., Nonlinear Control of Engineering Systems: A Lyapunov-Based Approach, pp. 252 - 268.

[19] De Queiroz, M. S., Kapila, V., Yan, Q., "Adaptive Nonlinear Control of Multiple Spacecraft Formation Flying," *AIAA Journal of Guidance, Control, and Dynamics*, Vol. 23, No. 3, 2000, pp. 385-390.

[20] Wong, H., Pan, H., De Queiroz, M. S., and Kapila, V., "Adaptive learning control for spacecraft formation flying," *Proceedings of the IEEE Conference on Decision and Control*, Vol. 2, Orlando, FL, Dec 4-7 2001, pp. 1089 - 1094.

[21] Breger, L. S., "Model Predictive Control for Formation Flying Spacecraft," M.Sc. Dissertation, Aeronautics and Astronautics Dept., MIT., Massachusetts, MA, 2004.

[22] Hui, L., Junfeng, L., and Baoyin, H., "Sliding mode control for low-thrust Earth-orbiting spacecraft formation maneuvering," *Aerospace science and technology*, Vol. 10, No. 7, 2006, pp. 636-643.

[23] Massey, T. and Shtessel, Y., "Continuous traditional and high-order sliding modes for satellite formation control," *Journal of Guidance, Control, and Dynamics*, Vol. 28, No. 4, 2005, pp. 826 - 831.

[24] Crassidis, J. L., Vadali, S. R., and Landis Markley, F., "Optimal Variable-Structure Control Tracking of Spacecraft Maneuvers," *AIAA Journal of Guidance, Control, and Dynamics: Engineering Notes*, Vol. 23, No. 3, 2000, pp. 564-x.

[25] Lim, H. C., Bang, H. C., Park, K. D., and Park, P. H., "Tracking control design using sliding mode techniques for satellite formation flying," *Journal of Astronomy and Space Sciences,* Vol. 20, No. 4, 2003, pp. 365 - 374.

[26] Yeh, H. H., Nelson, E., and Sparks, A., "Nonlinear Tracking Control for Satellite Formations," *AIAA Journal of Guidance, Control, and Dynamics*, Vol. 25, No. 2, 2002, pp. 376-386.

[27] Palmer, P., "Optimal Relocation of Satellites in Near-Circular-Orbit Formations," *AIAA Journal of Guidance, Control, and Dynamics*, Vol. 29, No. 3, 2006, pp. 519-526.

[28] Vadali, S. R., Vaddi, S. S., and Alfriend, K. T., "An Intelligent Control Concept for Formation Flying Satellites," *International Journal of Robust Control and Nonlinear Control*, 2002, pp. 97-115.

[29] Kumar, K., Bang, H., and Tahk, M., "Satellite Formation Flying Using Along-Track Thrust," *Acta Astronautica*, Vol. 61, No. 6, 2007, pp. 553-564.

[30] McVittie, G., Kumar, K. D., and Liu, G., "Control of Satellite Formation using Along Track Thrust," *Proc. The 21st Canadian Congress of Applied Mechanics (CANCAM 2007)*, Toronto, June 3-7, 2007.

[31] Starin, S., "Design Of A Linear Control System Of Reduced Inputs For Multiple Spacecraft Formation Flying," M.Sc. Dissertation, Dept. of Aerospace, Ohio State University, OH, 2000.

[32] Starin, S., Yedavalli, R. K., and Sparks, A. G., "Spacecraft Formation Flying Maneuvers Using Linear-Quadratic Regulation with No Radial Inputs," *AIAA Guidance, Navigation, and Control Conference and Exhibit*, August 6, 2001.

[33] Leonard, C., Hollister, W., and Bergmann, E., "Orbital Formationkeeping with Differential Drag," *AIAA Journal of Guidance, Control, and Dynamics*, Vol. 12, No. 1, 1987, pp. 108-113.

[34] Kumar, B. S., Ng, A., Yoshiwara, K., and De Rutier, A., "Differential drag as a means of spacecraft formation control," *IEEE 2007 Aerospace Conference*, March 3-10, 2007, pp. 1-9.

[35] Larson, W. L. and Wertz, J. R. (ed.), Space Mission Analysis and Design, 3rd ed., Kluwer Academic Publisher, Boston, 1999.

[36] Hill, G., "Researches in the lunar theory," *American Journal of Mathematics*, Vol. 1, 1878, pp. 5-26.

[37] Clohessy, W. and Wiltshire, R., "Terminal guidance systems for satellite rendezvous," *Journal of the Astronautical Sciences*, Vol. 27, No. 9, 1960, pp. 653 - 658.

[38] Zäk, S. H, *Systems and control*, Oxford University Press, New York, 2003.

[39] Hammett, K. D., Hall, C. D., and Ridgely, D. B., "Controllability Issues in Nonlinear State-Dependent Riccati Equation Control," *AIAA Journal of Guidance, Control, and Dynamics*, Vol. 21, No. 5, 1998.

[40] Sabol, C., Burns, R., and McLaughlin, C. A., "Satellite Formation Flying Design and Evolution," *AIAA Journal of Guidance, Control, and Dynamics*, Vol. 38, No. 2, 2001, pp. 270-278.

[41] DeRusso, P. M., Roy, R. J., Close, C. M., and Desrochers, A. A., *State Variables for Engineers*, 2nd ed., John Wiley & Sons, Toronto, 1998.

[42] Xu, C., Tsoi, R., and Sneeuw, N., "Analysis of J_2-Perturbed Relative Orbits for Satellite Formation Flying," *Gravity, Geoid and Space Missions 2004 IAG International Symposium*, Porta, Portugal, August 30, 2004.

[43] Utkin, V. I., "Variable Structure Systems with Sliding Modes," *IEEE Transactions on Automatic Control*, Vol. AC-22, No. 2, April 1977, pp. 212 – 222.

[44] Fossard, A. J. and Floquet, T., *Sliding Mode Control in Engineering*, Marcel Dekker, New York, NY, 2002, Chap. 1.

[45] Slotine, J. E. and Li, W., *Applied Nonlinear Control*, Prentice-Hall, Upper Saddle River, NJ, 1991.

[46] Pan, Y., Kumar, K. D., Liu, G., and Furuta, K., "Design of Variable Structure Control System with Nonlinear Time-Varying Sliding Sector," *IEEE Transactions on Automatic Control*, 2008.

[47] Hara, S, "Adaptive nonstationary positioning control of vibration systems by means of solutions of time-varying Riccati equations," *Microsystem Technologies*, Vol. 13, No. 8-10, 2007, pp. 1063-1075.

[48] Hui, S. and Zak, S. H., "Robust Control Synthesis for Uncertain/Nonlinear Dynamical Systems," *Automatica*, Vol. 28, No.2, 1992, pp. 289-298.

[49] Arnold, W. F. and Laub, A. J., "Generalized eigenproblem algorithms and software for algebraic Riccati equations," *Proceedings of the IEEE*, Vol. 72, No. 12, December, 1984, pp. 1746 - 1754.